Charge Trapping Mechanism in Organic Semiconductor Devices

Thesis submitted for the
Degree of Doctor of Philosophy (Science)
Of
Jadavpur University
2023

by

Sudipta Sen

Condensed Matter Physics Research Centre
Department of Physics
Jadavpur University
Kolkata 700 032

CERTIFICATE FROM THE SUPERVISOR

*This is to certify that the thesis entitled "**Charge Trapping Mechanism in Organic Semiconductor Devices**", submitted by **Sri Sudipta Sen** who got his name registered on **23rd February 2018** For the award of Ph. D. (Science) degree of Jadavpur University, is absolutely based upon his own work under the supervision of **Professor Nabin Baran Manik** and that neither this thesis nor any part of it has been submitted for either any degree / diploma or any other academic award anywhere before.*

24.04.2023

Dr. Nabin Baran Manik
Supervisor
Professor
Condensed Matter Physics Research Centre
Department of Physics
Jadavpur University
Kolkata-700032

Dr. NABIN BARAN MANIK
Professor
Department of Physics
Jadavpur University
Kolkata - 700 032

DECLARATION BY THE AUTHOR

*I do hereby declare that the work embodied in this thesis entitled "**Charge Trapping Mechanism in Organic Semiconductor Devices**", which is being submitted for the degree of Doctor of Philosophy (Science), is my own work and that, to the best of my knowledge and belief, neither the thesis nor any part thereof has been accepted for the award of any other degree or diploma of the university or other institute of higher learning, except where due acknowledgement has been made in the text.*

Sudipta Sen

Signature of the Candidate

Acknowledgement

Firstly, I would like to convey my gratitude to my supervisor Prof. Nabin Baran Manik for giving me an opportunity to do my Ph.D from Department of Physics, Jadavpur University. I have indebted to him for his unflinching support during my research tenure. Without his supervision, it would not have been possible for me to reach where I stand today. I joined his laboratory as a Research Scholar having UGC – JRF fellowship and thereafter got myself registered as a scholar under his supervision. His profound knowledge of the equipments and rigorous attitude towards research is highly exceptional. Dr. Manik's proper instructions and insightful knowledge made it possible for me to be in the right track throughout my research endeavor. I am also thankful to him for sharing his insightful knowledge beyond academics which helped me shape my attitude and personality in the research field.

I also owed a lot to the seniors and colleagues of my laboratory who have assisted me a lot during my research work. I would particularly like to thank Dr. A. Haldar, Dr. S. Maity, Dr. Md. R. Islam, Dr. S. Saha, Dr. P. Dalapati, Dr. S. Chakraborty, Mr. P. K. Das, Mr. S. Bhunia, Mr. D. Sahoo, Mr. A. K. Karan, Ms. S. Rakshit, Mr. A. Gucchait and Mrs. S. Guhathakurata for their valuable suggestions regarding my work.

Further, I would like to convey my gratefulness to all the members of the CMPRC group, Department of Physics, Jadavpur University, for their help and cooperation.

Finally, I would like to acknowledge University Grants Commission (UGC), India for their financial assistance without which it would not have been possible to conduct the research.

.

List of Abbreviations

Al	Aluminium
Al–M	Aluminium Coated Mylar
CB	Conduction Band
CNT	Carbon Nanotubes
COOH	Carboxylic Acid Functionalized
CV	Crystal Violet
C -V	Capacitance - Voltage
DCM	Dichloromethane
DSSC	Dye Sensitized Solar Cell
DOS	Density of States
E_F	Fermi level
E_t	Trap Energy
HOMO	Highest Occupied Molecular Orbital
ILC	Injection Limited Current
I -V	Current - Voltage
ITO	Indium Tin Oxide
M/O	Metal - Organic
LUMO	Lowest Unoccupied Molecular Orbital
MG	Malachite Green
MR	Methyl Red
MWCNT	Multi Walled Carbon Nanotubes
NP	Nanoparticles
N_C	Effective Density of States
N_D	Concentration of Donor Atoms
OPV	Organic Photovoltaics
PMMA	Poly Methyl Methacrylate
PSF	Phenosafranin
PVA	Poly Vinyl Alcohol
PV	Photovoltaics
R-S	Richardson - Schottky
SCLC	Space - Charge Limited Current
SWCNT	Single Walled Carbon Nanotubes
TiO_2	Titanium Dioxide

T_C	Characteristic Temperature
VB	Valence Band
V_a	Voltage Difference between Anode and Cathode
V_d	Diffusion Potential
V_{th}	Threshold Voltage/ Transition Voltage
W_d	Depletion Layer Width/ Space - Charge Layer Width
ZnO	Zinc Oxide

List of Tables

List of Figures

Contents

Chapter 3

Effect of Different Nanoparticles on Barrier Potential, Band Bending and Charge Trapping of Phenosafranin (PSF) Dye Based Device

Chapter 4

Impact of Single Walled Carbon Nanotubes (SWCNT) on Junction Properties of Safranin - T Dye Based Device

Chapter 5

Study on the Effect of Carboxyl-Functionalized Single Walled Carbon Nanotubes (COOH - SWCNT) and Different Sized Multi Walled Carbon Nanotubes (MWCNT) on Trap Energy and Junction Barrier of Malachite Green (MG) Dye Based Device

Chapter 8

Findings and Conclusion

Preface

The work embodied in the thesis entitled "Charge Trapping Mechanism in Organic Semiconductor Devices", is specifically concerned with the charge trapping and charge injection mechanisms of organic dye based devices. The charge injection of these devices is largely governed by metal-organic semiconductor interface and it is related to the presence of traps at the interface as organic devices are prone to traps. Due to interfacial trap density, the barrier height of the metal - organic layer interface is generally high. There is no significant work regarding the improvement of charge injection mechanism of these devices considering the effect of interfacial barrier height which has motivated the author to pursue research in this field.

The author started his research work as a Junior Research Fellow (JRF) funded by University Grants Commission (UGC), India. This work was carried out in the laboratory of Professor Nabin Baran Manik. The laboratory is in the Department of Physics, Jadavpur University. Thereafter, the author had done his Ph.D registration under the supervision of Dr. N. B.Manik, Professor, Department of Physics, Jadavpur University, Kolkata - 700032.

The electrical characteristics of the organic devices have been studied in this work. For studying the electrical characteristics, dark I -V measurements have been done. By analyzing the dark I -V measurements, the different electrical parameters related to charge injection mechanism such as barrier height, trap energy, ideality factor, depletion layer width, image barrier lowering effect and threshold voltage have been calculated. Attempts have been made to address some of the above mentioned problems both from experimental and theoretical perspective so that the charge injection process of the organic dye based devices can be improved.

To improve the charge injection process at metal - organic dye interface considering the effect of interfacial barrier height, we have incorporated different nanoparticles and nanotubes such as, Zinc Oxide (ZnO) Nanoparticles, Titanium Dioxide (TiO_2) nanoparticles and Carbon Nanotubes (CNT), in these organic dye based devices. As we all know that organic devices are prone to traps, the interfacial barrier height at metal - organic contact also influences the concentration of traps.

Zinc Oxide (ZnO) nanoparticles and Titanium Dioxide (TiO_2) nanoparticles reduce the barrier height, band bending at metal - organic semiconductor contact resulting in improvement of charge injection mechanism of organic devices.

The effects of CNT on the interfacial barrier height, trap concentration and depletion layer width of these devices have been extensively studied. We have incorporated both Single Walled Carbon Nanotubes (SWCNT) and different sized Multi Walled Carbon Nanotubes (MWCNT) in these organic devices. Our experiment reveals that SWCNT enhances the charge flow better than that of MWCNT in organic devices. It is observed that due to the addition of CNT, the interfacial barrier height, the concentration of traps and depletion layer width reduce which results in lowering of the device's threshold voltage. CNT provides easy percolation path ways which assist the easy migration of charges, which in turn improves the charge injection process of organic devices.

In this work, we have studied a series of dyes such as, Phenosafranin (PSF), Safranin - T, Malachite Green (MG) and Methyl Red (MR) dyes with and without adding different nanoparticles. From the dark I -V characteristics it is observed that both barrier height and trap energy get reduced. The I -V curves are studied by using Richardson - Schottky (R-S) thermionic emission model in presence of trap states and the relation between the trap energy, barrier height, and threshold voltage is discussed. We have also measured the interfacial barrier height by using Norde's method to check the consistency of the experimental data. We have also estimated the interfacial barrier height by varying the back electrode of the Crystal Violet (CV) dye based organic device.

Though the study in this field of organic dye based devices is relatively new and although numerous works are being done, there is no unique theory to explain charge transport process in all the systems. A theory which fits for a certain system may deviate a lot in case of other systems. So, further study is required for better understanding of these problems. The outcome of this work will be extremely helpful to understand the charge injection mechanism of the organic devices considering the barrier height, trap concentration, band bending and depletion layer width in presence of different nanoparticles.

Chapter 1

Motivation and Outline

1.1 Introduction

1.2 Objectives of the Work

1.3 Background of the Work

1.4 Outline of the Work

1.5 References

1.1 Introduction

Organic materials are currently being researched extensively to create various electronic and optoelectronic devices. Organic devices may be produced across a large area and are more agile, portable, and inexpensive. The characteristics of amorphous thin films of organic materials can be attuned over a broad range. Organic semiconductor devices are appealing as they can be deposited at low temperatures on substrates including glass, plastic, etc. to make viable devices by using cost effective manufacturing techniques **[1-4]**. Amidst these benefits, organic systems have some limitations. These devices' propensity to traps, which results in a high barrier height (ϕ_b) at metal - organic (M/O) interface, constitutes one of the major limitations. The charge infusion at interface is minimal because of the high barrier. The reliance of barrier potential on trap energy in organic devices has not received much attention. It is essential to make an effort to reduce the trap energy in order to maximize charge injection at M/O contact and subsequently decrease the barrier potential. Interfacial band bending and image barrier lowering are prerequisites for understanding how organic devices work. The interfacial electronic structure at M/O contact has a significant effect on the device performance. It affects how charges are injected into the contact **[5–6]**. The electrostatic model based on the density of states (DOS) in the material can also be used to investigate the band bending process in organic semiconductors **[7]**. There may be a correlation between the interfacial band deformation and interfacial barrier height (ϕ_b) **[8]**. Due to high barrier height and consequently minimal charge injection from metal to organic layer, the threshold voltage (V_{th}) is higher. The charge injection is significantly impacted by the contact barrier. The current focus of study is on how trap energy and barrier height influence the infusion of charges at M/O interface. The effects of various nanoparticles and nanotubes, such as Zinc Oxide (ZnO) nanoparticles, Titanium Dioxide (TiO_2) nanoparticles, Single Walled Carbon Nanotubes (SWCNT) and Multi Walled Carbon Nanotubes (MWCNT) have also been observed. Barrier heights and trap energy are being correlated analytically as well. The thickness of the depletion layer, the lowering of image charge barrier, barrier inhomogeneities in the presence and absence of various nanoparticles and nanotubes, have all been examined throughout this study.

1.2 Objectives of the Work

Investigating the various factors related to charge injection and charge trapping process at the M/O junction is the main objective of the ongoing study. Following that, it seeks to look into how different nanoparticles and nanotubes affect those factors in various organic dye based devices. The charge injection procedure is significantly influenced by the barrier potential at the M/O contact. The organic

dye based devices' charge injection technique significantly depends on interfacial band bending. The steady state current - voltage (I -V) characteristics of the organic device will be investigated to measure various electrical parameters, such as barrier potential, trap energy, depletion layer width, image force barrier lowering, and barrier inhomogeneities in presence and absence of various nanoparticles and nanotubes, which will influence the charge infusion process.

In our research, we have chosen a few organic dyes namely Phenosafranin (PSF), Safranin - T, Malachite Green (MG), Methyl Red (MR) and Crystal Violet (CV) dyes for our study. We have prepared devices with and without incorporating guest materials such as, ZnO, TiO_2 and CNT with these dyes. Different electrical properties are measured and compared to find the effect of these different nanoparticles and nanotubes. Along with all these experimental works, there has been an attempt to understand the injection mechanism at the contact area of metal and organic material.

In this research, varieties of literatures on the charge injection and charge entrapment at M/O interface have been discussed. We have also looked at the function of various nanoparticles and nanotubes in dye based organic devices. Dye/polymer solution is typically employed in spin coating process at regular room temperature. Additionally, there is no such obstacle to the fabrication of the device or the widespread deposition of the film.

As several aspects that affect the injection process have been thoroughly researched, the results of this work will be helpful to overcome some concerns linked to charge infusion at M/O interface. This endeavor will also demonstrate device physics application for various nanoparticles and nanotubes in the realm of organic electronics.

1.3 Background of the Work

Analyzing the performance of the organic device critically depends on charge transfer at the M/O interface. This work clarifies present understanding of parameters connected to injection current and formation of M/O contacts. When an electron or hole goes from the metal into the organic material's LUMO or HOMO states, the charge infusion takes place **[9]**. Amorphous van der Waals solids are what make up organic semiconductors **[10]**. According to the Richardson - Schottky (R-S) model of thermionic emission from the delocalized states of the metal into the localized states of the semiconductor, infusion of charges is commonly characterized. The energy of these states is formed with significant help from the mean barrier height, image potential, energetic disorder, and applied electric field **[11]**. Lack of a comprehensive, effective analytical theory nonetheless, when applied to

well-characterized surfaces, the injection current exhibits behaviour consistent with the thermionic emission process **[12–13]**.

Numerous applications in the field of organic electronics are currently being, or soon will be, commercialized. As a result, the effective operation of organic devices is well-known in numerous fields and has been documented in several scientific publications **[14–15]**. However, the process of charge transfer at the contact of metal - organic material is still an important area of study. One of the causes is a lack of thorough discernment brought on by the interface's intricacy as well as the chemical, structural, and morphological elements that have an impact on the charge injection procedure. If there is significant advancement in the knowledge of the infusion approach in terms of device physics, organic electronics' commercial success will increase dramatically **[16-17]**.

One or more layers of the active organic materials are sandwiched between two electrodes to form basic structure of the majority of these organic dye based devices. The charge injection procedure takes place when the charge carrier traverses the contact, overcoming the energy barrier. Their performance depends on the effective transfer of charge across the interface **[18]**. When the contact is created, equilibrium occurs when charge flow from one material to other continues until Fermi level alignment happens. The Mott-Schottky rule, which states that the vacuum levels align at the interface when a transferred charge occupies only dopant levels in the bulk, is then produced. This additional charge then lies in the depletion zone that is created by ionizing donor or acceptor dopants and results in band bending **[19]**. Absence of intentional dopant in organic semiconductors makes it difficult to measure Fermi level. The analysis of image potential, which pushes charges towards the interface and leads to incorrect interpretation of experimental results, depends on it **[20–21]**.

1.4 Outline of the Work

The charge trapping and carrier infusion process of organic semiconductor devices is what we intend to investigate in the current work. Due to the propensity of organic devices to traps, the metal – organic semiconductor interface controls the charge injection of these devices in a significant way. The barrier height and thickness of depletion layer of M/O contact are typically large due to interfacial trap density. However, there aren't many research works that use an organic semiconductor to estimate these parameters at the junction of M/O layer when traps are present.

In consideration of the charge trapping, it is of interest to us to investigate barrier and space - charge layer width of organic semiconductor devices. Interfacial barrier has strong correlation with the interfacial band bending and image force barrier lowering effect of these organic devices. We have a

plan to measure these parameters from I -V characteristics of these devices and correlate it with the trap energy. We will confide our study with a series of organic dyes such as Phenosafranin (PSF), Safranin -T, Malachite Green (MG), Methyl Red (MR) and Crystal Violet (CV) dyes and also in presence of some nanoparticles such as ZnO and TiO_2 and different nanotubes, such as SWCNT and MWCNT.

The overall outline of our work has been summarized below. There are eight chapters in this present thesis.

In **Chapter 1**, the variables that will impact the charge infusion at M/O contact are discussed. The goals and background of this work have also been mentioned in this context.

In **Chapter 2**, the basic working principle of the organic devices, different charge trapping models and its effect on charge injection process, different charge injection models and the above mentioned parameters such as interfacial barrier height, concentration of traps, depletion layer width, band bending, image force barrier lowering and barrier inhomogeneities that affect the charge trapping and charge injection process have been discussed in detail. Different nanotubes and nanoparticles which have been incorporated in different organic dye based devices have also been mentioned in this chapter.

In **Chapter 3**, we have analyzed PSF dye based device's barrier height, charge trapping, and band bending at the M/O layer interface. We have looked at the impact of two distinct nanoparticles, such as ZnO and TiO_2, on these characteristics. On this organic device, changing the concentration of TiO_2 nanoparticles has also been done. According to the steady state dark I -V plots of the organic device, adding ZnO and TiO_2 nanoparticles enhances device's ability to inject charges by reducing interfacial barrier and trap density. In this chapter, an effort has been made to analytically relate interfacial barrier and trap density. Using Norde's method, interfacial barrier height has also been calculated and is still compatible with the value determined by using I -V characteristics. Presence of both nanoparticles has reduced band bending at the M/O dye contact. This chapter goes into great detail about the findings. It has been found that when TiO_2 nanoparticles concentration is highest while maintaining the same PSF dye concentration, barrier height, trap concentration, and band bending are least, allowing higher injection of carriers at the junction.

In **Chapter 4**, Safranin - T dye based organic device’s trap energy, barrier potential, barrier inhomogeneity, and depletion layer width, both without and after taking into account the image charge effect have been analyzed and how SWCNT affects these electrical properties has been studied. SWCNT reduces the aforementioned factors, lowering the device's threshold voltage and

improving the charge infusion process. In this chapter, we have also looked at the relationship between contact barrier and depletion layer width. Additionally, this chapter has demonstrated how the applied field affects space - charge layer width and barrier height. This chapter has stated a possible justification for origin of these alterations.

In **Chapter 5**, pertaining to junction barrier and trap energy, we have discussed the effects of both COOH - SWCNT and MWCNT on charge infusion process of MG dye based device. Fabrication of devices and as well as experimental methods has been discussed in detail. I -V measurements are used to characterize these devices. Norde's method is employed to examine the congruency of the interfacial barrier derived from I -V characteristics, and both approaches are in strong agreement with one another. The possible reason has been furnished.

In **Chapter 6**, we have investigated the effects of SWCNT and MWCNT on various parameters related to charge infusion and trapping process, such as contact barrier, trap energy, depletion layer width, and image barrier lowering of MR dye based device. In this chapter, findings are thoroughly addressed.

In **Chapter 7**, we have seen how the back electrode affects the concentration of traps and junction barrier of an organic device based on CV dye. As a result of changing the back electrode, we are able to optimize the charge flow at the junction by lowering concentration of traps and junction barrier.

In **Chapter 8**, the summary and overall findings of our work have been highlighted. This chapter contains overall conclusion of our work and also the future scope of this work in this research field of organic semiconductor.

1.5 References

[1] S. R. Forrest, "The path to ubiquitous and low-cost organic electronic appliances on plastic", Nature, 2004, **428**, 911-918

[2] T. H. Lim, S. H. Kim and K. W. Oh, "Fabrication of Organic Materials for Electronic Textiles", In: Handbook of Smart Textiles, 2014, [1st ed.], Springer Singapore, 1-29

[3] Q. Zhang, W. Hu, H. Sirringhaus and K. Müllen, "Recent Progress in Emerging Organic Semiconductors", Advanced Materials, 2022, **34**, 1-4

[4] F. M. Li, A. Nathan, Y. Wu and B. S. Ong, "Organic Thin Film Transistor Integration: A Hybrid Approach", 2011, [1st ed.], Wiley-VCH Verlag GmbH & Co. KGaA, Weinheim, Germany, 1-11

[5] V. Coropceanu, J. Cornil, D. A. da Silva Filho, Y. Olivier, R. Silbey and J. –L. Brédas, "Charge Transport in Organic Semiconductors", Chemical Reviews, 2007, **107**, 926-952

[6] M. T. Greiner and Z. –H. Lou, "Thin-film metal oxides in organic semiconductor devices: their electronic structures, work functions and interfaces", NPG Asia Materials, 2013, **5**, 1- 16

[7] M. Oehzelt, N. Koch and G. Heimel, "Organic semiconductor density of states controls the energy level alignment at electrode interfaces", Nature Communications, 2014, **5**, 1-8

[8] P. Zhang, S. Zhao, H. Wang, J. Zhang, J. Shi, H. Wang and D. Yan, "Relation between Interfacial Band- Bending and Electronic Properties in Organic Semiconductor Pentacene", Advanced Electronic Materials, 2017, **3**, 1700136-1-1700136-6

[9] N. F. Mott, "Electrons in Disordered Structures", Advances in Physics, 1967, **16**, 49-144

[10] K. W. Böer and U. W. Pohl, "Defects in Amorphous and Organic Semiconductors", In: Semiconductor Physics, 2018, [1st ed.], Springer Cham, 781-812

[11] C. Liu, Y. Xu and Y. –Y. Noh, "Contact Engineering in Organic Field-Effect Transistors", Materials Today, 2015, **18**, 79-96

[12] S. Jung, C. H. Kim, Y. Bonnassieux and G. Horowitz, "Injection barrier at metal/organic semiconductor junctions with a Gaussian density-of-states", Journal of Physics D: Applied Physics, 2015, **48**, 395103-1- 395103-10

[13] J. C. Scott, "Metal - Organic Interface and Charge Injection in Organic Electronic Devices", Journal of Vacuum Science & Technology A, 2003, **21**, 521-533

[14] S. Ahmad, "Organic semiconductors for device applications: current trends and future prospects", Journal of Polymer Engineering, 2014, **34**, 279-338

[15] A. Kumatani, Y. Li, P. Darmawan, T. Minari and K. Tsukagoshi, "On Practical Charge Injection at the Metal/Organic Semiconductor Interface", Scientific Reports, 2013, **3**, 1-6

[16] T. W. Kelley, P. F. Baude, C. Gerlach, D. E. Ender, D. Muyres, M. A. Haase, D. E. Vogel and Steven D. Theiss, "Recent Progress in Organic Electronics: Materials, Devices, and Processes", Chemistry of Materials, 2004, **16**, 4413-4422

[17] N. Armbrust, F. Schiller, J. Güdde and U. Höfer, "Model potential for the description of metal/organic interface states", Scientific Reports, 2017, **7**, 1-8

[18] S. Chen, Z. Zhao and H. Liu, "Charge Transport at the M/O Interface", Annual Review of Physical Chemistry, 2013, **64**, 221-245

[19] H. Ishii, N. Hayashi, E. Ito, Y. Washizu, K. Sugi, Y. Kimura, M. Niwan, Y. Ouchi, and K. Seki, "Kelvin probe study of band bending at organic semiconductor/metal interfaces: examination of Fermilevel alignment", Physica Status Solidi (A), Applied Research, 2004, **201**, 1075-1094

[20] W. Schottky, "Halbleitertheorie der Sperrschicht", Naturwissenschaften, 1938, **26**, 843-843

[21] A. J. Twarowski, "Energy level bending at molecular crystal surfaces", The Journal of Chemical Physics, 1982, **77**, 1458-1460

Chapter 2

Physical Principles and Theoretical Analysis of Charge Trapping and Charge Injection Process in Organic Semiconductors

2.1 Introduction

In the preceding chapter, we described the context and aims of our current work. The preceding chapter also provided a structure for the current thesis work as well as a potential outcome. The basic operating principle of organic devices, various charge injection models, and factors like trap concentration, interfacial barrier height, depletion layer width, band bending, image charge barrier lowering and barrier inhomogeneities that influence the charge infusion and trapping process at the M/O contact will be covered in detail in this chapter. Properties of different nanoparticles which will be incorporated in these different organic dye based devices will also be elucidated in this chapter.

2.2 Working Principle of Organic Dye Based Devices

Since 1990, organic dye based devices have got significant attentions among the researchers. Due to the fact that organic dye based devices are made of very thin layers and most organic semiconductors are p-type semiconductors with a substantially high optical band gap, production costs are reduced **[1-2]**. In sp^2-hybridized states of carbon atoms, organic materials are made of π -bonded electrons that can travel through delocalized π -orbitals **[3]**. In our work, we have formed M/O contact in the prepared organic device. The work function of the metal electrode and the Lowest Unoccupied Molecular Orbital (LUMO) and Highest Occupied Molecular Orbital (HOMO) energy levels of organic materials both remain at their original values prior to M/O contact establishment. The alignment of energy levels would occur after the creation of M/O contact. When the work function of the metal electrode is more than LUMO energy level of organic materials, the electro-potential will cause electrons to be transported from the metal electrode to organic materials and when work function of the metal electrode is less than the LUMO energy level, the electron will be moved from organic materials to the metal electrode **[4-5]**. Electric field will be created from organic materials towards metal electrode. The electrons moving from organic materials to metal electrode, would encounter an energy barrier due to this electric field **[6-7]**.

2.3 Charge Carrier Trapping and Its Exponential Distribution at Metal - Organic Interface

Any defect that generates localized electronic states that are energetically and spatially spread throughout the semiconductor's band gap is referred to be an electronic trap. According to their relative energy locations from trap depth at a particular temperature, traps can be distinguished as

shallow traps and deep traps. Shallow traps remain close to the band edges (a few kT) and deep traps remain considerably away (many kT) from the band edges.

In organic semiconductor materials, impurities, structural defects, geminate pairs, and self-trapping are a few potential sources of trap states. A submerged molecule's HOMO or LUMO will establish a trap state if it is positioned between the host molecules since the molecular interactions in organic materials is weak **[8]**. A conjugation length fluctuation caused by structural defects can result in the creation of some tail states below the transport energy. These constitute up the states of the trap. However, structural flaws are not just limited to the creation of tail states; any kind of flaw in the structure is more likely to create trap states **[9–11]**.

A pair of Coulomb bond charge carriers is known as a geminate pair. A Coulomb trap is created when the recombination probability of a geminate pair is suppressed. Only the presence of both types of charge carriers permits the occurrence of these traps **[12]**.

Polaron and bipolaron formation are not actually traps because they move. But polaron or bipolaron mobility is at least one or two orders of magnitude inferior than that of a free carrier. Self-trapping is the process of these charge carriers creating their own trap state when the energy of the polarons or bipolarons is lowered by several hundreds of meV **[13]**.

Shallow traps are typically described as localized tail states in band gap. Charge carrier may be momentarily captured and restrained by a trap, up and till it is returned to band by an electric field or thermal energy or a photon. For example, a localized shallow trap state in the band gap traps charges travelling within delocalized states in the multiple-trap and release (MTR) model, which subsequently uses thermal energy to release the charges back into the energy band **[14–15]**. Trapped charge carriers can take part in transport by thermally activated hopping or tunneling from one localized state to another if high trap densities are there **[16]**. If the trap depth is low, de-trapping of charge carriers is conceivable by thermal energy. At a particular temperature, probability of returning to the band by thermal energy is more likely for carriers present in shallow traps but for deep traps, it is more unlikely **[17]**. These deep states frequently serve as charge carrier recombination sites, shortening their total lifetime. Traps can have discrete energy or a energy distribution, which can be modeled using exponential or a Gaussian function **[18–21]**.

Only, exponential distribution of traps has been taken into consideration for our analysis.

Fig. 2.1 shows schematic of localized trap states between HOMO and LUMO band of organic material.

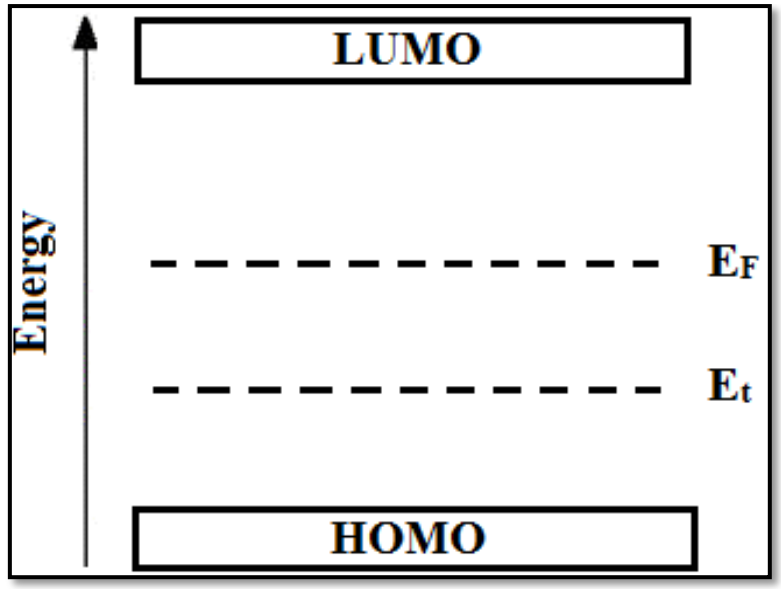

Fig. 2.1 Diagrammatic Illustration of Localized Trap States in Organic Material between HOMO and LUMO Band

Equation (2.1) and **equation (2.2)** represent one-dimensional single (double) carrier drift current and Poisson equations (for electrons, holes, or both) respectively.

$$J_d = nq\mu E \quad \textbf{(2.1)}$$

$$\frac{dE}{dx} = \frac{q}{\epsilon}(n + n_t) \quad \textbf{(2.2)}$$

Where, J_d is the drift current density, μ is the carrier mobility, E is the electric field strength, n and n_t are the free and trapped charge concentrations respectively and q is electronic charge. The above equations can be solved for two cases as follows

Case I: When free carrier density is substantially higher than the trap charge density ($n>>n_t$)

Then, **equation (2.1)** may be written as

$$\frac{dE}{dx} = \frac{q}{\varepsilon}n \quad \textbf{(2.3)}$$

Free charge carriers consist of both injected and thermally generated charges. Depending on the relative proportions of these two types of free carriers, two cases may arise. There are always some thermally generated free carriers present in the material. Let it be denoted by n_0. For metals, this number is very high so that injected space - charge density n is negligible compared to n_0. For insulators, n_0 is negligible for high injection level. But for very small external field, injection of

carriers into the insulator is very low. Therefore, for low external voltages considering free carriers, **equation (2.1)** takes the form, which is shown in **equation (2.4)**

$$J_d = \{n(x) + n_0\}q\mu E \quad \textbf{(2.4)}$$

$$\frac{dE}{dx} = \frac{q}{\varepsilon}n(x) \quad \textbf{(2.5)}$$

At the low injection level n(x) may be approximated as n(x) ~0, then, **equation (2.4)** takes the form

$$J_d = n_0 q\mu E \quad \textbf{(2.6)}$$

E = constant

This is well known Ohm's law.

For high injection levels, injected carriers dominate over thermally generated free carriers. By putting the value of n(x) from **equation (2.4)** in the **equation (2.5)**, we have,

$$\frac{dE}{dx} = \frac{1}{\mu\epsilon E}J_d$$

$E = -\frac{dV}{dx}$ where, V is the potential.

Putting the value of E in terms of V we get,

$$\frac{d}{dx}\left\{\left(\frac{dV}{dx}\right)^2\right\} = \frac{2J_d}{\mu\epsilon}$$

Integrating with respect to x we get,

$$\frac{dV}{dx} = \sqrt{\frac{2J_d}{\mu\epsilon}}x + \text{constant} \quad \textbf{(2.7)}$$

If we take field E to be zero at x = 0 then the above constant is zero. Taking sample thickness to be L and by integrating the above equation with respect to x between x = 0 to x = L we get,

$$\int_0^V dV = \sqrt{\frac{2J_d}{\mu\varepsilon}} \int_0^L x^{1/2} dx$$

By integrating, we get,

$$V = \sqrt{\frac{2J_d}{\mu\varepsilon}} \frac{L^{3/2}}{3/2}$$

Therefore,

$$V^2 = \left(\frac{2J_d}{\mu\varepsilon}\right) \frac{4}{9} L^3$$

The current density $J_d = V/L$ is written as

$$J_d = \frac{9}{8} \mu\varepsilon \frac{V^2}{L^3} \quad \textbf{(2.8)}$$

This is the current density equation for space - charge limited current.

Case II. When free carrier density is considerably lower than the trap charge density ($n << n_t$)

Equation (2.2) takes the form

$$\frac{dE}{dx} = \frac{q}{\varepsilon} n_t \quad \textbf{(2.9)}$$

The above **equation (2.9)** along with **equation (2.3)** cannot be solved if we do not know the relation between n and n_t. n_t is given as

$$n_t = H_n \exp\left(\frac{F_n}{kT_c}\right) \quad \textbf{(2.10)}$$

Where, T_c is the characteristic temperature, where $T_c = E_t/k$, where, E_t is trap energy, H_n is trap density, F_n is the electron Fermi energy. n_t and n are interrelated as follows:

$$n_t = H_n \exp\left(\frac{F_n}{kT_c}\right)$$

$$n = N_c \exp\left(\frac{F_n}{kT}\right)$$

$$n_t = H_n \exp\left(\frac{F_n}{kT} * \frac{T}{T_c}\right)$$

$$n_c = H_n \left(\frac{n}{N_c}\right)^{1/m}$$

$$n_t = C n^{1/m} \qquad \textbf{(2.11)}$$

Where, $m = T_c/T$ and $C = H_n/(N_c^{1/m})$

Therefore from **equation (2.3)**, we have

$$\frac{dE}{dx} = \frac{q}{\varepsilon} C n^{1/m}$$

Putting E in terms of V

$$\frac{d^2V}{dx^2} * \left(\frac{dV}{dx}\right)^{1/m} = \frac{q}{\varepsilon} C \left(\frac{J}{q\mu}\right)^{1/m}$$

Integrating with respect to x, we get

$$\left(\frac{dV}{dx}\right)^{(1+m)/m} \times \frac{m}{1+m} = \frac{q}{\varepsilon} C \left(\frac{J}{q\mu}\right)^{1/m} x + \text{constant}$$

The value of this constant is zero because at x = 0, dV/dx = 0. Therefore

$$\frac{dV}{dx} = \left(\frac{m+1}{m}\right)^{m/m+1} \times \left(\frac{C}{\varepsilon}\right)^{m/m+1} \times q^{m-1/m+1} \times \left(\frac{J}{\mu}\right)^{m/m+1} \times x^{m/m+1}$$

Integrating again with respect to x between x = 0 to x = L, the sample thickness we have

$$\int_0^V dV = \left(\frac{m+1}{m}\right)^{m/m+1} \times \left(\frac{C}{\varepsilon}\right)^{m/m+1} \times q^{m-1/m+1} \times \left(\frac{J}{\mu}\right)^{m/m+1} \int_0^L x^{m/m+1} dx$$

$$V = \left(\frac{m+1}{m}\right)^{m/m+1} \times \left(\frac{C}{\varepsilon}\right)^{m/m+1} \times q^{m-1/m+1} \times \left(\frac{J}{\mu}\right)^{m/m+1} \times \frac{m+1}{2m+1} \times L^{2m+1/m+1}$$

The current density can be stated from the above expression which is expressed in **equation (2.12)**

$$J = N_c \mu \left(\frac{2m+1}{m+1}\right)^{m+1} \left(\frac{\varepsilon m}{(m+1)H_n}\right)^m q^{m-1} \frac{V^{m+1}}{L^{2m+1}} \qquad \textbf{(2.12)}$$

This is Trap Charge Limited Conduction process.

The power law dependence $J \sim V^{m+1}$ is the most significant aspect of the aforementioned **equation (2.12)**. The particular I -V relation develops as a result of traps that are evenly spaced between the

LUMO and HOMO. The best fit for our current - voltage (I -V) experimental results is provided by this model **[22]**.

2.4 Interface Barriers

Current section will elucidate the contact barrier creation at metal - organic junction. We will also go through various experimental methods for characterizing these contact barriers which are formed at the convergence of a metal and an organic layer. This section will also comprise of band bending, image force barrier lowering, and barrier inhomogeneities.

2.4.1 Interface Barrier Formation

An interfacial barrier (ϕ_b) is created at the M/O contact when metal comes into contact with an organic semiconductor. The creation of an interfacial barrier between an organic substance and a metal relies on the synchronization of both metal and organic substance's respective energy levels. It is necessary to get through the barrier, to transport electrical charges from metal to the organic material. Barrier regulates the passage of electrical charges. The charge flow across the interface will differ depending on interface barrier's magnitude. To transport an electrical charge from metallic electrode into the HOMO or LUMO of the organic, or vice versa, this barrier must be overcome. Due to their resemblance to schottky contacts in conventional semiconductors, M/O interfaces were the first contacts in organic electronics to be thoroughly reported **[23]**.

2.4.2 Different Types of Interface Barrier

According to theoretical calculations, at room temperature, injection limited current (ILC) flows when ϕ_b is more than 0.3 eV but space - charge limited current (SCLC) flows when ϕ_b is less than 0.3 eV **[24]**.

2.4.3 Experimental Characterization of Different Interface Barriers in Organic Devices

To estimate the interfacial barriers at metal - organic contact in organic dye based devices, generally, four methods are used **[25]**. These four methods are as follows:

(i) Current – Voltage measurement
(ii) Capacitance – Voltage measurement
(iii) Activation – Energy measurement

(iv) Photoelectric measurement

In our work, Keithley 2400 source meter is used for the measurement of dark I -V characteristics of the device and afterwards, junction barrier is calculated from dark I -V. Norde method is used to verify reliability of contact barrier value acquired from dark I -V measurement. We have also employed capacitance-voltage (C -V) measurements to estimate the interfacial barrier in some of our works. There are times when the presence of traps at the junction can be used to explain a small discrepancy among the calculated values of interfacial barrier obtained using various approaches.

2.4.4 Band Bending

The concept of band bending was first proposed by Schottky and Mott to explain the rectifying effect of metal - semiconductor contacts **[26-27]**. It is frequently thought that organic semiconductors and metals will exhibit band bending with Fermi level alignment. Band bending is the process of continuously shifting the organic semiconductor's energy band edges in space - charge region due to electric field produced as charge transfers between organic semiconductor and metal. When the work function of metal (ϕ_m) is more than the work function of the organic semiconductor (ϕ_s), the energy bands bend upward toward the interface and the energy bands bend downward when $\phi_s > \phi_m$. The schematic representation of band bending has been shown in **Fig. 2.2**, in which $\phi_m < \phi_s$.

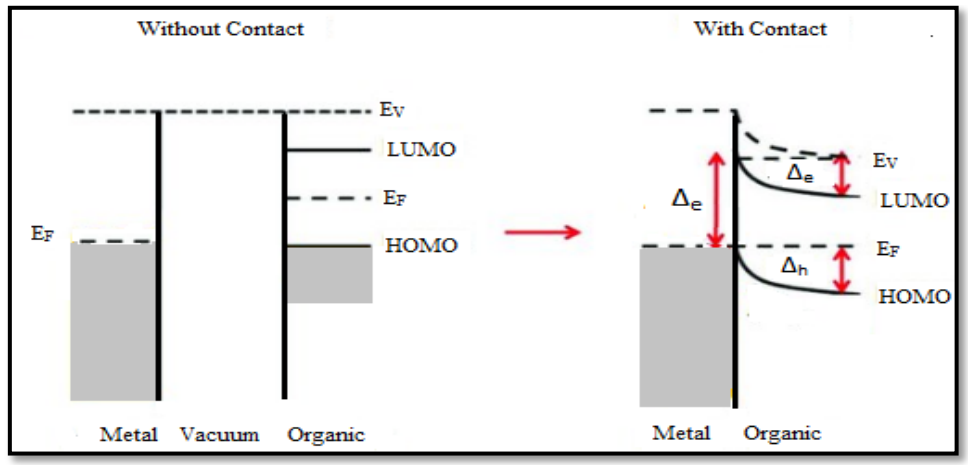

Fig. 2.2 Schematic Diagram of Band Bending at Metal - Organic Contact for $\phi_m < \phi_s$

Although, in our present work, we have estimated the interfacial band bending at metal - organic contact using a method which is proposed by Ryo Nouchi **[28]**, which is expressed by the **equation (2.13)**.

$$n_{if} = [1 - \frac{\delta\phi_{if}^{0}}{4q|V_i^0|}]^{-1} \quad \textbf{(2.13)}$$

Where, n_{if} = ideality factor and $q|V_i^0|$ = zero – bias band bending, $\delta\phi_{if}^{0}$ = image barrier lowering. By using **equation (2.13)**, we have also estimated the interfacial band bending without and with different nanoparticles.

2.4.5 Image Force Barrier Lowering

This work also discusses the influence of image charges on decreasing barriers. At M/O interface, charge infusion is significantly influenced by image force barrier lowering effect. An external electric field and the Coulomb field work together to limit the carrier infusion at M/O contact **[29]**.

Fig. 2.3 depicts schematic diagram of infusion of charge at M/O junction without and with image charge at the interface.

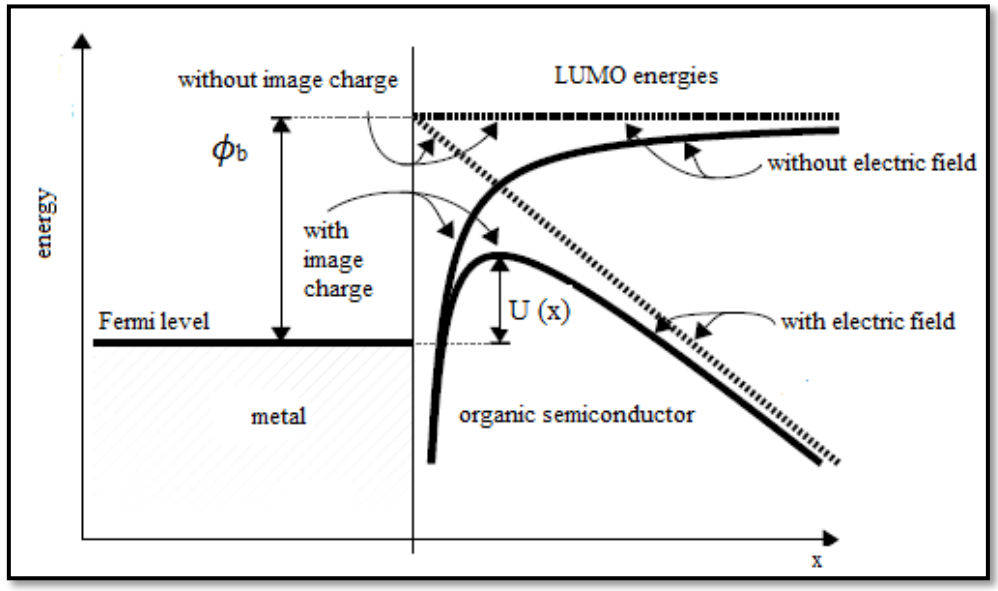

Fig. 2.3 Schematic Diagram of Charge Injection from Metal to Organic Semiconductor via Schottky Emission without and with Image Charge

Both carrier and image carrier on the electrode are bounded by superposition, as indicated by the subsequent **equation (2.14)**

$$U(x) = \phi_b - \frac{q^2}{16\pi\varepsilon_0\varepsilon x} - eFx \quad \textbf{(2.14)}$$

U (x) = Interfacial barrier in presence of image charge, x = distance from interface, F = external field (V/cm) and other notations have standard meaning.

2.4.6 Barrier Inhomogeneities

The lateral fluctuation of the junction barrier can be used to explain barrier inhomogeneities. The interfacial property and fabrication technique are responsible for this variation in the interfacial barrier **[30–33]**. Werner and Güttler developed Schottky barrier inhomogeneity model **[34]**. To explain I -V characteristics deviation of these devices, this model makes the assumption that the contact barrier has a Gaussian distribution. In our research, we have employed the Werner and Güttler model and looked at how nanoparticles affect the barrier inhomogeneity at the interface.

Taking into consideration of the presence of barrier inhomogeneties at the interface, the charge flow can be represented by the **equation (2.15)**,

$$I(V) = \int_{-\infty}^{+\infty} I(\phi_b, V) P(\phi_b)\, d\phi_b \quad \textbf{(2.15)}$$

Where,

$$P(\phi_b) = \frac{1}{\sigma_0\sqrt{2\pi}} \exp\left[-\frac{(\phi_b-\phi_0)^2}{2\sigma_0^2}\right] \quad \textbf{(2.16)}$$

Where, $P(\phi_b)$ is Gaussian distribution of barrier potential, pre exponential term is normalization constant and σ_0 is a standard deviation from mean barrier potential (ϕ_0).

When the distribution of interfacial barrier is described by Gaussian function, the current flow can be represented by **equation (2.17)**

$$I(V) = AA^*T^2 \exp[-\beta\left(\phi_0 - \frac{\beta\sigma_0^2}{2}\right)]\exp\left(\frac{\beta V}{n}\right)[1-\exp(-\beta V)] \quad \textbf{(2.17)}$$

Where,

$$I_0 = AA^*T^2\exp(-\beta\phi_a) \quad \textbf{(2.18)}$$

Where, I_0 = saturation current, ϕ_a = apparent barrier potential, A = area of device, A* = effective Richardson constant, T = absolute temperature, n = ideality factor.

Equation (2.19) demonstrates how ϕ_a is interrelated to σ_0.

$$\phi_a = \phi_0 - \frac{\beta\sigma_0^2}{2} \quad \textbf{(2.19)}$$

Where, $\beta = \frac{q}{kT}$

ϕ_a depends on ϕ_0, σ_0 and also on the temperature. The intercept at the ordinate axis in the plot of ϕ_a vs 1/2kT defines ϕ_0 and slope indicates σ_0. Fitting procedure can be used to detect interface inhomogeneity of the prepared device.

2.5 Different Charge Injection Models in Organic Dye Based Devices

When current flow at M/O interface is constrained by infusion process, then it is called ILC. In this work, four different charge injection models in organic devices have been discussed. Four different charge injection models are as follows:

(i) Richardson - Schottky Thermionic Emission Model
(ii) Drift-Diffusion Charge Injection Model
(iii) Hopping Charge Injection Model
(iv) Fowler-Nordheim Tunneling Model

2.5.1 Richardson - Schottky Thermionic Emission Model

Interfacial charge flow at M/O contact can be analyzed by R-S Thermionic Emission model. This model is described in the following manner.

Considering, x direction which is perpendicular to surface of electron emitting solid, the critical value of the electron's momentum in the x direction can be written as shown in **equation (2.20)**

$$\frac{p_{x_0}^2}{2m} = E_F + \phi_b \quad \textbf{(2.20)}$$

Where, E_F = Fermi level, ϕ_b = barrier height.

Let, N (p_x) determines number of electrons per unit volume having momentum values p_x and $p_x + dp_x$ in the x direction. When the electron with momentum p_x reaches the surface, its velocity becomes p_x/m.

Consequently, the quantity of electrons arriving at the unit surface area at unit time is

$$\int_{p_{x_0}}^{\infty} \frac{p_x}{m} N(p_x) dp_x$$

Thus, the emission current density is shown in **equation (2.21)**.

$$J = \frac{e}{m} \int_{p_{x_0}}^{\infty} p_x N(p_x) dp_x \qquad \textbf{(2.21)}$$

N (p_x) is the product of the number of possible states of momentum p_x and the probability that an electron is in each state. The amount of states with momentum values within the range of p and p + dp can be written as shown in **equation (2.22)**

$$Z(p)\, dp = \left(\frac{8\pi}{h^3}\right) p^2\, dp \qquad \textbf{(2.22)}$$

The above **equation (2.22)** gives the momentum values of p in any direction but particularly, we are interested in momentum in the x direction. The number of electrons with a momentum in the particular range dp_x at p_x when p_y and p_z values are unrestricted needs to be determined. We need to have a momentum space where each point represents a specific combination of momentum components p_x, p_y and p_z with $p^2 = p_x^2 + p_y^2 + p_z^2$. Considering, a spherical shell with $p = \sqrt{p_x^2 + p_y^2 + p_z^2}$ as radius and dp as thickness, then each quantum state with momentum values within p and p + dp lies in shell. Thus, the fraction of the states at momentum p which have momentum values within the interval p_x to $p_x + dp_x$, p_y to $p_y + dp_y$ and p_z to $p_z + dp_z$, is given by the ratio of the volume $dp_x dp_y dp_z$ to the volume of the spherical shell of radius p and thickness dp, which is shown in **equation (2.23)**.

$$dp_x dp_y dp_z = \frac{dp_x\, dp_y\, dp_z}{4\pi p^2 dp} \qquad \textbf{(2.23)}$$

Total states in the range of momentum interval $dp_x dp_y dp_z$ is estimated by multiplying the above **equation (2.23)** by the total states in the momentum interval dp at momentum p and this is expressed in **equation (2.24)**

$$Z\left(p_x p_y p_z\right) dp_x dp_y dp_z = \left(\frac{8\pi}{h^3}\right) p^2\, dp\, \frac{dp_x\, dp_y\, dp_z}{4\pi p^2 dp}$$

$$= \left(\frac{2}{h^3}\right) dp_x dp_y dp_z \qquad \textbf{(2.24)}$$

The number of states per cubic metre having a momentum component in the x direction that is between the values p_x to $p_x + dp_x$ is given by **equation (2.24)** and similarly, for p_y and p_z.

The electrons per unit volume with momentum values p_x and $p_x + dp_x$ in the x direction is given by **equation (2.25)**

$$N(p_x)\, dx = \left(\frac{2}{h^3}\right) dp_x \int \frac{dp_y\, dp_z}{1 + e^{\frac{E - E_F}{k_B T}}}$$

$$= \left(\frac{2}{h^3}\right) dp_x \int_{p_y = -\infty}^{\infty} \int_{p_z = -\infty}^{\infty} \frac{dp_y\, dp_z}{1 + e^{\frac{E - E_F}{k_B T}}} \qquad \textbf{(2.25)}$$

At 300 K, $(E - E_F) \gg k_B T$, hence 1 is neglected. We also know that,

$$E = \frac{1}{2m}\left(p_x^2 + p_y^2 + p_z^2\right)$$

Then, the **equation (2.25)** becomes

$$N(p_x)\, dx = \left(\frac{2}{h^3}\right) dp_x \int_{p_y = -\infty}^{\infty} \int_{p_z = -\infty}^{\infty} e^{-\frac{E}{k_B T}} e^{\frac{E_F}{k_B T}} dp_y\, dp_z$$

$$= \left(\frac{2}{h^3}\right) dp_x \int_{-\infty}^{\infty} \int_{-\infty}^{\infty} e^{\frac{E_F}{k_B T}} e^{-\frac{p_x^2 + p_y^2 + p_z^2}{2mk_B T}} dp_y\, dp_z$$

$$= \left(\frac{2}{h^3}\right) dp_x e^{\frac{E_F}{k_B T}} e^{-\frac{p_x^2}{2mk_B T}} \int_{-\infty}^{\infty} e^{-\frac{p_y^2}{2mk_B T}} dp_y \int_{-\infty}^{\infty} e^{-\frac{p_z^2}{2mk_B T}} dp_z \qquad \textbf{(2.26)}$$

The integrals have the standard form of $\int_{-\infty}^{\infty} e^{-\alpha x^2} = \sqrt{\frac{\pi}{\alpha}}$

Thus, the **equation (2.26)** becomes

$$N(p_x)\,dx = \left(\frac{2}{h^3}\right) e^{\frac{E_F}{k_B T}} e^{-\frac{p_x^2}{2mk_B T}} dp_x \sqrt{2\pi m k_B T}\sqrt{2\pi m k_B T}$$

$$= \left[\frac{4\pi m k_B T}{h^3}\right] e^{\frac{E_F}{k_B T}} e^{-\frac{p_x^2}{2mk_B T}}\, dp_x$$

Substituting the above value in **equation (2.21)**

$$J = \frac{e}{m}\int_{p_{x_0}}^{\infty} \left[\frac{4\pi m k_B T}{h^3}\right] e^{\frac{E_F}{k_B T}} e^{-\frac{p_x^2}{2mk_B T}} p_x dp_x \qquad \textbf{(2.27)}$$

Substituting $(-\frac{p_x^2}{2m})$ from the **equation (2.20)**, we get,

$$J = \left(\frac{e}{m}\right)\left[\frac{4\pi m k_B T}{h^3}\right] \int e^{\frac{E_F}{k_B T}} e^{-\frac{E_F}{k_B T}} e^{-\frac{\phi_b}{k_B T}}\, m\, d\phi_b$$

$$J = \left(\frac{e}{m}\right)\left[\frac{4\pi m k_B T}{h^3}\right] m \int_{\phi_b}^{\infty} e^{-\frac{\phi_b}{k_B T}}\, d\phi_b$$

$$J = \left[\frac{4\pi e m k_B T}{h^3}\right] \left[-k_B T\, e^{-\frac{\phi_b}{k_B T}}\right]_{\phi_b}^{\infty}$$

$$J = \left[\frac{4\pi e m k_B^2 T^2}{h^3}\right] e^{-\frac{\phi_b}{k_B T}}$$

$$J = \left[\frac{4\pi e m k_B^2}{h^3}\right] T^2\, e^{-\frac{\phi_b}{k_B T}}$$

$$J = A^* T^2\, e^{-\frac{\phi_b}{k_B T}} \qquad \textbf{(2.28)}$$

Where, A* = effective Richardson constant.

Now, $J = \frac{I}{A}$

So, the **equation (2.28)** can be expressed as

$$I = AA^* T^2\, e^{-\frac{\phi_b}{k_B T}} \qquad \textbf{(2.29)}$$

The removal of electrons by an external electric field is not assumed in this theory. However, without electric field, a space - charge will exist at metal - semiconductor interface, reducing the device's current flow. Thus, external electric field is necessary to prevent the reduction in current. Potential energy barrier at interface is lowered during application of electric field, which increases flow of

current. Schottky effect is the term used to describe this increase in current flow and its dependency on the surrounding electric field **[35-37]**.

According to the R-S model, an electron from a metal can be infused after it has garnered sufficient thermal energy to overcome maximum potential caused by the superposition of the external electric field and the image charge potential **[38]**. This model can be used to describe and analyze the current flow at interface when junction of metal and organic material is formed. In the current thesis, we have used this model to analyze current flow in the prepared organic devices.

2.5.2 Drift-Diffusion Charge Injection Model

The drift-diffusion model of charge injection can be used to assess device's current flow where diffusion is the primary process for charge flow.

The Poisson's equation and the drift- diffusion equation are the two fundamental equations on which the drift - diffusion model is constructed.

Equation (2.30) and **equation (2.31)**, which are given below, show the Poisson's equation and the drift-diffusion equation, respectively, for positive charge carriers.

$$\frac{d^2V}{dx^2} = -\frac{dE}{dx} = -\frac{qp(x)}{\epsilon} \quad \textbf{(2.30)}$$

$$J = qp\mu E - qD\frac{dp}{dx} \quad \textbf{(2.31)}$$

In the equations above, V denotes for electric potential, E for electric field, p for positive charge carrier density, ϵ for semiconductor permittivity, J for current density, q for electron charge, μ for mobility, and D for diffusion coefficient **[39]**. Diffusion constant can also be written as $D = \frac{\mu kT}{q}$.

Schottky's diffusion theory is formulated by solving Poisson's equation and drift-diffusion equation, both of which are depicted in **equation (2.30)** and **equation (2.31)**, respectively.

$$E_v(x) = E_v(0) + \frac{q^2 N_A}{\varepsilon}\left(W_d x - \frac{x^2}{2}\right) \quad \textbf{(2.32)}$$

Where,

$$W_d = \sqrt{\frac{2\varepsilon}{qN_A}\left(V_d - V_a - \frac{kT}{q}\right)} \quad \textbf{(2.33)}$$

In the above equation, W_d is the space - charge layer width, N_A is dopant density, V_d is diffusion potential and V_a is applied potential.

The **equation (2.31)** is used to calculate current density, which is given in the **equation (2.34)** below.

$$J = \mu kT\left(\frac{p}{kT}\frac{dE_v}{dx} - \frac{dp}{dx}\right) \quad \textbf{(2.34)}$$

The integration of **equation (2.34)** is then done using the integrating factor $\exp\left(-E_v/kT\right)$.

$$J\int_0^{W_{sc}} \exp\left(-\frac{E_v}{kT}\right) dx = -\mu kT\left[p\exp\left(-\frac{E_v}{kT}\right)\right]_0^{W_{sc}} \quad \textbf{(2.35)}$$

The Fermi level of metal can be used as the reference energy to provide the boundary conditions.

$$E_v(0) = -E_{bp} \quad \textbf{(2.36)}$$

$$E_v(W_{sc}) = -E_p + q(V_d - V_a) \quad \textbf{(2.37)}$$

$$p(0) = N_v \exp\left(-\frac{E_{bp}}{kT}\right) \quad \textbf{(2.38)}$$

$$p(W_{sc}) = N_v \exp\left(-\frac{E_p}{kT}\right) \quad \textbf{(2.39)}$$

At the metal - semiconductor junction, E_{bp} is the height of hole barrier, and E_p is the difference in energy between Fermi level and the valence band edge of bulk of semiconductor. The valence band edge's effective state density is denoted by N_v.

When the aforementioned equations are combined, the current density can be stated as

$$J = J_d\left(\exp\frac{qV_a}{kT} - 1\right) \quad \textbf{(2.40)}$$

$$J_d = q\mu N_v F(0)\exp\left(-\frac{E_{bp}}{kT}\right) \quad \textbf{(2.41)}$$

F (0) = electric field at metal - organic contact at x = 0.

The metal-insulator-metal (MIM) model assumes that space - charge layer covers the whole semiconductor layer in an organic device since the dopant density and semiconductor thickness are too low. In such cases, constant electric field and equilibrium potential varies linearly with distance.

The valence band edge's variation is shown in **equation (2.42)**.

$$E_V(x) = E_V(0) - q(V_d - V_a)\frac{x}{d} \quad \textbf{(2.42)}$$

In this equation, d stands for the semiconductor's thickness, V_d for the difference in energy between work functions of two electrodes, and V_a for difference of voltage applied between anode and cathode.

Now that **equation (2.35)** has been integrated over whole semiconductor's thickness, then it becomes,

$$J = q\mu p_0 \frac{V_d - V_a}{d} \frac{\exp\left(qV_a/kT\right) - 1}{\exp\left(qV_d/kT\right) - \exp\left(qV_a/kT\right)} \quad \textbf{(2.43)}$$

Where, at the anode ($x = 0$), $p_0 = N_v \exp\left(-E_b^{an}/kT\right)$ is the density of hole and E_b^{an} is the injection hole barrier at anode.

The potential profile's form not changing with application of voltage is the underlying premise of **equation (2.43)**. **Equation (2.32)** illustrates that with a schottky diode, this condition is essentially true.

Mott first presented the SCLC model, a helpful approximation of drift- diffusion model. The diffusion component of the current is ignored in this model **[40]**. At higher applied voltages and when barrier at the interface is less than 0.3 eV, the SCLC regime is valid.

This study considers only the effect of ILC on the current injection mechanism and does not consider the effect of SCLC. If the height of barrier is more than 0.25-0.30 eV, it is known that current flow is injection limited in an organic device, and at lower barriers, charge flow is governed by SCLC **[41]**. Regardless of temperature and bias, the barrier height is the single factor that will determine the relative contributions of injection and space - charge effects to the observed I -V characteristics. We have only taken into account ILC because ϕ_b is greater than 0.30 eV. In this work, we have employed R-S thermionic emission model only to examine I -V characteristics of organic device.

2.5.3 Hopping Charge Injection Model

Related to Bässler's hopping transport model, Arkhipov formulated a hopping injection model for the M/O layer interface **[42]**,

$$J=ev_0 \int_a^{\infty} dx_0 \; w_{esc}(x_0) \exp(-2\gamma x_0) \int_{-\infty}^{\infty} dE \; Bol(E) g(U-E) \quad \textbf{(2.44)}$$

Where, e is charge of electron, v_0 is frequency of attempt-to-jump, a is the distance to the nearest-neighbor, γ is inverse localization radius, x_0 is distance of hopping, $w_{esc}(x_0)$ is probability of escape which is expressed in the **equation (2.45)**.

$$w_{esc}(x_0) = \frac{\int_a^{x_0} dx \exp\left[-\frac{e}{k_B T}\left(Fx + \frac{e}{16\pi\varepsilon_0\varepsilon x}\right)\right]}{\int_a^{\infty} dx \exp\left[-\frac{e}{k_B T}\left(Fx + \frac{e}{16\pi\varepsilon_0\varepsilon x}\right)\right]} \quad \textbf{(2.45)}$$

Bol (E) represents the jump rate's energy dependence.

$$Bol(E) = \begin{cases} 1 & E < 0 \\ \exp\left(-\frac{E}{k_B T}\right) & E > 0 \end{cases} \quad \textbf{(2.46)}$$

$$U(x) = \phi_b - \frac{e^2}{16\pi\varepsilon_0\varepsilon x} - eFx \quad \textbf{(2.47)}$$

The organic Gaussian DOS is g, which is shown in **equation (2.48)**

$$g(U-E) = \frac{N}{\sigma\sqrt{2\pi}} \exp\left(-\frac{U-E}{2\sigma^2}\right) \quad \textbf{(2.48)}$$

Where σ is Gaussian distribution's variance and N is total spatial density of localized intrinsic molecular orbital states.

2.5.4 Fowler-Nordheim Tunneling Model

Presence of LUMO and HOMO energy levels is linearly dependent on position inside the organic layer when the tunneling process is the main process of charge injection without localized states. Tunneling through a barrier of triangular shape at metal/organic interface, as shown in **Fig. 2.4**, allows charge carriers to be injected at the contact.

$$J = q \int_{-\infty}^{\infty} P(W)dW \quad \textbf{(2.49)}$$

Where, P (W) is equal to the equilibrium flux of electrons incident on the interface [N(W)] times the quantum mechanical probability that carrier passes through barrier [D(W)] under the assumption that carriers of metal continue to be in thermal equilibrium despite those that are tunneling from metal **[43]**.

The number N (W) is then

$$N(W) = \left[\frac{4\pi m k_B T}{h^3}\right] \ln\left[1 + \exp\left(-\frac{W-\mu}{k_B T}\right)\right] \quad \textbf{(2.50)}$$

Where, m is the effective mass, k_B is the Boltzmann constant, h is the Planck constant and μ is the metal's Fermi energy.

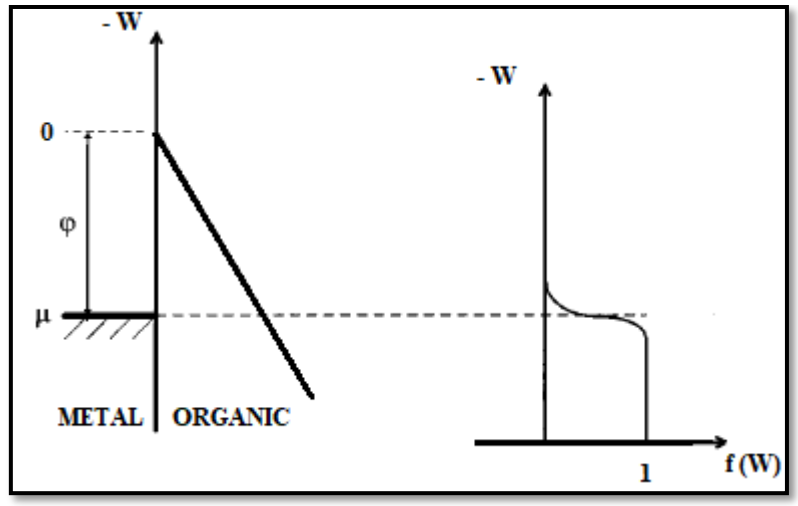

Fig. 2.4 At Temperatures Higher than 0 K, Band Scheme for Metal/Polymer Interface with Applied Field and Fermi–Dirac Distribution Function f (W)

In the Wentzel-Kramers-Brillouin (WKB) approximation, the tunneling probability for a triangular shaped barrier is

$$D(W) = \exp\left(\frac{-4(2m)^{1/2}|W|^{3/2}}{3Fq\hbar}\right) \quad \textbf{(2.51)}$$

Where, F is electric field and $\hbar = \frac{h}{2\pi}$.

Combining **equation (2.50)** and **equation (2.51)**, P (W) dW is obtained by **equation (2.52)**.

$$P(W)\,dW = \left[\frac{4\pi m k_B T}{h^3}\right]\exp\left(\frac{-4(2m)^{1/2}|W|^{3/2}}{3Fq\hbar}\right) \times \ln\left[1+\exp\left(-\frac{W-\mu}{k_B T}\right)\right]dW \quad \textbf{(2.52)}$$

The first two terms of a Taylor expansion around W = μ can be used to approximate the exponent in D (W), then **equation (2.52)** becomes

$$P(W)\,dW = \left[\frac{4\pi m k_B T}{h^3}\right]\exp\left(\frac{-4(2m)^{1/2}\phi_b^{3/2}}{3Fq\hbar}\right)\exp[\beta(W-\mu)] \times \ln\left[1+\exp\left(-\frac{W-\mu}{k_B T}\right)\right]dW \quad \textbf{(2.53)}$$

$$\beta = \frac{2(2m)^{1/2}\phi_b^{1/2}}{Fq\hbar} \quad \textbf{(2.54)}$$

The approximation in logarithmic function in **equation (2.53)** is to yield the Fowler-Nordheim theory. For $\phi_b/k_BT \gg 1$, this approximation is accurate. To obtain a more accurate description, the logarithmic function in **equation (2.53)** is integrated. The temperature dependency of the tunneling current is moderate, and according to **equation (2.49)** and **equation (2.53)** the tunneling current is

$$J(T) = q\left(\frac{4\pi m k_B^2 T^2}{h^3}\right)\exp\left(\frac{-4(2m)^{1/2}\phi_b^{3/2}}{3Fq\hbar}\right) \times \int_0^\infty \xi^{\beta k_B T-1}\ln\left(1+\frac{1}{\xi}\right)d\xi \quad \textbf{(2.55)}$$

Where, $\xi = \exp[(W-\mu)/k_B T]$.

Parts of integration in **equation (2.55)**, results in a standard form, which becomes

$$J(T) = \frac{q^2\pi k_B T}{h^2}\left(\frac{m}{2\phi_b}\right)^{1/2} F \times \exp\left(\frac{-4(2m)^{1/2}\phi_b^{3/2}}{3Fq\hbar}\right)\frac{1}{\sin(\beta\pi k_B T)} \quad \textbf{(2.56)}$$

The limit of applicability of **equation (2.56)** obtained keeping P (W) small in the energy interval $\mu < W < 10^6$. This presumption suggests that

$$\beta < \frac{1}{k_B T} - \frac{1}{\phi_b} \quad \textbf{(2.57)}$$

The dominant mode of current at M/O contact is thermionic emission if **equation (2.57)** is not satisfied.

2.6 Formation of Depletion Layer and Its Effect on Charge Injection Process

In thermal equilibrium, a portion of the organic semiconductor which is nearer to the M/O junction gets depleted of mobile charge carriers when no voltage is applied externally. Depletion region/ space - charge region (W_d) is the term given to this portion. The accumulation of density of ionized dopants and the density of trapped charges in localized states form net charge density in depletion zone **[44]**. Using the organic device's capacitance - voltage (C - V) characteristics, space - charge layer width can be estimated **[45]**. In our work, same technique has also been employed for the measurement of space - charge layer width. It has been estimated by the **equation (2.58)**.

$$W_d = \mp\sqrt{\frac{2\varepsilon_0\varepsilon_s V_d}{qN_D}} \qquad \textbf{(2.58)}$$

W_d = space - charge layer width, ε_0 = free space permittivity, ε_s = semiconductor permittivity, V_d = diffusion potential, q = charge of an electron, N_D = donor atoms concentration.

C^{-2} - V characteristics are used for measuring both diffusion potential and interfacial barrier. While estimating interfacial barrier from both the C - V and I -V techniques, there will be slight difference between these two processes as C - V method averages over entire region to measure barrier **[46]**. Susceptibility to traps can be attributed to these variations. Charge injection process at the junction considerably improves when depletion layer width decreases.

2.7 Different Nanoparticles and Nanotubes in Organic Devices and their Properties

We have prepared various organic dye based devices and we have also added different nanoparticles and nanotubes such as ZnO, TiO_2, SWCNT and MWCNT respectively in these prepared devices. These nanoparticles and nanotubes and their properties have been elucidated in the subsequent subsections.

2.7.1 Zinc Oxide (ZnO) Nanoparticles

Zinc Oxide (ZnO) is an inorganic material. It is white in colour at room temperature but when it is heated its colour become yellow. ZnO is not soluble in water **[47]**. ZnO can exist in three different crystal structures, which are wurzite, rocksalt and zinc blende. **Fig. 2.5** depicts the schematic representation of these crystal structures **[48-49]**. However, under ambient conditions, the wurzite structure is the only one that is thermodynamically stable.

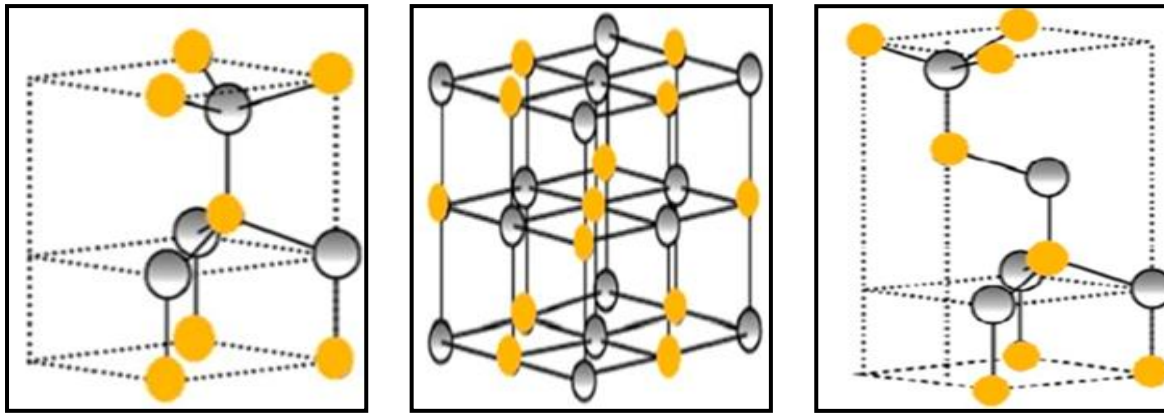

(a) **(b)** **(c)**

Fig. 2.5 Schematic Diagram of **(a)** Hexagonal Wurtzite, **(b)** Rock Salt and **(c)** Zinc Blende Structure of ZnO. Yellow and Grey Spheres denote O and Zn atoms

Wurtzite ZnO has a hexagonal structure and it has sp^3 covalent bonding with tetrahedral coordination **[50]**. Wurtzite ZnO is one of the most significant and successfully utilized materials at the nanoscale as it has a wide band gap and high excitonic energy **[51]**. Certain properties such as cost effectiveness, high electron mobility, good electron acceptor, and low crystalline temperatures make ZnO nanoparticles propitious inorganic metal oxides for use in organic devices **[52]**. Through reducing the charge recombination process and lengthening the active charge carrier lifetime, ZnO nanoparticles enhance the performance of organic devices **[53]**.

2.7.2 Titanium Dioxide (TiO_2) Nanoparticles

TiO_2 has many unique properties, subsuming non-toxicity, resistance to photochemical and chemical erosion and cost effectiveness. Owing to such advantages, TiO_2 finds utilization in self-cleaning surfaces, solar cells, chemical sensors, hydrogen gas evolution, pigments, and environmental purification **[54]**. The oxide nanoparticles created by various processes are becoming extremely valuable because of their better electrical, optical, and magnetic properties in comparison to their bulk equivalents **[55]**. Three main solid polymorphs of TiO_2 are anatase, rutile, and brookite, though it also exists in amorphous and crystalline forms **[56]**. **Fig. 2.6** displays a schematic representation of these three crystal structures of TiO_2 **[57].** TiO_2 thin films have been used in dye-sensitized solar cells (DSSC) due to its extensive surface area, interconnected pore networks, and capacity for significant dye adsorption. In the lab, Gratzel et al. have already obtained a conversion efficiency of 11% or more **[58]**. Utilizing electrodes with TiO_2 nanoparticles of superior properties can be used to improve stability and efficiency of DSSCs **[59]**. TiO_2 in its anatase form has been utilized in our research.

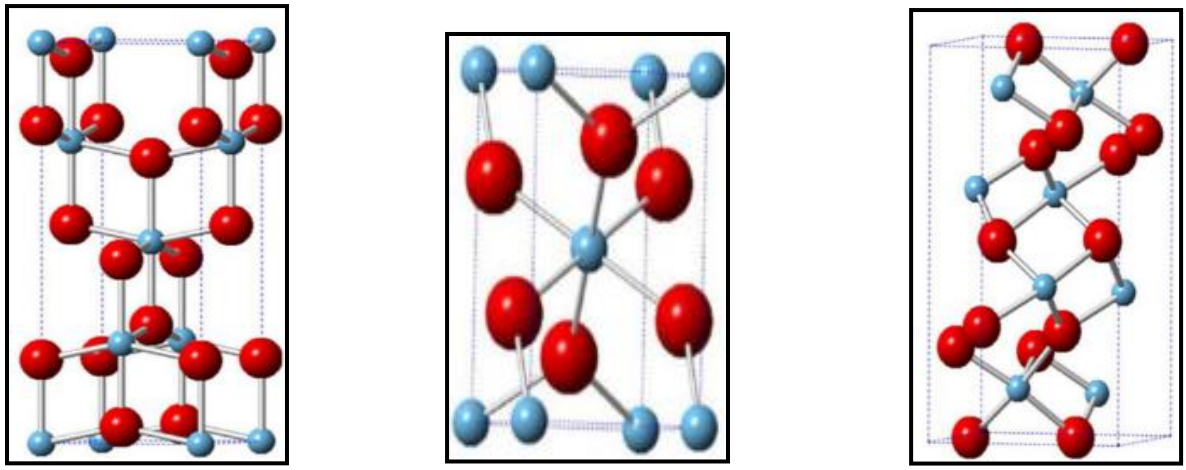

(a) **(b)** **(c)**

Fig. 2.6 Schematic Diagram of **(a)** Anatase, **(b)** Rutile and **(c)** Brookite Structure of TiO_2. Red and Blue Spheres denote O and Ti atoms.

2.7.3 Single Walled Carbon Nanotubes (SWCNT)

Carbon nanotubes (CNTs) have considerable researcher's attention, since its discovery in 1991 by Japanese scientist "Sumio Iijima" **[60]**. This is because of their distinctive physical, mechanical, and conductive qualities **[61]**. It is electrically very conductive, equivalent to copper (Cu). SWCNTs and MWCNTs are the two primary subtypes of CNTs. CNTs also belong to the group of one-dimensional (1D) nanostructures. SWCNTs are made up of a single layer of graphene that can take the form of a cylinder. **Fig. 2.7** displays the schematic diagram of SWCNT. They are varieties of the sp^2 hybridized carbon and similar to graphite, the structure produces hexagonal-shaped six-atom carbon rings. The SWCNTs typically have a tube thickness of just one atom and a circumference of only ten atoms. Nanotubes can be thought of as having a practically one-dimensional structure due to their typical enormous length-to-diameter ratio (aspect ratio) of roughly 1000 **[62]**. At very low temperatures, SWCNTs have numerous characteristics, such as Coulomb blockade and single-electron charging, that are similar to those of quantum dots and wires. Utilizing these and other phenomena, active electronic and optoelectronic devices of previously unheard-of size can be created **[63]**. SWCNTs typically have a diameter of less than 4 nm and a length of the micrometer order **[64-65]**. SWCNTs come in three various shapes, including armchair, chiral, and zigzag, depending on how the graphene sheet is rolled up into a cylindrical shape **[66]**.

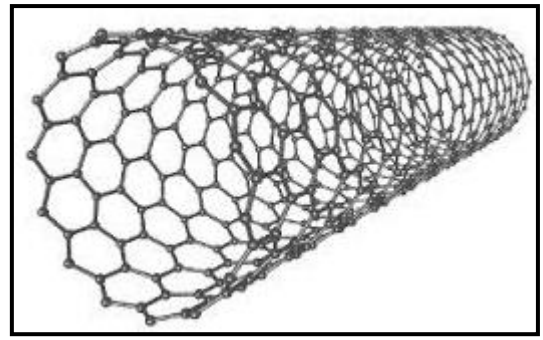

Fig. 2.7 Structural Diagram of Single Walled Carbon Nanotubes (SWCNT)

The various SWCNT forms are depicted in **Fig. 2.8**. A pair of indices (n, m) describes the chiral vector and they are used to describe the structure of SWCNT. The integers n and m determine the number of unit vectors in the hexagonal crystal lattice of graphene along two directions. Zigzag nanotubes are created when m = 0; when n = m, armchair nanotubes are created, and other states are referred to as chiral. The armchair form is often metallic, although alternative forms can turn nanotubes into semiconductors **[67]**.

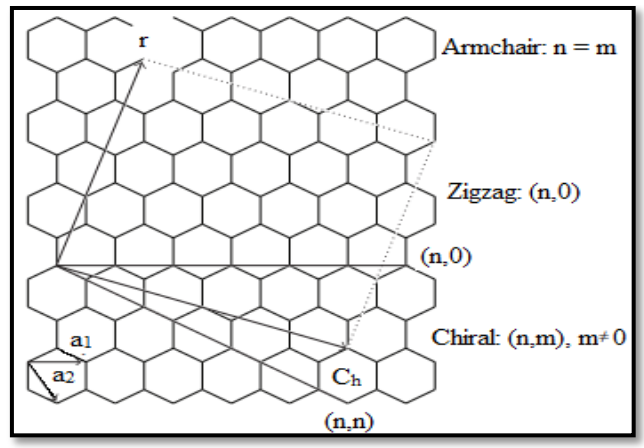

Fig. 2.8 Schematic Diagram of three different forms of Single Walled Carbon Nanotubes (SWCNT)

2.7.4 Multi Walled Carbon Nanotubes (MWCNT)

A few to a few tens of concentric cylinders spaced at regular intervals around a typical centre hollow make up MWCNTs. **Fig. 2.9** displays the schematic diagram of MWCNT.

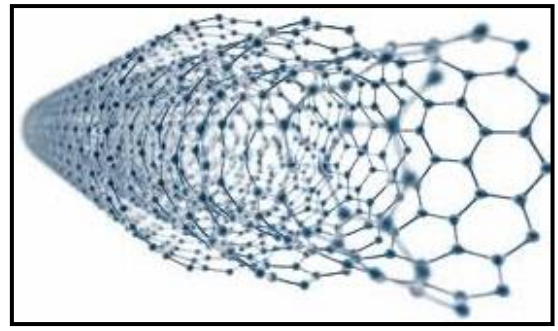

Fig. 2.9 Structural Diagram of Multi Walled Carbon Nanotubes (MWCNT)

The interlayer spacing of MWCNT ranges from 0.34 to 0.39 nm approximately. The MWCNT's inner and outer diameters range from 0.4 to a few nm and 2 to 30 nm, respectively **[68-69]**. The axial size of MWCNT varies from 1 µm to a few cm, and both tips are typically closed with pentagonal ring defects capping the ends. The tube can be closed at both ends due to a defect in the Pentagonal ring **[70]**. Due to their multilayer construction, MWCNTs have better tensile strengths than SWCNTs and their outside walls protect the inner carbon nanotubes from outside chemicals.

2.8 Conclusions

This chapter looks into the different parameters involved in the charge injection mechanism, such as trap concentration, interfacial barrier, depletion layer width, band bending, image force barrier lowering, and barrier inhomogeneities at the junction of metal and organic semiconductors, and then it investigates the effects of ZnO, TiO_2, SWCNT and MWCNT on these parameters. To understand and analyze these parameters, the basic working principle of organic devices, different charge injection models namely Richardson - Schottky Thermionic emission model, Drift-Diffusion charge injection model, Hopping charge injection model and Fowler-Nordheim tunneling model have been discussed in this present chapter. Trapping effect on charge carriers and exponential distribution of traps has also been discussed. The parameters that affect the charge carrier infusion process can be measured from steady state I -V characteristics and C - V characteristics. Certain properties of ZnO, TiO_2, SWCNT and MWCNT, which have been incorporated in different organic dye based devices, have also been studied.

In the following chapter, the junction barrier and band bending of PSF dye based devices will be elucidated, after which impact of ZnO and TiO_2 nanoparticles on both of these characteristics will be evaluated. Interrelationship between barrier potential and charge trapping will also be investigated.

Additionally, it will be predicted for PSF dye containing devices how varying TiO_2 nanoparticle concentrations affect barrier and charge entrapment.

2.9 References

[1] S. Antohe, S. Iftimie, L. Hrostea, V. A. Antohe and M. Girtan, "A critical review of photovoltaic cells based on organic monomeric and polymeric thin film heterojunctions", Thin Solid Films, 2017, **642**, 219-231

[2] A. Eatemadi, H. Daraee, H. Karimkhanloo, M. Kouhi, N. Zarghami, A. Akbarzadeh, M. Abasi, Y. Hanifehpour and S. W. Joo, "Carbon nanotubes: properties, synthesis, purification, and medical applications", Nanoscale Research Letters, 2014, **9**, 1-13

[3] N. Saifuddin, A. Z. Raziah, and A. R. Junizah, "Carbon Nanotubes: A Review on Structure and Their Interaction with Proteins", Journal of Chemistry, 2013, **2013**, 1-18

[4] H. Ishii, K. Sugiyama, E. Ito and K. Seki, "Energy level alignment and interfacial electronic structures at organic/metal and organic/organic interfaces", Advanced Materials, 1999, **11**, 605-625

[5] N. Koch and A. Kahn, "Conjugated organic molecules on metal versus polymer electrodes: Demonstration of a key energy level alignment mechanism", Applied Physics Letters, 2003, **82**, 70-72

[6] S. Braun, W. R. Salaneck and M. Fahlman, "Energy-Level Alignment at Organic/Metal and Organic/Organic Interfaces", Advanced Materials, 2009, **21**, 1450-1472

[7] C. Yi, X. Hu, X. Gong and A. Elzatahry, "Interfacial engineering for high performance organic photovoltaics", Materials Today, 2016, **19**, 169-177

[8] F. Gutman and L. E. Lyons, "Organic Semiconductors", 1967, [1st ed.], John Wiley & Sóns, New York, 776

[9] T. Kondo, "Current-voltage characteristics of organic semiconductors: interfacial control between organic layers and electrodes", 2007, [Doctoral Thesis, Georgia Institute of Technology], 20-22

[10] R. Schmechel, "Hopping transport in doped organic semiconductors: A theoretical approach and its application to p-doped zinc-phthalocyanine", Journal of Applied Physics, 2003, **93**, 4653-4660

[11] S. D. Baranovskii, H. Cordes, F. Hensel and G. Leising, "Charge-carrier transport in disordered organic solids", Physical Review B, 2000, **62**, 7934-7938

[12] N. von Malm, J. Steiger, R. Schmechel and H. von Seggern, "Trap engineering in organic hole transport materials", Journal of Applied Physics, 2001, **89**, 5559-5563

[13] P. D. Townsend and R. H. Friend, "Photoexcitation in Durham-route polyacetylene: Self-localization and charge transport", Physical Review B, 1989, **40**, 3112-3120

[14] H. F. Haneef, A. M. Zeidell and O. D. Jurchescu, "Charge carrier traps in organic semiconductors: a review on the underlying physics and impact on electronic devices", Journal of Materials Chemistry C, 2020, **8**, 759-787

[15] G. Horowitz, P. Lang, M. Mottaghi and H. Aubin, "Extracting Parameters from the Current–Voltage Characteristics of Organic Field-Effect Transistors", Advanced Functional Materials, 2004, **14**, 1069–1074

[16] M. C. J. M. Vissenberg and M. Matters, "Theory of the field-effect mobility in amorphous organic transistors", Physical Review B: Condensed Matter and Materials Physics, 1998, **57**, 12964 – 12967

[17] A. Salleo, "Organic Electronics", 2013, Wiley-VCH Verlag GmbH & Co. KGaA, Weinheim, Germany

[18] E. A. Silinsh, "Organic Molecular Crystals: Their electronic states", 1980, Springer Berlin Heidelberg, Berlin, Heidelberg

[19] E. A. Silinsh, "On the physical nature of traps in molecular crystals", Physica Status Solidi (A), 1970, **3**, 817–828

[20] A. Rose, "Space-Charge-Limited Currents in Solids", Physical Review, 1955, **97**, 1538–1544

[21] J. Sworakowski and K. Pigon, "Trap distribution and space-charge limited currents in organic crystals: Anthracene", Journal of Physics and Chemistry of Solids, 1969, **30**, 491–496

[22] Md. R. Islam, S. Maity, A. Haldar, N. B. Manik and A. N. Basu, "Photocurrent growth and decay behavior of crystal violet dye based photo electrochemical cell In photovoltaic mode", Ionics, 2012, **18**, 209-214

[23] M. G. Helander, Z. Wang and Z. H. Lu, "Electrode–Organic Interface Physics", 2016, In: Bhushan B. (eds) Encyclopedia of Nanotechnology. Springer, Dordrecht

[24] V. I. Arkhipov, H. von Seggern and E. V. Emelianova, "Charge injection versus space-charge-limited current inorganic light-emitting diodes", Applied Physics Letters, 2003, **83**, 5074–5076

[25] Ö. Güllü and A. Türüt, "Electrical Analysis of Organic dye-Based MIS Schottky Contacts", Microelectronic Engineering, 2010, **87**, 2482-2487

[26] H. Ishii, N. Hayashi, E. Ito, Y. Washizu, K. Sugi, Y. Kimura, M. Niwan, Y. Ouchi, and K. Seki, "Kelvin probe study of band bending at organic semiconductor/metal interfaces: examination of Fermi level alignment", Physica Status Solidi (A), Applied Research, 2004, **201**, 1075-1094

[27] Z. Zhang and J. T. Yates Jr., "Band Bending in Semiconductors: Chemical and Physical Consequences at Surfaces and Interfaces", Chemical Reviews, 2012, **112**, 5520–5551

[28] R. Nouchi, "Extraction of the Schottky parameters in metal-semiconductor-metal diodes from a single current-voltage measurement", Journal of Applied Physics, 2014, **116**, 184505-1-184505-6

[29] V. I. Arkhipov, U. Wolf and H. Bässler, "Current injection from a metal to a disordered hopping system. II. Comparison between analytic theory and simulation", Physical Review B, 1998, **59**, 7514 - 7520

[30] H. Bässler and A. Köhler, "Charge Transport in Organic Semiconductors", In: Metzger R. [eds.], Unimolecular and Supramolecular Electronics I. Topics in Current Chemistry, 2011, **312**, Springer, Berlin, Heidelberg

[31] Y. Miura, K. Hirose, K. Aizawa, N. Ikarashi and H. Okabayashi, "Schottky barrier inhomogeneity caused by grain boundaries in epitaxial Al film formed on Si (111)", Applied Physics Letters, 1992, **61**, 1057-1059

[32] S. Zhu, R. L. Van Meirhaeghe, C. Detavernier, F. Cardon, G. -P. Ru, X. -P. Qu and B. -Z. Li, "Barrier height inhomogeneities of epitaxial $CoSi_2$ Schottky contacts on n-Si (100) and (111)", Solid State Electronics, 2000, **44**, 663–671

[33] G. M. Vanalme, L. Goubert, R. L. Van Meirhaeghe, F. Cardon and P. Van Daele, "A ballistic electron emission microscopy study of barrier height inhomogeneities introduced in Au/III-V semiconductor Schottky barrier contacts by chemical pretreatments", Semiconductor Science and Technology, 1999, **14**, 871-877

[34] J. H. Werner and H. H. Güttler, "Barrier inhomogeneities at Schottky contacts", Journal of Applied Physics, 1991, **69**, 1522-1533

[35] A. Asherya, A. A. M. Farag, M. A. Moussad and G. M. Turky, "Enhancement of electrical and dielectrically performance of graphene-based promise electronic devices", Synthetic Metals, 2020, **261**, 1-10

[36] S. O. Pillai, "Solid State Physics- Structure and Electron Related Properties", 1994, [2nd ed.], Wiley Eastern Limited, New Delhi, 271-275

[37] N. A. Torkhov, "Effect of Photovoltage on Current Flow in Metal-Semiconductor Schottky-Barrier Contacts", Semiconductors, 2011, **45**, 935-943

[38] Z. Chiguvare, J. Parisi, and V. Dyakonov, "Current limiting mechanisms in indium-tin-oxide/poly3-hexylthiophene/ aluminum thin film devices", Journal of Applied Physics, 2003, **94**, 2440-2448

[39] G. Horowitz, "Drift-diffusion current in organic diodes", Condensed Matter- Mesoscale and Nanoscale Physics, 2017, **1702**, 1-11

[40] N. F. Mott and R. W. Gurney, "Electronic processes in ionic crystals", 1940, [2nd ed.], Oxford, Clarendon Press, 168-169

[41] T. V. Woudenbergh, "Charge Injection into Organic Semiconductors", 2005, [Doctoral Thesis, University of Groningen], 9-12

[42] H. Bässler, "Charge transport in disordered organic photoconductors: a Monte carlo simulation study", Physica Status Solidi. B. Basic research, 1993, **175**, 15-56

[43] M. Koehler and I. A. Hümmelgen, "Temperature dependent tunnelling current at metal/polymer interfaces—potential barrier height determination", Applied Physics Letters, 1997, **70**, 3254- 3256

[44] E. H. Rhoderick and R. H. Williams, "Metal-Semiconductor Contacts", 1988, [2nd ed.], Oxford, Clarendon Press, 226–231

[45] N. Li, X. D. Gao, B. F. Ding, X. Y. Sun, X. M. Ding and X. Y. Hou, "Determination of capacitance-voltage characteristics of organic semiconductor devices by combined current-voltage and voltage decay measurements", Science China Technological Sciences, 2011, **54**, 826-829

[46] Ö. Güllü, "Barrier Modification by Methyl Violet Organic Dye Molecules of Ag/P-Inp Structures", European Journal of Interdisciplinary Studies, 2016, **2**, 7-17

[47] S. Sabir, M. Arshad and S. K. Chaudhari, "Zinc Oxide Nanoparticles for Revolutionizing Agriculture: Synthesis and Applications", The Scientific World Journal, 2014, **2014**, 1-8

[48] P. J. P. Espitia, N. F. F. Soares, J. S. R. Coimbra, N. J. Andrade, R. S. Cruz and E. A. A. Medeiros, "Zinc Oxide Nanoparticles: Synthesis, Antimicrobial Activity and Food Packaging Applications", Food and Bioprocess Technology, 2012, **5**, 1447–1464

[49] M. Zare, K. Namratha, S. Ilyas, A. Sultana, A. Hezam, M. A. Surmeneva and K. Byrappa, "Emerging Trends for ZnO Nanoparticles and Their Applications in Food Packaging", ACS Food Science & Technology, 2022, **2**, 763-781

[50] K. Nomura, H. Ohta, K. Ueda, T. Kamiya, M. Hirano and H. Hosono, "Thin-film transistor fabricated in single-crystalline transparent oxide semiconductor", Science, 2003, **300**, 1269–1272

[51] X. Wang, Y. Ding, C. J. Summers, and Z. L. Wang, "Large scale synthesis of six-nanometer-wide ZnO nanobelts", Journal of Physical Chemistry B, 2004, **108**, 8773–8777

[52] S. Saravanan, Y. A. M. Ismail, M. Silambarasan, N. Kishi and T. Soga, "ZnO nanoparticles with different concentrations inside organic solar cell active layer", Advances in Energy Research, 2016, **4**, 275-284

[53] A. Wibowo, M. A. Marsudi, M. I. Amal, M. B. Ananda, R. Stephanie, H. Ardy and L. J. Diguna, "ZnO nanostructured materials for emerging solar cell applications", RSC Advances, 2020, **10**, 42838-42859

[54] M. R. Hoffmann, S. T. Martin, W. Choi and D. W. Bahnemann, "Environmental Applications of Semiconductor Photocatalysis", Chemical Reviews, 1995, **95**, 69-96

[55] H. Xu, X .Wang and L. Zhang, "Selective preparation of nanorods and micro-octahedrons of Fe_2O_3 and their catalytic performances for Thermal decomposition of ammonium perchlorate", Powder Technology, 2008, **185**, 176-180

[56] S. Mahshid, M. Askari, and M. S. Ghamsari, "Synthesis of TiO_2 nanoparticles by hydrolysis and peptization of titanium isopropoxide Solution", Journal of Materials Processing Technology, 2007, **189**, 296-300

[57] A. H. Navidpour, S. Abbasi, D. Li, A. Mojiri and J. L. Zhou, "Investigation of Advanced Oxidation Process in the Presence of TiO_2 Semiconductor as Photocatalyst: Property, Principle, Kinetic Analysis, and Photocatalytic Activity", Catalysts, 2023, **13**, 1-29

[58] M. Grätzel, "Conversion of sunlight to electric power by nanocrystalline dye-sensitized solar cells", Journal of Photochemistry and Photobiology A: Chemistry, 2004, **164**, 3-14

[59] A. Hagfeldt and M. Grätzel, "Molecular photovoltaics", Accounts of Chemical Research, 2000, **33**, 269-277

[60] S. Iijima, "Helical microtubules of graphitic carbon", Nature, 1991, **354**, 56-58

[61] S. M. Fatemi and M. Foroutan, "Review on carbon nanotubes and carbon nanotube bundles for gas/ion separation and water purification studied by molecular dynamics simulation", International Journal of Environmental Science and Technology, 2016, **13**, 457-470

[62] J. Pitroda, B. Jethwa and S. K. Dave, "A Critical Review on Carbon Nanotubes", International Journal of Constructive Research in Civil Engineering, 2016, **2**, 36-42

[63] J. E. Fischer and A. T. Johnson, "Electronic properties of carbon nanotubes", Current Opinion in Solid State and Materials Science, 1999, **4**, 28-33

[64] L. Chico, V. H. Crespi, L. X. Benedict, S. G. Louie and M. L. Cohen, "Pure Carbon Nanoscale Devices: Nanotube Heterojunctions", Physical Review Letters,1996, **9**, 971–974

[65] S. Paliwal, K. Pandey, S. Pawar, H. Joshi and N. Bisht, "A Review on Carbon Nanotubes: As a Nano carrier Drug Delivery System", Indian Journal of Pharmaceutical Sciences, 2020, **82**, 766-772

[66] E. T. Thostenson, Z. Ren and T.W. Chou, "Advances in the science and technology of carbon nanotubes and their composites: a review", Composites Science and Technology, 2001, **61**, 1899–1912

[67] A. Aqel, K. M. M. Abou El-Nour, R. A. A. Ammar and A. Al-Warthan, "Carbon nanotubes, science and technology part (I) structure, synthesis and characterization", Arabian Journal of Chemistry, 2012, **5**, 1-23

[68] P. M. Ajayan and T. W. Ebbesen, "Nanometre-size tubes of carbon", Reports on Progress in Physics, 1997, **60**, 1025-1062

[69] O. V. Kharissova and B. I. Kharisov, "Variations of interlayer spacing in carbon nanotubes", RSC Advances, 2014, **4**, 30807-30815

[70] J. O. Min, S. Y. Kim, U. S. Shin, and B. E. Yoon, "Multi-walled carbon nanotubes change morpho-functional and GABA characteristics of mouse cortical astrocytes", Journal of Nanobiotechnology, 2015, **13**, 1-10

Chapter 3

Effect of Different Nanoparticles on Barrier Potential, Band Bending and Charge Trapping of Phenosafranin (PSF) Dye Based Device

3.1 Introduction

In earlier chapter, the basic operating principle of organic devices, various charge injection models, and factors like trap concentration, interfacial barrier height, depletion layer width, band bending, image force barrier, and barrier inhomogeneities that influence the charge infusion process had been mentioned. Earlier chapter also elucidated the characteristics of various nanoparticles that will be used in these various organic dye based devices.

Present chapter will investigate barrier potential and charge trapping behaviour of organic device based on the dye Phenosafranin (PSF), and then we will look at the impact of Zinc Oxide (ZnO) and Titanium Dioxide (TiO_2) nanoparticles on these parameters. We all know that the charge flow at M/O contact, which occurs when an organic dye is sandwiched between two metal electrodes with various work functions, has a significant impact on the performance of organic electronic devices. Interfacial band bending is crucial in this situation for realizing the function of organic devices or for enhancing device performance. It has been demonstrated that the interfacial band bending at the metal - inorganic semiconductor junction influences several electronic characteristics for inorganic device constructions **[1-2]**. However, little research has been done on how nanoparticles affect junction barrier and bending of bands at M/O interface. In this chapter, we will also look at the interfacial band bending effect when TiO_2 and ZnO nanoparticles are present. The device's performance may be impacted by the organic or metal electrode contacts **[3]**. To obtain desirable electrical parameters, such as a reduction in high barrier height (ϕ_b) and trap concentration (E_t) at M/O interface, optimal customization of band bending is necessary. Poor charge transfer from metal to organic layer is caused by high barrier height. Charge infusion is very much reliant on barrier height, which may also result in greater threshold voltage (V_{th}). In this chapter, we will change the TiO_2 nanoparticles concentration while keeping the PSF dye concentration constant to study the effects of various nanoparticle concentrations. The trap distribution will also be shown on a G (V) - V plot.

The difference between fermi energy levels of metal and organic material's energy band is what is responsible for the barrier potential **[4]**. Charge infusion of constructed device is examined using R-S model of thermionic emission.

According to theoretical calculations, current is injection limited when contact barrier is larger than 0.3 eV **[5]**. As, contact barrier was determined to be more than 0.3 eV in our research, we have deemed the current flow to be injection-limited.

3.2 Experimental Details with the Incorporation of ZnO and TiO_2 nanoparticles

This section will describe barrier and interfacial band bending at M/O contact and effect of ZnO and TiO_2 nanoparticles on these parameters will also be studied.

3.2.1 Materials and Sample Preparation

PSF dye is an example of cationic dye of phenazinium group of chemicals, which is purchased from Sigma Aldrich in Germany and is depicted in **Fig. 3.1 (a)**. Molecular weight of it is 322.79 g/mol. $C_{18}H_{15}ClN_4$ is the empirical formula for it. The use of phenazinium dyes in semiconductors is widespread **[6]**. It is also utilized in numerous photochemical biological applications. Due to its electrical, mechanical, and optical capabilities, ZnO nanoparticles have been investigated throughout the past few decades **[7-9]**. ZnO nanoparticles can be used in photocatalysts, dye-sensitized solar cells, ultra violet photodetectors, gas sensors, dye-sensitized solar cells, and more **[10-13]**. TiO_2 nanoparticles have also a wide range of uses in photocatalysis, solar cells, and in the treatment of environmental pollution because they are widely accessible, affordable, and low hazardous, and we have exploited this nanoparticle in its anatase form **[14-17]**. Both nanoparticles are 100 nm in size and are imported from Sigma-Aldrich in Germany. ZnO nanoparticles and TiO_2 nanoparticles have molecular weights of 81.37 g/mol and 79.90 g/mol, respectively. **Fig. 3.1 (b)** and **Fig. 3.1 (c)** show the structural visualization of ZnO and TiO_2, respectively.

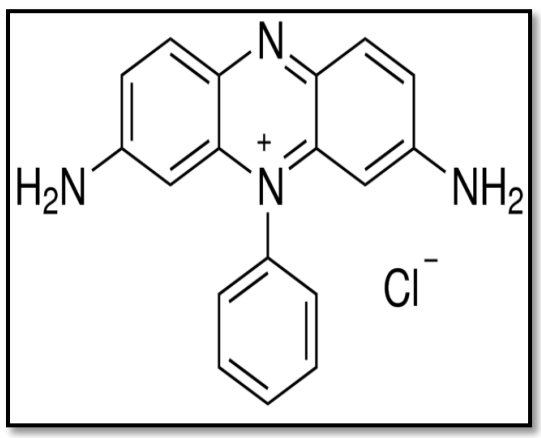

(a)

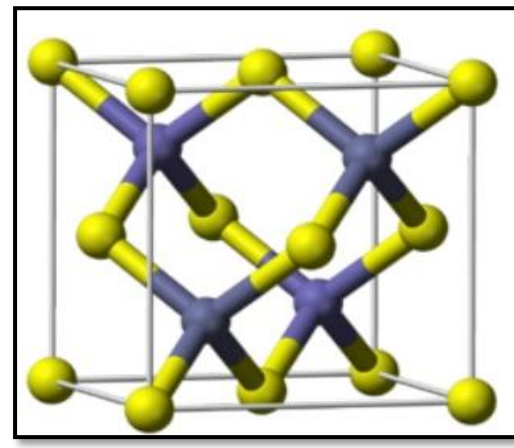

(b)

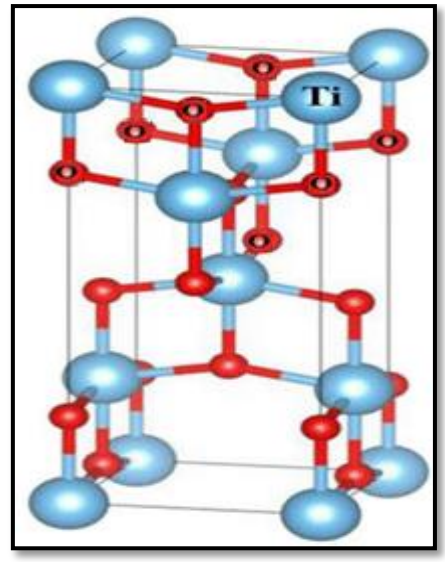

(c)

Fig. 3.1 Structural Visualization of **(a)** PSF dye, **(b)** ZnO and **(c)** TiO_2

15 mL of distilled water have been poured into a clean beaker. Then, 3 mg of highly viscous Poly Vinyl Alcohol (PVA) have been added, and the mixture has been swirled for 30 minutes at 70^0C using a magnetic stirrer. PVA is bought from S. D. Fine Chem. Ltd. in Boisar, India. To create a solution that resembles gel, PVA serves as a transparent inert binder. PVA's molecular weight is nearly 125000. To bind the dye solution to the electrodes, PVA is utilized. 2 mg PSF dye is added to PVA solution, and the mixture is swirled once more for an additional 10 minutes. In three test tubes that have already been cleaned, this solution is then split into three equal portions. One test tube contains PSF solution without nanoparticles. To make solution which contains PSF dye with ZnO nanoparticles and PSF dye with TiO_2 nanoparticles, other two test tubes contain 2 mg of ZnO nanoparticles and 2 mg of TiO_2 nanoparticles respectively along with 2 mg of PSF dye.

PSF dye solution is spin coated on a pre-cleaned ITO coated glass at 1000 rpm speed and it is then dried at 3000 rpm speed. An Al electrode undergoes spin coating of the same solution. The PSF cell is formed by sandwiching these two electrodes together. To make PSF cells with ZnO and TiO_2 nanoparticles, PSF solutions with both the nanoparticles are also spin coated separately. These cells are dried in vacuum for 12 hours before being characterized **[18]**. The prepared device's schematic is depicted in **Fig. 3.2**.

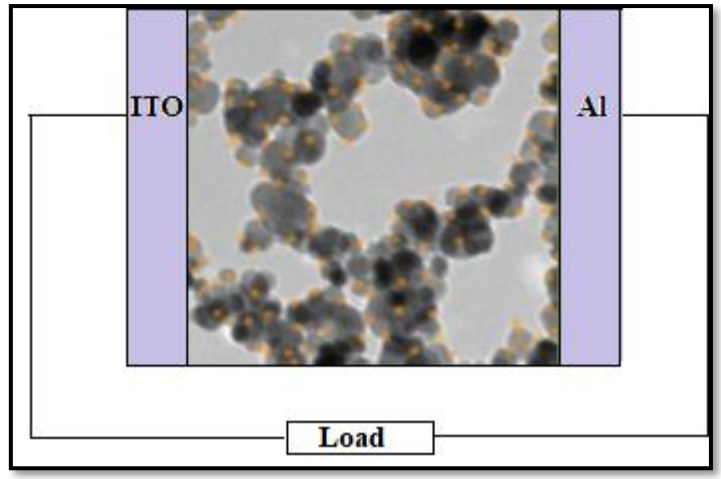

Fig. 3.2 Schematic Diagram of a Sandwich Type Organic Device with Nanoparticles

Fig. 3.3 (a) shows different chemicals of our laboratory. **Fig. 3.3 (b)**, **Fig. 3.3 (c) and Fig. 3.3 (d)** show spin coater, weighing machine and Keithley 2400 source meter respectively, which we have used in our laboratory.

(a)

(b)

(c)

(d)

Fig. 3.3 (a) Different Chemicals in our laboratory, **(b)** Spin Coater, **(c)** Weighing Machine and **(d)** Keithley 2400 source meter of our laboratory

3.2.2 Measurements

SEM images are useful for finding out how the nanoparticles are positioned in the active substance. **Fig. 3.4 (a)** and **Fig. 3.4 (b)** in this study exhibit SEM images for PSF with ZnO cell and PSF with TiO_2 cell correspondingly. A JSM-6700F is used for SEM analysis. The two cells' I -V properties are measured using Keithley 2400 source measuring unit. The positive and negative terminals of battery are linked to ITO and Al electrodes, respectively. With a delay of 1500 ms, the applied voltage is tuned from 0 to 6 V in intervals of 0.5 V. Room temperature is kept at 25^0C throughout the experiment **[19]**.

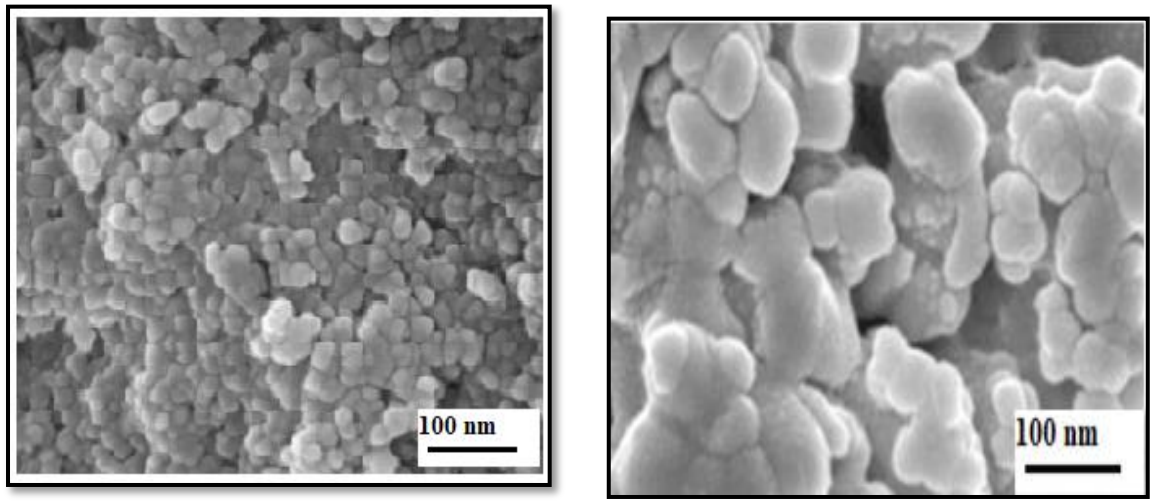

(a) **(b)**

Fig. 3.4 SEM images of **(a)** PSF + ZnO cell and **(b)** PSF + TiO_2 cell respectively

3.2.3 Results and Discussions

Both of these organic devices' current-voltage (I -V) properties are consistent with the thermionic emission theory. The following **equation (3.1)** to **equation (3.3)** can be used to describe the interfacial flow of current.

$$I = AA^{*}T^{2} \exp\left(-\frac{q\phi_b}{kT}\right)\left(\exp\left(\frac{qV}{nkT}\right) - 1\right) \quad \textbf{(3.1)}$$

The above **equation (3.1)** can also be rewritten as

$$I = I_0(\exp(\frac{qV}{nkT}) - 1) \quad \textbf{(3.2)}$$

Where I_0 is given in following **equation (3.3)**

$$I_0 = AA^*T^2 \exp(-\frac{q\phi_b}{kT}) \quad \textbf{(3.3)}$$

The meaning of the given symbols is conventional **[20 -24]**. ϕ_b is derived from extrapolation of I_0 from ln I -V plot. From **equation (3.4)**, ϕ_b is calculated and the **equation (3.4)** has been deduced from the **equation (3.3) [25-27]**

$$\phi_b = \frac{kT}{q}\ln\left(\frac{AA^*T^2}{I_0}\right) \quad \textbf{(3.4)}$$

Fig. 3.5 (a) and **Fig. 3.5 (b)** depict I -V plots of device without and with ZnO and TiO_2 nanoparticles, respectively. Inclusion of both nanoparticles improves the current flow. With ZnO nanoparticles and TiO_2 nanoparticles, the magnitude of current has almost multiplied by three and four times, respectively. The process of filling the trap can also be responsible for this increase in current.

To obtain ϕ_b, ln I -V plots of device without and with ZnO and TiO_2 nanoparticles have been illustrated in **Fig. 3.6 (a)** and **Fig. 3.6 (b)** respectively. For V > kT/ q, extrapolated intercept at V = 0 axis gives I_0. By putting the value of I_0 in **equation (3.4)**, ϕ_b has been calculated.

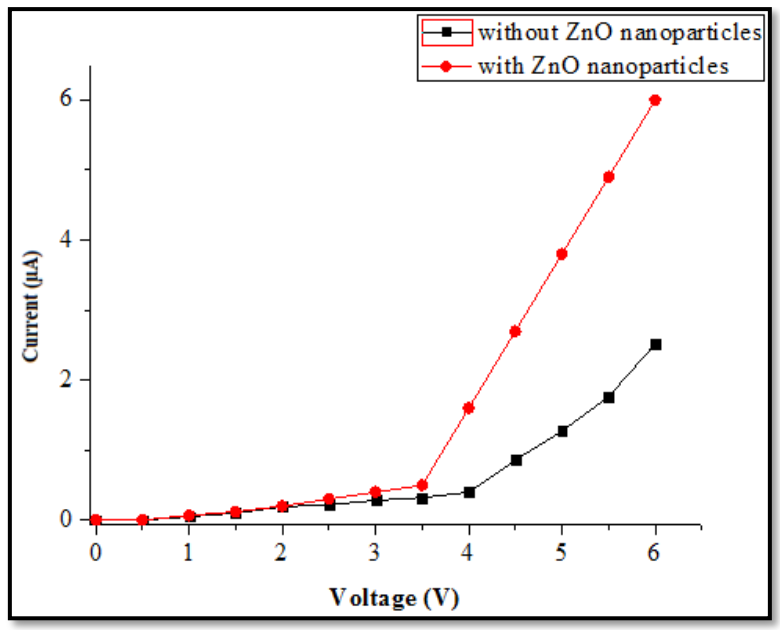

(a)

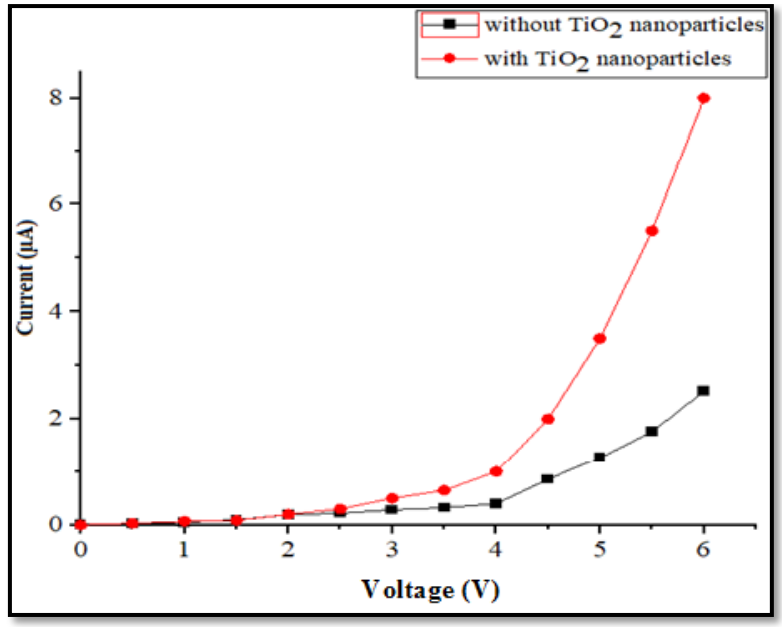

(b)

Fig. 3.5 I -V plots of device **(a)** without and with ZnO nanoparticles and **(b)** without and with TiO_2 nanoparticles

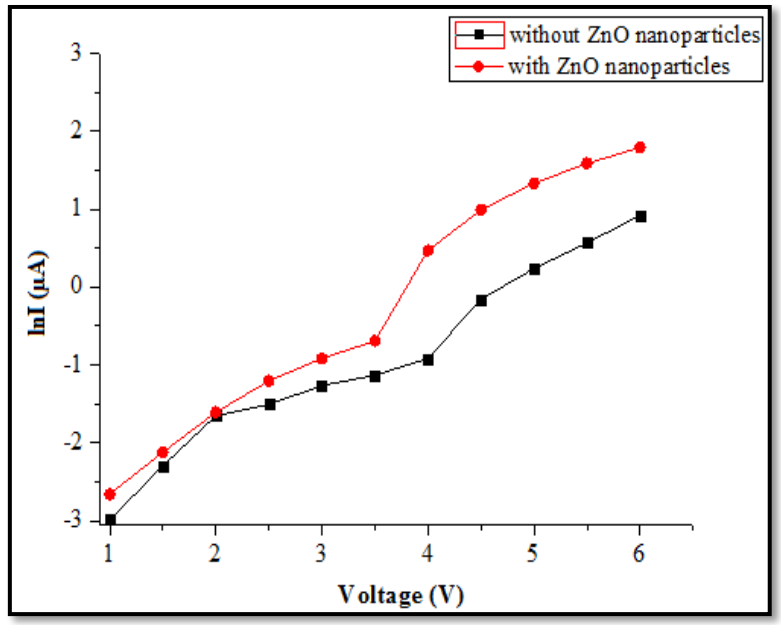

(a)

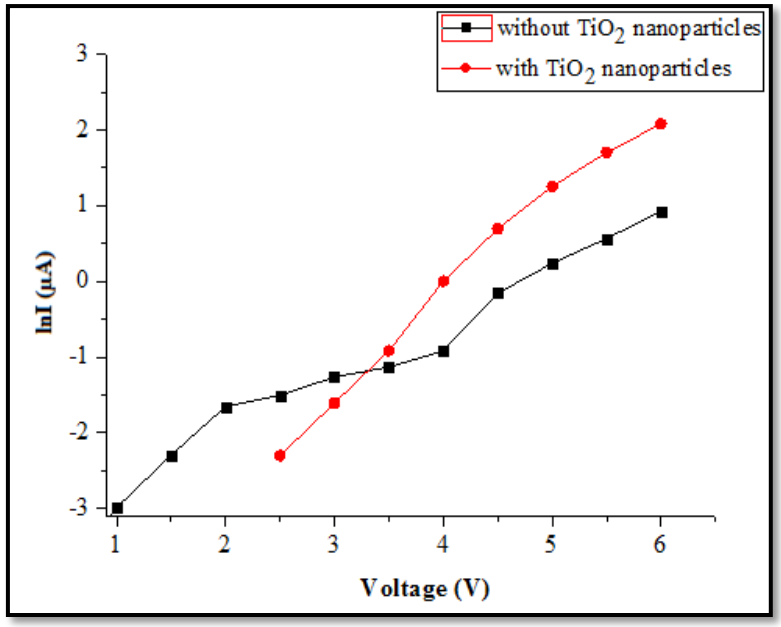

(b)

Fig. 3.6 ln I -V plots of device **(a)** without and with ZnO nanoparticles and **(b)** without and with TiO_2 nanoparticles

Fig. 3.6 (a) and **Fig. 3.6 (b)**, indicate that with ZnO and TiO_2 nanoparticles, the barrier potential lessens as the value of I_0 increases as shown in **equation (3.4)**.

Barrier at M/O contact is also estimated by using Norde's function. **Equation (3.5)** expresses the Norde's function, where I (V) is determined from device's I-V characteristics **[28]**.

$$F(V) = \left(\frac{V}{X}\right) - \frac{kT}{q}\ln\left(\frac{I(V)}{AA^{*}T^{2}}\right) \quad \textbf{(3.5)}$$

X is the first integer greater than n. I (V_0) corresponding to minimum value of F (V_0), where V_0 is the corresponding voltage **[29-30]**.

By calculating the derivative of **equation (3.5)** with respect to V and putting $\frac{dF(V)}{dV} = 0$. V_0 is expressed as

$$V_0 = \frac{kT}{q} + \ln\left(\frac{I_0}{AA^{*}T^{2}}\right) \quad \textbf{(3.6)}$$

and **equation (3.7)** shows the minimum value of F (V)

$$F(V_0) = \frac{V_0}{X} - \frac{kT}{q}\left(\frac{I_0}{AA^{*}T^{2}}\right) \quad \textbf{(3.7)}$$

In **Fig. 3.7 (a)** and **Fig. 3.7 (b)**, for the organic device structure, without and with ZnO and TiO_2 nanoparticles respectively, the barrier ϕ_b has been estimated by **equation (3.8)**.

$$\phi_b = F(V_0) + \frac{V_0}{X} - \frac{kT}{q} \qquad \textbf{(3.8)}$$

Both **Fig. 3.7 (a)** and **Fig. 3.7 (b)** of Norde's function plots depict barrier lowering with ZnO and TiO_2 nanoparticles. Lessening of contact barrier is also consistent with estimation of barrier derived from device's steady state I -V characteristics.

M/O contact entirely controls band bending process in organic device. Schematic visualization of bending of bands is depicted in **Fig. 3.8**. Charge transfer occurs due to interaction between HOMO and LUMO based on frontier molecular orbital (FMO) theory of chemical reactivity **[31]**.

Equation (3.9) can be used to calculate the amount of bands bend at the contact area.

$$n_{if} = \left[1 - \frac{\delta\phi_{if}^{0}}{4q|V_i^0|}\right]^{-1} \qquad \textbf{(3.9)}$$

Where, n_{if} = ideality factor and $q|V_i^0|$ = zero – bias band bending, $\delta\phi_{if}^{0}$ = image barrier lowering **[32]**.

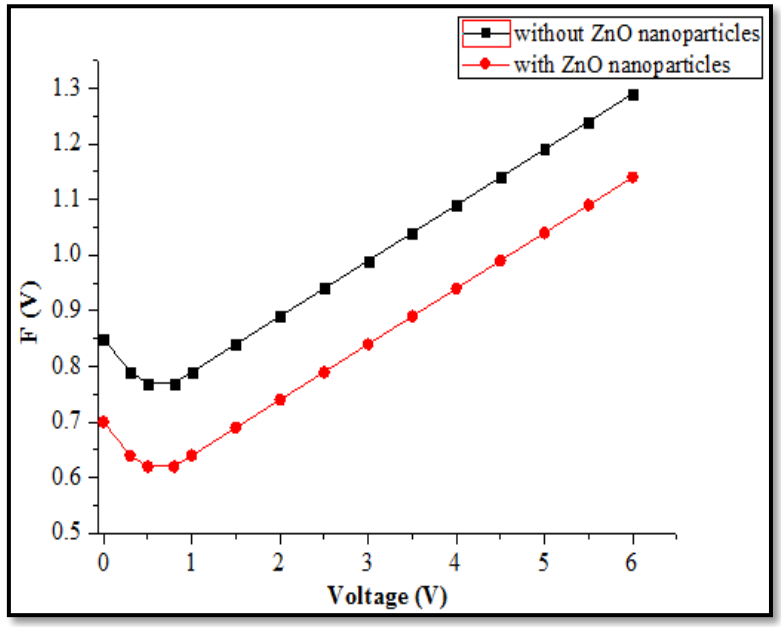

(a)

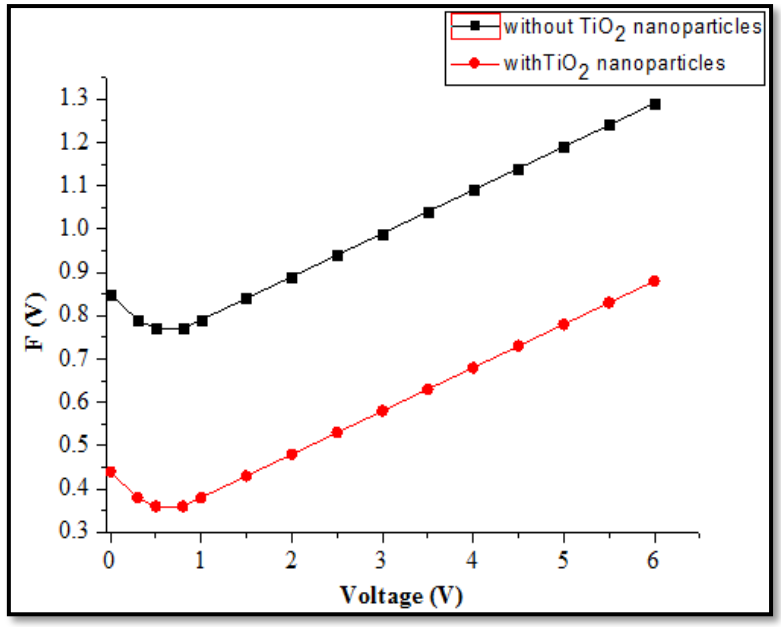

(b)

Fig. 3.7 Norde Function plots of device **(a)** without and with ZnO nanoparticles and **(b)** without and with TiO_2 nanoparticles

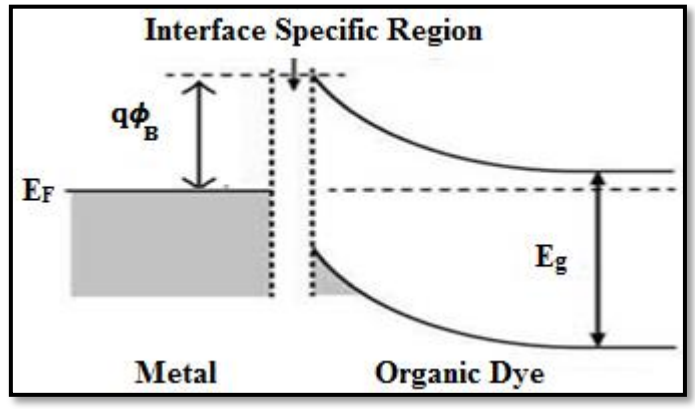

Fig. 3.8 Schematic diagram of bending of bands at M/O contact

The values of threshold voltage, barrier potential and band bending of devices without any nanoparticles, with ZnO and TiO_2 nanoparticles are shown in **Table 3.1**.

It can be seen from **Table 3.1** that TiO_2 nanoparticles enhance device performance more than ZnO nanoparticles do. That can be explained by TiO_2 nanoparticles' higher porosity when compared to ZnO nanoparticles. Because of the high porosity, the TiO_2 nanoparticles is the recipient of more

injected electrons and provides better conductive pathway from the site of electron injection to the collecting electrode compared to ZnO nanoparticles.

Table 3.1 Calculation of threshold voltage, barrier potential and band bending of PSF dye based devices without and with ZnO nanoparticles and TiO_2 nanoparticles

PSF dye based devices	Threshold Voltage (V)	Barrier Potential from I -V characteristics (eV)	Barrier Potential using Norde's Function (eV)	Band Bending (eV)
Without nanoparticle	4.000	0.810	0.830	0.218
With ZnO nanoparticles	3.500	0.670	0.690	0.183
With TiO_2 nanoparticles	2.500	0.440	0.470	0.153

3.3 Experimental Details with Variation of Different Concentration of TiO_2 nanoparticles

In this section, we will look at how varied TiO_2 nanoparticle concentrations affect junction barrier of PSF dye based organic devices. Also, we will try to correlate organic device's barrier potential and charge entrapment.

3.3.1 Materials and Sample Preparation

First, a PSF dye solution devoid of any nanoparticle is formed. We have discussed the procedure for creating PVA solutions in **section 3.2.1**. The solution is now given a 2 mg PSF addition, and it is swirled for 10 minutes. This solution's one part is set aside in a test tube that has already been cleaned. Afterwards 2 mg of TiO_2 nanoparticles are added and well mixed into the remaining PSF dye solution. We keep this PSF: TiO_2 = 1:1 solution apart. To make the ratio 1:2, 4 mg of TiO_2 is added to solution which contains 2 mg of PSF. Similar to this, higher TiO_2 concentrations are used to create PSF: TiO_2 solutions, which are 1: 3 and 1: 4. PSF solution without any nanoparticle is spin coated at

1500 rpm speed and dried at 3500 rpm speed over a glass substrate that has been previously cleaned and coated with ITO. Similar to this, the solution is applied to Al, and the cell is created by sandwiching ITO-coated glass and Al. This cell is vacuum dried for 12 hours, together with other cells composed of different ratios of TiO_2 nanoparticles. The other four cells have PSF: TiO_2 ratios of 1:1, 1:2, 1:3, and 1:4.

3.3.2 Measurements

The same measurement method as described in **section 3.2.2** is used. With a delay of 1000 ms, the voltage ranges from 0 to 6 V in steps of 0.5 V. A 25^0C ambient temperature is maintained throughout experiment.

3.3.3 Results and Discussions

In **Fig. 3.9**, I -V curves of a device with various TiO_2 nanoparticle concentrations and one without any nanoparticle is displayed.

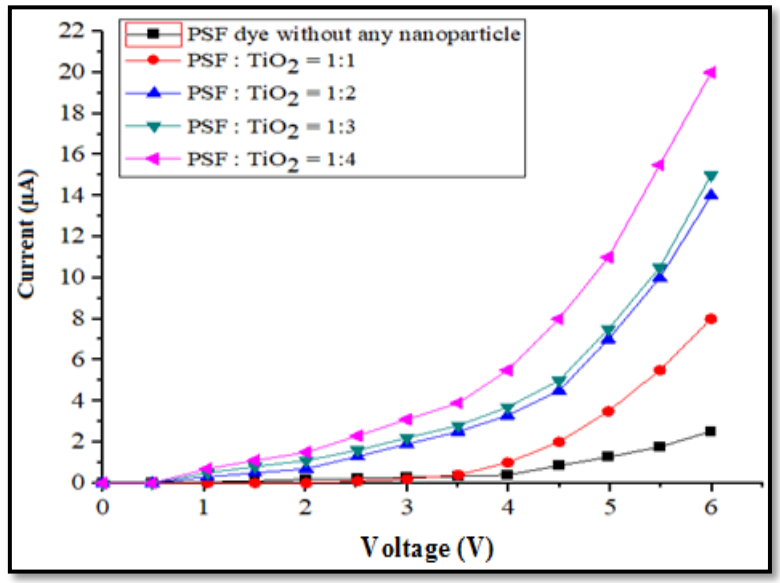

Fig. 3.9 I -V plots of device without any nanoparticle and with different concentrations of TiO_2 nanoparticles

According to **Fig. 3.9**, current gets better as the concentration of TiO_2 nanoparticles rises. Current flow in device is highest when PSF and TiO_2 concentration ratio is 1:4. I -V plots indicate that the charge infusion improves with nanoparticles, which may be associated to trap filling. Traps function

as recombination centres as well. When TiO_2 nanoparticles are present, charge flow is enhanced by filling the traps, which also lowers the barrier at interface.

Junction barrier is calculated using ln I -V plot, as illustrated in **Fig. 3.10**. This graph demonstrates how the barrier is decreased with the addition of TiO_2 nanoparticles. For this device, barrier is highest when it is devoid of nanoparticle and it is lowest when ratio of PSF dye to TiO_2 nanoparticles is 1:4.

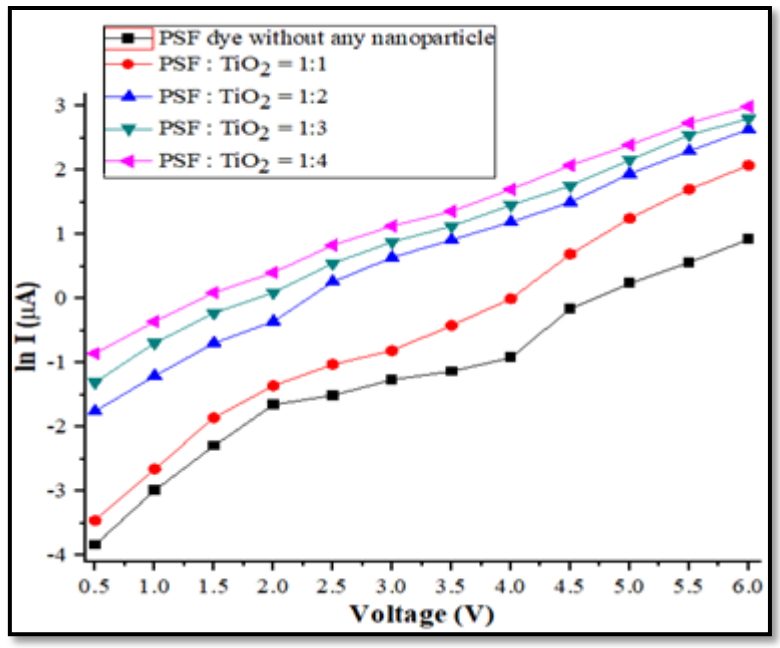

Fig. 3.10 ln I -V plots of device without any nanoparticle and with different concentrations of TiO_2 nanoparticles

We have used the same model that has been shown in **equation (3.1)** to **equation (3.3)** to study I -V characteristics of this device. In a similar manner, **equation (3.4)** can be used to estimate the barrier of the device. In addition, we have determined the junction barrier using the Norde function, as illustrated in **equation (3.5)** to **equation (3.8)**.

As seen in **Fig. 3.11**, barrier is reduced when TiO_2 nanoparticles are present, and the estimated values for this parameter are similar with those found on the device's I -V plot. The junction barrier is also calculated using Norde function from which similar inference can be drawn.

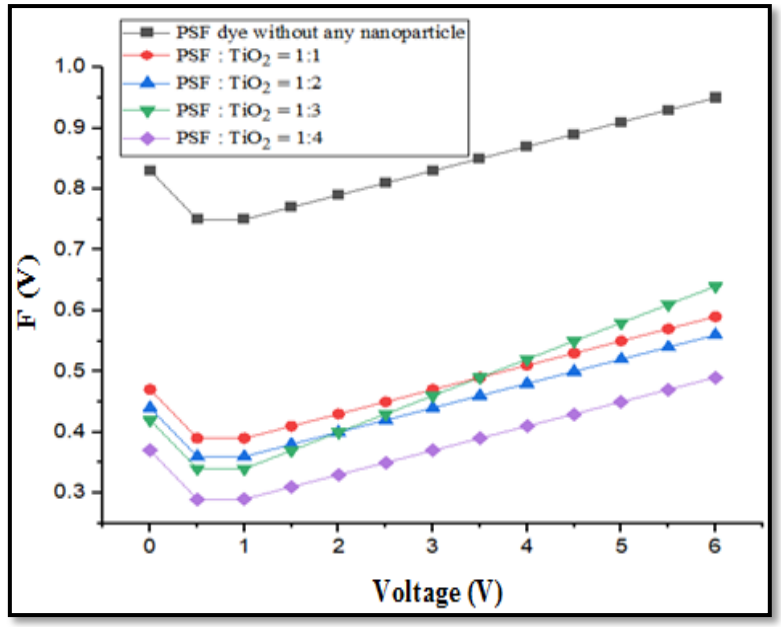

Fig. 3.11 Norde Function plots of device without and with different concentrations of TiO_2 nanoparticles

Organic devices are susceptible to trapping, so we have used a method suggested by Rizvi et al. to assess the charge trapping effect **[33]**, as seen by the **equation (3.10)** below

$$G(V) = \frac{d\log(I)}{d\log(V)} \qquad \textbf{(3.10)}$$

G (V) would have a peak due to traps filling up.

Sharp peaks in G (V) - V plot of **Fig. 3.12** show the traps are filled with TiO_2 nanoparticles, which lowers junction barrier resulting in improvement of charge infusion at the interface.

Trapping of charges can be expressed in **equation (3.11) [34]**

$$E_t = mkT \qquad \textbf{(3.11)}$$

Equation (3.4) and **equation (3.11)** can be compared, and it can be concluded that if additional parameters are taken into account, $\phi_b \propto E_t$. Hence, the barrier lowers as the charge trapping reduces **[35]**.

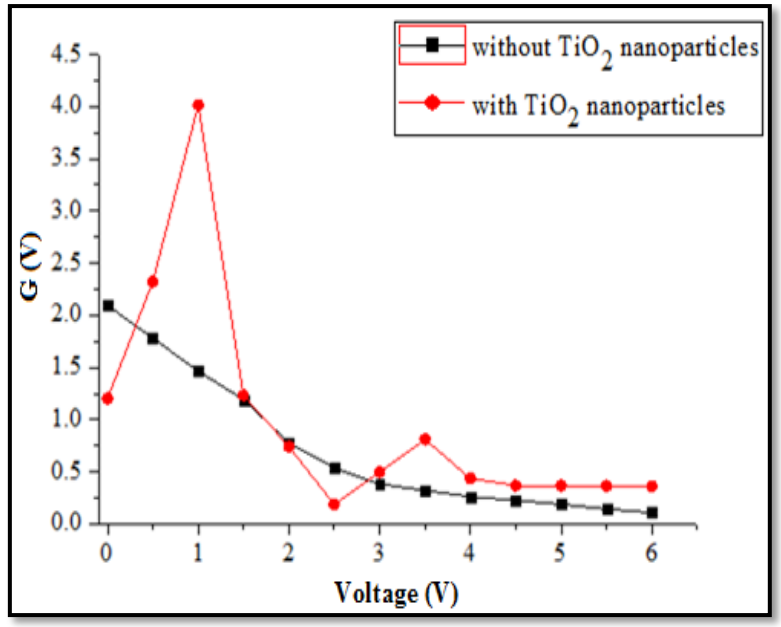

Fig. 3.12 G (V) - V plots of devices without and with TiO_2 nanoparticles

The values of threshold voltage, barrier potential and band bending of PSF dye based organic devices without any nanoparticle and with different concentrations of TiO_2 nanoparticles are shown in **Table 3.2**.

Table 3.2 Estimation of threshold voltage, barrier potential, and band bending of PSF dye devices with and without various concentrations of TiO_2 nanoparticles

Devices (PSF:TiO_2)	**Threshold Voltage (V)**	**Barrier Potential from I -V plot (eV)**	**Barrier Potential from Norde Function (eV)**	**Band Bending (eV)**
Without any nanoparticle	4.000	0.810	0.830	0.218
1:1	2.500	0.440	0.470	0.153
1:2	2.250	0.430	0.440	0.147
1:3	2.000	0.400	0.420	0.136
1:4	1.750	0.380	0.370	0.127

3.4 Conclusions

Current chapter analyzes interfacial band bending and junction barrier of PSF dye based devices. Both these properties have been affected by ZnO and TiO_2 nanoparticles. The barrier height for ZnO and TiO_2 nanoparticles are computed utilizing dark I -V plots as well as Norde's approach for these devices. Both approaches exhibit strong consistency with one another. It can be said that the interfacial band bending and injection barrier at M/O interface have decreased with ZnO and TiO_2 nanoparticles. Moreover, ZnO and TiO_2 nanoparticles lower the device's threshold voltage, enabling it to be turned on at considerably lower voltages. We have also demonstrated how the barrier potential and charge trapping are related in this chapter. The relationship between these two variables is proportional. When one parameter declines, the other parameter also declines. Also, the effects of various TiO_2 nanoparticle concentrations on the barrier potential and charge trapping effect of devices have been studied. In comparison to concentration ratios of PSF and TiO_2 nanoparticles, which are 1:1, 1:2, 1:3 and 1:4, the barrier at interface is lowest when the concentration ratio of PSF and TiO_2 nanoparticles is 1:4. When the device is devoid of any nanoparticle, the value of barrier is at its peak. Our findings suggest that by decreasing the barrier potential, TiO_2 nanoparticle concentrations enhance charge flow. The G (V) - V characteristics show that TiO_2 nanoparticles lower the trap concentration. Value of barrier declines as the trap-filling process is improved. Due to better charge flow, these devices will exhibit improved charge infusion at M/O contact and better conductivity.

3.5 References

[1] Y. Jiao, A. Hellman, Y. Fang, S. Gao and M. Käll, “Schottky barrier formation and band bending revealed by first principles calculations”, Scientific Reports, 2015, **5**, 11374-1-11374-8

[2] R. T. Tung, “The physics and chemistry of the Schottky barrier height”, Applied Physics Reviews, 2014, **1**, 011304-1-011304-54

[3] M. C. Heiber, A. Wagenpfahl and C. Deibel, “Handbook of Organic Materials for Electronic and Photonic Devices”, 2018, [2nd ed.], Woodhead Publishing, Cambridge, 309-348

[4] N. Armbrust, F. Schiller, J. Güdde and U. Höfer, “Model Potential for the description of metal/ organic interface states, Scientific Reports, 2017, **7**, 1-8

[5] V. I. Arkhipov, H. V. Seggern and E. V. Emelianova, “Charge injection versus space-charge-limited current in organic light-emitting diodes”, Applied Physics Letters, 2003, **83**, 5074-5076

[6] I. Saha, M. Hossain, and G. S. Kumar, “Sequence-Selective Binding of Phenazinium Dyes Phenosafranin and Safranin O to Guanine−Cytosine Deoxyribopolynucleotides: Spectroscopic and Thermodynamic Studies”, The Journal of Physical Chemistry B, 2010, **114**, 15278-15287

[7] L. M. Mahajan and D. S. Patil, "Structural, optical and electrical properties of post annealed K-doped ZnO films for optoelectronics applications", Materials Research Express, 2019, **6**, 076437-1-076437-11

[8] A. Chernikov, S. Horst, T. Waitz, M. Tiemann and S. Chatterjee, "Photoluminescence Properties of Ordered Mesoporous ZnO", The Journal of Physical Chemistry C, 2011, **115**, 1375-1379

[9] C. K. Kasar, J. P. Bange and D. S. Patil, "Effect of cerium composition on optical and structural properties of cerium doped ZnO nanowires", Journal of Materials Science: Materials in Electronics, 2017, **28**, 11217-11221

[10] M. J. S. Spencer and I. Yarovsky, "ZnO Nanostructures for Gas Sensing: Interaction of NO_2, NO, O, and N with the ZnO $(10\bar{1}0)$ Surface", The Journal of Physical Chemistry C, 2010, **114**, 10881-10893

[11] J. A. Anta, E. Guillen and R. Tena-Zaera, "ZnO – Based Dye - Sensitized Solar Cells", The Journal of Physical Chemistry C, 2012, **116**, 11413-11425

[12] Y. Jin, J. Wang, B. Sun, J. C. Blakesley and N. C. Greenham, "Solution-Processed Ultraviolet Photodetectors Based on Colloidal ZnO Nanoparticles", Nano Letters, 2008, **8**,1649-1653

[13] A. Mclaren, T. Valdes-Solis, G. Li and S. C. Tsang, "Shape and Size Effects of ZnO Nanocrystals on Photocatalytic Activity", Journal of the American Chemical Society, 2009, **131**, 12540-12541

[14] D. R. Coronado, G. R. Gattorno , M.E. Espinosa-Pesqueira, C. Cab, R. D. Coss and G. Oskam, "Phase-pure TiO_2 nanoparticles: anatase, brookite and rutile", Nanotechnology, 2008, **19**, 145605-1-145605-10

[15] Y. Lai, L. Wang, D. Liu, Z. Chen and C. Lin, "TiO_2-Based Nanomaterials: Design, Synthesis, and Applications", Journal of Nanomaterials, 2015, **2015**, 1-3

[16] M. Rani and S. K. Tripathi, "A Comparative Study of Nanostructured TiO_2, ZnO and Bilayer TiO_2/ZnO Dye-Sensitized Solar Cells", Journal of Electronic Materials, 2015, **44**, 1151-1159

[17] J. Jia, H. Yamamoto, T. Okajima and Y. Shigesato, "On the Crystal Structural Control of Sputtered TiO_2 Thin Films", Nanoscale Research Letters, 2016, **11**, 324-1-324-9

[18] S. Sen and N. B. Manik, "Effect of Zinc Oxide (ZnO) Nanoparticles on Interfacial Barrier Height and Band Bending of Phenosafranin (PSF) Dye Based Organic Device", Journal of Electronic Materials, 2020, **49**, 4647-4652

[19] S. Sen and N. B. Manik,"Effect of Different Concentrations of Titanium Di Oxide Nanoparticles on the Potential Barrier of Organic Device", European Journal of Formal Sciences and Engineering, 2021, **4**, 1-10

[20] J. Svensson, E. E. B. Campbell, "Schottky barriers in carbon nanotube-metal contacts", Journal of Applied Physics, 2011, **110**, 111101-1−111101-16

[21] M. Shah, Kh. S. Karimov, Z. Ahmad and M. H. Sayyad, "Electrical Characteristics of Al/CNT/NiPc/PEPC/Ag Surface-Type Cell", Chinese Physics Letters, 2010, **27**, 106102-1-106102-4

[22] Z. Harrabi, S. Jomni, L. Beji and A. Bouazizi, "Distribution of barrier heights in Au/porous GaAs Schottky diodes from current–voltage–temperature measurements", Physica B, 2010, **405**, 3745-3750

[23] H. M. J. Al-Ta'ii, Y. M. Amin and V. Periasamy, "Calculation of the Electronic Parameters of an Al/DNA/p-Si Schottky Barrier Diode Influenced by Alpha Radiation", Sensors, 2015, **15**, 4810-4822

[24] Z. Ahmed and M. H. Sayyad, "Electrical characteristics of a high rectification ratio organic Schottky diode based on Methyl red", Optoelectronics and Advanced Materials – Rapid Communications, 2009, **3**, 509-512

[25] M. Yildirim, "Determination of Contact Parameters of Au/n-Ge Schottky Barrier Diode with Rubrene Interlayer", Journal of Polytechnic, 2017, **20**, 165-173

[26] B. Güzeldir, M. Saglam, A. Ates and A. Türüt, "Determination of the some electronic parameters of nanostructure copper selenide and Cu/Cu_3Se_2/n-GaAs/In structure", Journal of Alloys and Compounds, 2015, **627**, 200-205

[27] Z. Ul Islam , M. Tahir , W. A. Syed , F. Aziz , F. Wahab , S. M. Said , M. R. Sarker , S. H. Md. Ali and M. F. M. Sabri, "Fabrication and Photovoltaic Properties of Organic Solar Cell Based on Zinc Phthalocyanine", Energies, 2020, **13**, 1-14

[28] H. Norde, "A modified forward I-V plot for Schottky diodes with high series resistance", Journal of Applied Physics, 1979, **50**, 5052-5053.

[29] F. Yakuphanoglu, M. Shah and W. Aslam Farooq, "Electrical and Interfacial Properties of p-Si/P3HT Organic-on-Inorganic Junction Barrier", Acta Physica Polonica A, 2011, **120**, 558-562.

[30] A. Türüt, "Determination of barrier height temperature coefficient by Norde's method in ideal Co/n-GaAs Schottky contacts", Turkish Journal of Physics, 2012, **36**, 235-244

[31**]** K. Fukui, "Theory of Orientation and Stereo Selection", 1975, Springer - Verlag, Berlin, 50 -75

[32] R. Nouchi, "Extraction of the Schottky parameters in metal-semiconductor-metal diodes from a single current-voltage measurement", Journal of Applied Physics, 2014, **116**, 184505-1-184505-6

[33] S. M. H. Rizvi, P. Mantri and B. Mazhari, "Traps signature in steady state current-voltage characteristics of organic diode", Journal of Applied Physics, 2014, **115**, 244502-1-244502-9

[34] S. K. Dey, Md. R. Islam, N. B. Manik and A. N. Basu, "Study of the effect of trap levels on steady–state dark I–V characteristics in Safranine–T –based solid state thin film photoelectrochemical cell", Journal of Materials Science: Materials in Electronics, 2002, **13**, 249-252

[35] S. Sen and N. B. Manik, "Correlation between Barrier Potential and Charge Trapping under the Influence of Titanium Dioxide Nanomaterials in Organic Devices", Results in Materials, 2020, **8**, 1-6

Chapter 4

Impact of Single Walled Carbon Nanotubes (SWCNT) on Junction Properties of Safranin - T Dye Based Device

4.1 Introduction

4.2 Materials and Sample Preparation

4.3 Measurements

4.4 Results and Discussions

4.5 Conclusions

4.6 References

4.1 Introduction

Prior chapter discussed barrier potential and interfacial band bending of organic device and how ZnO and TiO_2 nanoparticles affected both of these properties. We also demonstrated how the barrier potential and charge trapping were proportional to each other. Also, the earlier chapter investigated the effects of various TiO_2 nanoparticle concentrations on both of these parameters.

In this chapter, we will study different parameters such as barrier inhomogeneity, barrier potential, barrier lowering caused by image charge carriers, and carrier entrapment and afterwards, effect of SWCNTs on these parameters will also be studied. To calculate charge carrier trapping and barrier potential, the produced organic device will undergo I -V characterization. R–S model will be used to study device's I -V characteristics **[1]**. A plot of apparent barrier potential with respect to 1/2kT will also be made in order to investigate barrier inhomogeneity and its relationship to junction barrier.

4.2 Materials and Sample Preparation

The cationic azine dye Safranin - T has the empirical formula $C_{20}H_{19}ClN_4$ **[2]**. 350.84 g/mol is the molecular weight of it. The source of this dye is Sigma-Aldrich. The Safranin - T structure is shown in **Fig. 4.1(a)**. SWCNT, which is acquired from Sisco Research Laboratory (SRL), India, is shown in **Fig. 4.1(b)**. The structural visualization of PVA is seen in **Fig. 4.1 (c)**.

The PVA solution is initially formed without any nanoparticle. This solution is now supplemented with 1 mg of Safranin - T, which is swirled for 30 minutes. This solution's one part is set aside in a test tube that has already been cleaned. Then 1 mg of SWCNT is added and thoroughly mixed into the remaining Safranin - T dye solution. Safranin - T dye solution without any nanoparticle is spin coated at 2500 rpm speed and dried at 4000 rpm speed over a glass substrate coated in ITO after the solutions have been prepared. In a similar manner, the solution is applied to Al, and then ITO coated glass and Al are sandwiched together to create the Safranin - T cell without the nanoparticles. To prepare Safranin - T cell made up of SWCNT, Safranin - T solution with SWCNT is also spin coated separately. Both of these cells are placed in a vacuum desiccator for 12 hours to dry before being characterized.

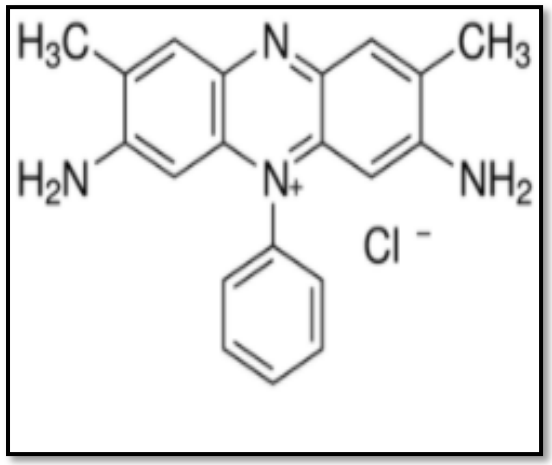

(a)

(b)

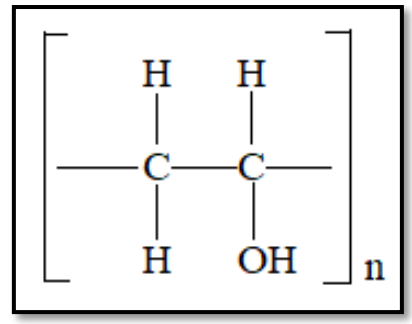

(c)

Fig. 4.1 Structural Visualization of **(a)** Safranin - T dye, **(b)** SWCNT and **(c)** PVA

The structural layout for organic device is shown in **Fig. 4.2**.

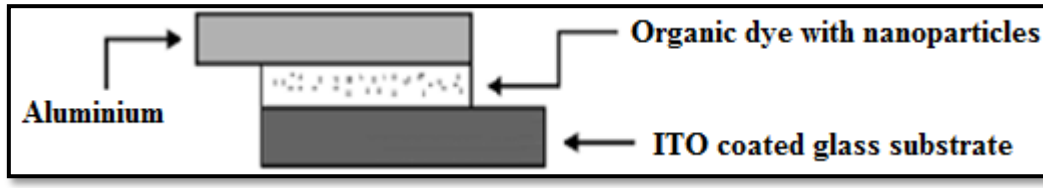

Fig. 4.2 Structural Layout of Prepared Device

4.3 Measurements

Keithley 2400 source measuring unit is used to test I -V characteristics of prepared two cells. At a delay of 1000 ms, the applied voltage is changed in stages of 0.2 V from 0 to 6 V. The experiment takes place at 25^0C room temperature.

4.4 Results and Discussions

The **equation (4.1)** depicts current at interface in accordance with the R-S hypothesis.

$$I = AA^*T^2 \exp\left(-\frac{q\phi_b}{kT}\right)\left(\exp\left(\frac{qV}{nkT}\right)\left[1 - \exp\left(\frac{-qV}{kT}\right)\right]\right) \quad \textbf{(4.1)}$$

Where,

$$I_0 = AA^*T^2 \exp\left(-\frac{q\phi_b}{kT}\right) \quad \textbf{(4.2)}$$

The interfacial barrier is determined from **equation (4.3)**

$$\phi_b = \frac{kT}{q}\ln\left(\frac{AA^*T^2}{I_0}\right) \quad \textbf{(4.3)}$$

All symbols carry their usual meaning **[3-8]**. The term $\frac{q}{kT}$ is changed to β.

Equation (4.3) can be rewritten as **equation (4.4)**

$$\phi_b = \frac{1}{\beta}\ln\left(\frac{AA^*T^2}{I_0}\right) \quad \textbf{(4.4)}$$

Fig. 4.3 illustrates I -V graphs of the device with and without SWCNTs. From **Fig. 4.3**, the threshold voltage has been computed. The semi logarithmic plots of **Fig. 4.3** are displayed in **Fig. 4.4** to calculate the barrier at junction.

Current flow can be described by the following **equation (4.5)** when barrier inhomogeneities at contact are taken into account **[9]**

$$I(V) = \int_{-\infty}^{+\infty} I(\phi_b, V)\, P(\phi_b)\, d\phi_b \quad \textbf{(4.5)}$$

Where,

$$P(\phi_b) = \frac{1}{\sigma_0\sqrt{2\pi}} \exp\left[-\frac{(\phi_b - \phi_0)^2}{2\sigma_0^2}\right] \quad \textbf{(4.6)}$$

All the notations have their standard meaning as proposed by Werner and Güttler [**10-11**].

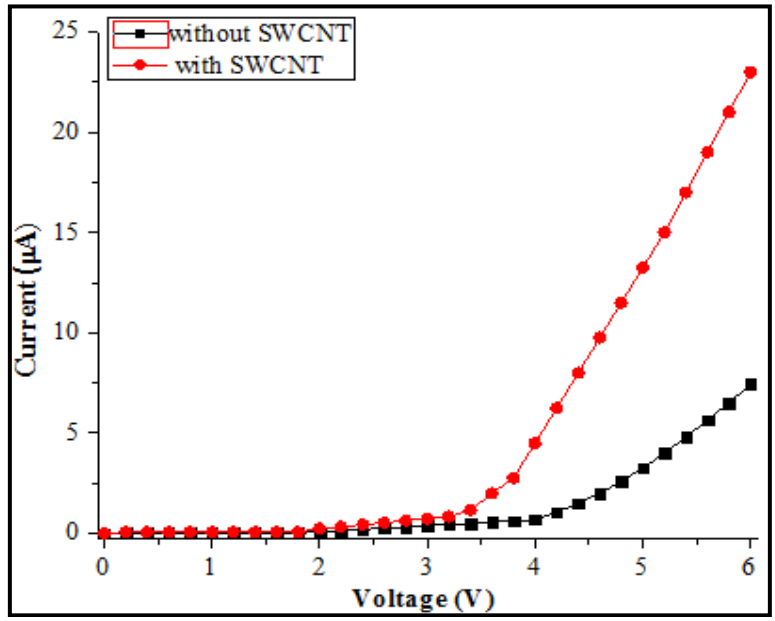

Fig. 4.3 I -V plots of device without and with SWCNT

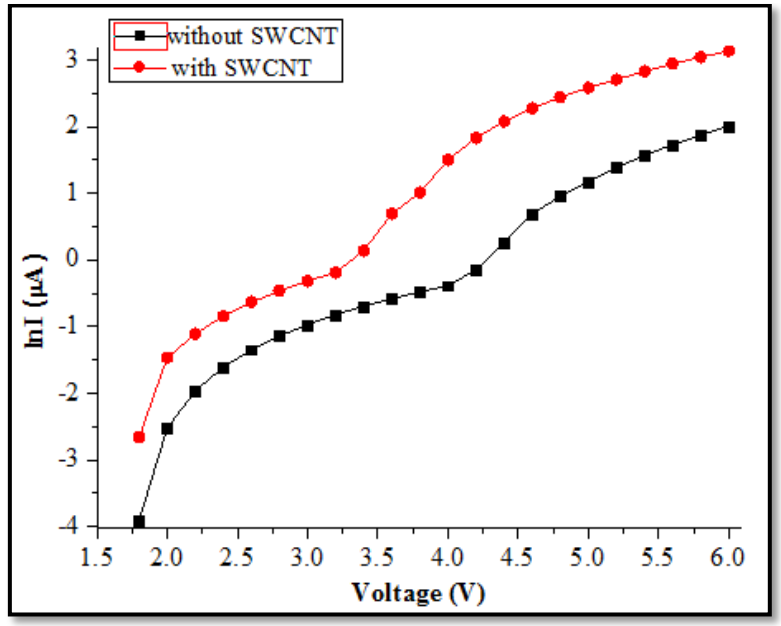

Fig. 4.4 ln I -V plots of device without and with SWCNT

Equation (4.7), which combines **equation (4.1)** and **equation (4.5)**, has been used to describe the device's current while taking into account the Gaussian distribution of the barrier.

$$I(V) = AA^{*}T^{2} \exp\left[-\beta\left(\phi_0 - \frac{\beta\sigma_0^2}{2}\right)\right] \exp\left(\frac{\beta V}{n}\right) [1 - \exp(-\beta V)] \quad \textbf{(4.7)}$$

$$I_s = AA^{*}T^{2} \exp(-\beta\phi_a) \quad \textbf{(4.8)}$$

Used symbols have their usual meaning **[12-14]**.

Equation (4.9) demonstrates how the apparent barrier potential (ϕ_a) and standard deviation from ϕ_0 are linked **[15-16]**

$$\phi_a = \phi_0 - \frac{\beta\sigma_0^2}{2} \quad \textbf{(4.9)}$$

Equation (4.7) is the same as **equation (4.1)**, with exception that it uses ϕ_a in place of ϕ_b.

ϕ_a with regard to 1/2kT is plotted in **Fig. 4.5**. It is clear from **equation (4.9)** that temperature, ϕ_0 and σ_0 all affect perceived barrier potential. The temperature range in **Fig. 4.5** has been changed from 290 K to 340 K. The values of the intercept and slope in **Fig. 4.5** are the values of ϕ_0 and σ_0 respectively. The values of ϕ_0 and σ_0 are, respectively, 0.75 eV and 0.17 eV without SWCNT, and both values are decreased to 0.70 eV and 0.13 eV with SWCNT. In general, the symbol σ_0 denotes barrier inhomogeneity. Barrier inhomogeneity is significantly present at the Safranin-T/Al schottky contact, according to calculated values of σ_0. As long as the barrier inhomogeneity value is kept low, device's charge infusion process will improve. The schottky contact's barrier inhomogeneity is decreased when SWCNT is present, which may lead to a better charge infusion at interface.

This work also discusses the influence of image charges on decreasing barriers. **Equation (4.10)** illustrates representation of effective barrier while taking the image charge effect into consideration.

$$U(x) = \phi_b - \frac{e^2}{16\pi\varepsilon_0\varepsilon x} - eFx \quad \textbf{(4.10)}$$

x = interfacial distance and all other symbols have their standard interpretations **[17]**.

In absence and presence of SWCNT, effective barrier is determined, when image charge effect is present. The dielectric constant is 3.2, and separation from interface is equal to 2 nm. A 10^4 V/cm applied field is used. Without and with SWCNT, the estimated effective barrier values for image charge effect are 0.79 eV and 0.74 eV, respectively. According to **Fig. 4.6**, the effective barrier in an organic device drops practically linearly as the applied field increases.

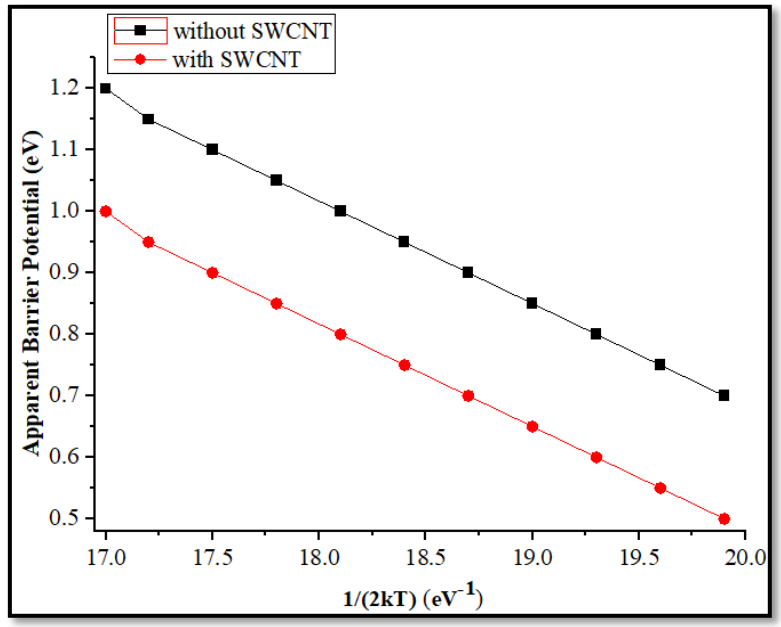

Fig. 4.5 Apparent Barrier Potential versus 1/2kT plot of device without and with SWCNT

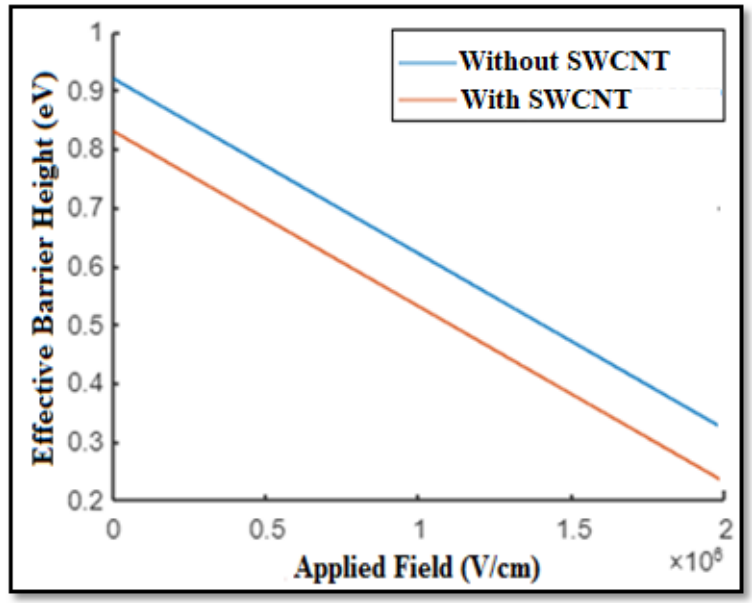

Fig. 4.6 Dependence of Effective Schottky Barrier on the Applied Field

Fig. 4.7 also shows the relationship between effective barrier height and distance from interfacial contact with and without SWCNT. The effective barrier height reduces as distance from the M/O interface rises, as seen in **Fig. 4.7**.

The space - charge layer width is estimated from **equation (4.11)**

$$W_d = \sqrt{\frac{2\varepsilon_0\varepsilon_s V_d}{qN_D}} \quad \textbf{(4.11)}$$

W_d = space - charge layer width, ε_0 = vacuum permittivity, ε_s = semiconductor permittivity, V_d = diffusion potential, q = charge of an electron, N_D = donor atom concentration.

Equation (4.12) correlates depletion layer width and junction barrier.

$$W_d = \frac{\phi_b}{F} \quad \textbf{(4.12)}$$

F = applied field.

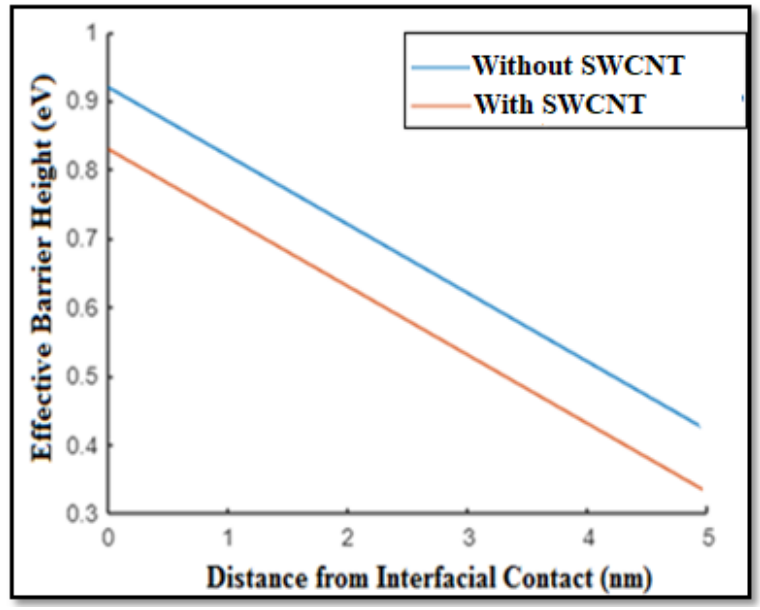

Fig. 4.7 Effective Junction Barrier on the Distance from Interfacial Contact with and without SWCNT

Fig. 4.8 shows interdependence of space - charge layer width with applied electric field. It is evident that the interfacial depletion region width has been decreased as the applied electric field increases.

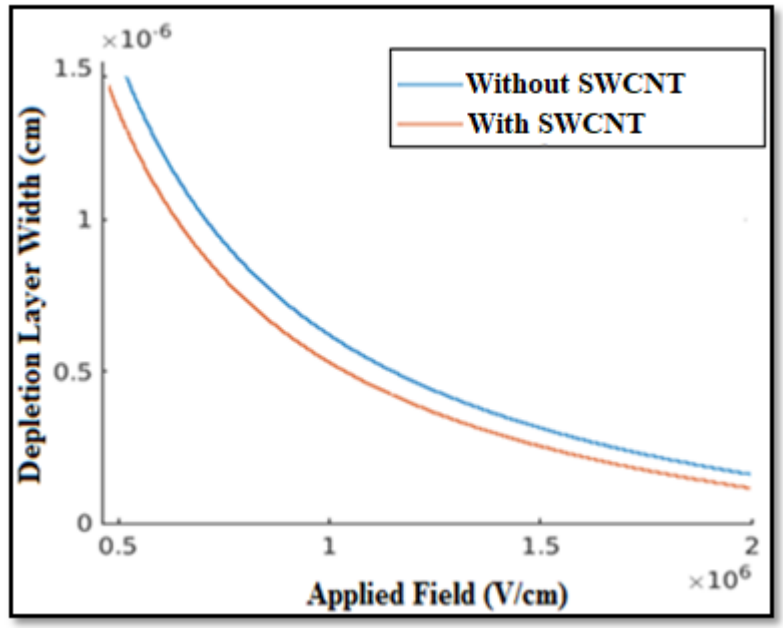

Fig. 4.8 Dependence of Depletion Layer Width on the Applied Field

In **Fig. 4.9**, the relationship between the effective schottky barrier and space - charge layer width has been depicted. It has been observed that space - charge layer width escalates with rising value of effective schottky barrier.

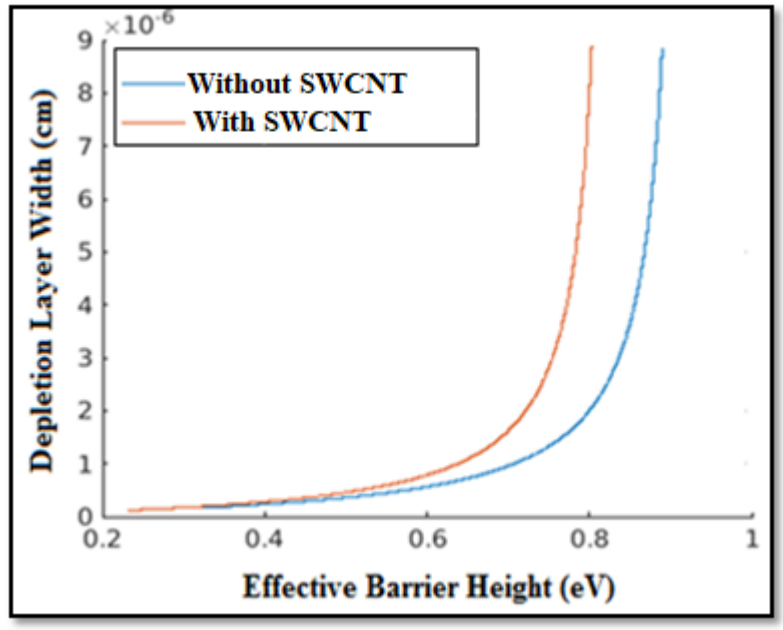

Fig. 4.9 Dependence of Depletion Layer Width on the Effective Schottky Barrier

Trap energy has been estimated from ln I - ln V plot which is shown in **Fig. 4.10**.

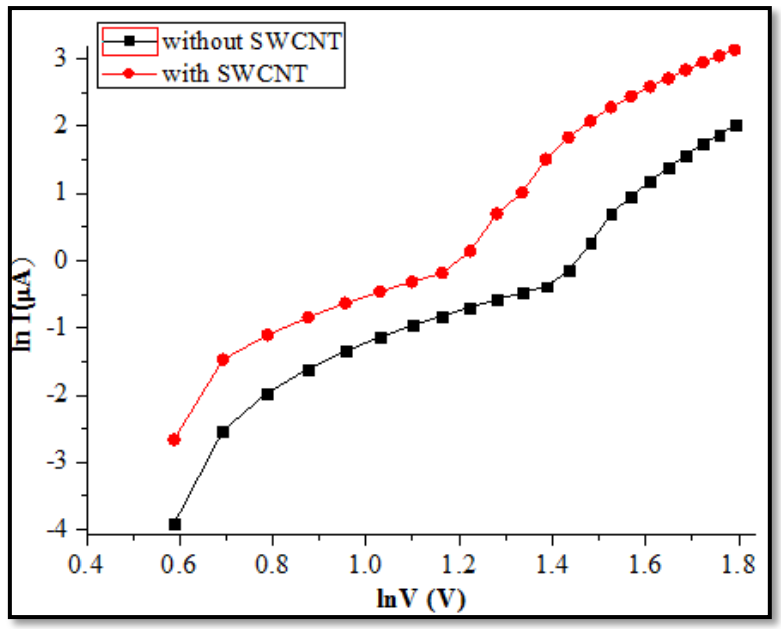

Fig. 4.10 ln I - ln V plot of device without and with SWCNT

Equation (4.13) can be used to describe the trap energy.

$$E_t = mkT \qquad \textbf{(4.13)}$$

Where, E_t = trap energy and other symbols carry their usual meaning **[18]**. m is estimated from **Fig. 4.10**.

The values of organic devices' threshold voltage, trap energy, barrier potential without and with considering image charge effect and barrier inhomogeneity with and without SWCNT are illustrated in **Table 4.1**.

Table 4.1 shows that presence of SWCNT reduces the parameters that hinder the charge flow in the device resulting in better device performance. It reduces trap energy and barrier potential to 30.51% and 4.93% respectively. Barrier inhomogeneity is lowered to approximately 23.53%. Effective barrier potential considering image charge effect also lowers to 6.33% with SWCNT. Lowering of these parameters will cause device to be switched on at lower voltages, whose approximate reduction is 18.75% with SWCNT.

Table 4.1 Calculation of threshold voltage, trap energy, barrier potential without and with image charge effect and barrier inhomogeneity of organic devices in absence and in presence of SWCNT

Safranin - T dye based devices	Threshold Voltage (V)	Value of m	Trap Energy (eV)	Barrier Potential (eV)	Effective Barrier Potential considering Image Charge (eV)	Barrier Inhomogeneity (eV)
Without SWCNT	4.000	2.270	0.059	0.810	0.790	0.170
With SWCNT	3.250	1.580	0.041	0.770	0.740	0.130

4.5 Conclusions

Different junction properties such as trap concentration, barrier potential without and with image charge effect, and barrier inhomogeneity, have been studied in this chapter. With application of electric field, the interdependence between space - charge layer width and schottky barrier has also been illustrated. Additionally, it has been shown how the space - charge layer width and schottky barrier rely on one another. Impact of SWCNT incorporation on these factors has also been done. According to device's I -V characteristics, both trap concentration and contact barrier without and with image charge has been lessened with SWCNT. In presence of SWCNT, the trap energy and barrier potential are reduced from 0.059 eV to 0.041 eV and 0.81 eV to 0.77 eV, respectively. Barrier potential has also been found to be affected by image charge, and with SWCNT, this effect is also lowered, going from 0.79 eV to 0.74 eV. The presence of SWCNT has also reduced barrier inhomogeneity at junction from 0.17 eV to 0.13 eV. All of these variables have a substantial impact on the charge infusion at M/O contact and this work's key finding is their interdependence. Another interesting finding is SWCNT’s high aspect ratio that reduces these parameters and it will enhance the charge flow at M/O interface and increase conductivity and device performance.

4.6 References

[1] A. Kumatani, Y. Li, P. Darmawan, T. Minari and K. Tsukagoshi, "On Practical Charge Injection at the Metal/Organic Semiconductor Interface", Scientific Reports, 2013, **3**, 1-6

[2] V. K. Gupta, A. Mittal, R. Jain, M. Mathur and S. Sikarwar, "Adsorption of Safranin-T from wastewater using waste materials— activated carbon and activated rice husks", Journal of Colloid and Interface Science, 2006, **303**, 80–86

[3] A. Kocyigit, M. Yılmaz, Ş. Aydogan and Ü. Incekara, "The effect of measurements and layer coating homogeneity of AB on the Al/AB/p-Si devices", Journal of Alloys and Compounds, 2019, **790**, 388-396

[4] V. R. Reddy, "Electrical and interfacial properties of Au/n-InP Schottky contacts with nickel phthalocyanine (NiPc) interlayer", Indian Journal of Physics, 2014, **89**, 463-469

[5] K. Zeghdar, L. Dehimi, A. Saadoune and N. Sengouga, "Inhomogeneous barrier height effect on the current–voltage characteristics of an Au/n-InP Schottky diode", Journal of Semiconductors, 2015, **36**, 1-6

[6] M. H. Ziko, A. Koel, T. Rang and M. H. Rashid, "Investigation of Barrier Inhomogeneities and Electronic Transport on Al-Foil/p-Type-4H-SiC Schottky Barrier Diodes Using Diffusion Welding", Crystals, 2020, **10**, 1-12

[7] K. Zeghdar, L. Dehimi, F. Pezzimenti, S. Rao and F. G. D. Corte, "Simulation and analysis of the current–voltage–temperature characteristics of Al/Ti/4H-SiC Schottky barrier diodes", Japanese Journal of Applied Physics, 2019, **58**, 1-7

[8] I. Jyothi, H. -D. Yang, K. -H. Shim, V. Janardhanam, S.-M. Kang, H. Hong and C. -J. Choi, "Temperature Dependency of Schottky Barrier Parameters of Ti Schottky Contacts to Si-on-Insulator", Materials Transactions, 2013, **54**, 1655 – 1660

[9] J. H. Werner and H. H. Güttler, "Barrier inhomogeneities at Schottky contacts", Journal of Applied Physics, 1991, **69**, 1522-1533

[10] J. H. Werner and H. H. Güttler, "Temperature dependence of Schottky barrier heights on silicon", Journal of Applied Physics, 1993, **73**, 1315-1319

[11] N. Yildirim, H. Dogan, H. Korkut and A. Türüt, "Dependence of characteristic diode parameters in Ni/n-GaAs contacts on thermal annealing and sample temperature", International Journal of Modern Physics B, 2009, **23**, 5237-5249

[12] H. H. Güllü, D. E. Yildiz, Ö. B. Sürücü, M. Terlemezoglu and M. Parlak, "Temperature dependence of electrical properties in In/$Cu_2ZnSnTe_4$/Si/Ag diodes", Bulletin of Materials Science, 2019, **42**, 1-8

[13] A. Asherya, A. A. M. Farag, M. A. Moussad and G. M. Turky, "Enhancement of electrical and dielectrically performance of graphene-based promise electronic devices", Synthetic Metals, 2020, **261**, 1-10

[14] S. Sen, P. K. Das and N. B. Manik, "Study on Effect of Single Walled Carbon Nanotubes on Junction Properties of Safranin – T Dye Based Organic Device", Journal of Physics Communications, 2021, **5**, 1-9

[15] V. I. Arkhipov, U. Wolf and H. Bässler, "Current injection from a metal to a disordered hopping system. II. Comparison between analytic theory and simulation", Physical Review B, 1998, **59**, 7514 - 7520

[16] S. Sen, P. K. Das and N. B. Manik, "Modification of Interfacial Properties of Organic Device in Presence of Single Walled Carbon Nanotubes", Journal of Materials Science and Surface Engineering, 2022, **9**, 1067-1070

[17] H. Bässler and A. Köhler, "Charge Transport in Organic Semiconductors", In: Metzger R. [eds.], Unimolecular and Supramolecular Electronics I. Topics in Current Chemistry, 2011, **312**, Springer, Berlin, Heidelberg

[18] A. Haldar, S. Maity and N. B. Manik, "Electrical and photovoltaic characterisations of methyl red dye doped solid-state photoelectrochemical cell", Ionics, 2009, **15**, 79-83

Chapter 5

Study on the Effect of Carboxyl - Functionalized Single Walled Carbon Nanotubes (COOH - SWCNT) and Different Sized Multi Walled Carbon Nanotubes (MWCNT) on Trap Energy and Junction Barrier of Malachite Green (MG) Dye Based Device

5.1 Introduction

The previous chapter covered the various junction parameters of Safranin - T dye based devices. On these factors, the impact of SWCNT incorporation was also seen. It also showed how the schottky barrier and space - charge layer width can be correlated.

MG dye will be used as the organic material in this chapter. Similar sandwich structured device will be formed between ITO and Al. The work function of ITO is 4.8 eV, while that of aluminium is 4.2 eV **[1]**. This chapter will look at the barrier potential or junction barrier and trap concentration at M/O interface. Additionally, the impact of both COOH - SWCNT and MWCNT on these two factors will be clarified. In general, functionalized CNTs have some benefits over their unfunctionalized counterparts. Functionalized SWCNTs make better dispersions in solvents and have stronger interfacial bonds compared to non-functionalized forms. Functionalized groups may be joined to the primary tube's ends or side chains in order to create a branch-like structure **[2]**. MWCNT will be used for its outstanding electrical, mechanical, and thermal properties **[3-5]**. One of the MWCNTs we will use has a diameter of 8 nm, while the other has a diameter of 30 nm. The addition of MWCNT will serve as filler, and it will aid in creating a simple path for charge percolation, increasing the device's current flow. Using the device's I -V plot, junction barrier and trap concentration will be estimated. The same I -V plot will be used to determine transition voltage as well. R – S model will be used to analyze device’s current flow. To confirm the congruency of the value obtained from the device's I -V plot, we will also use the Norde’s technique to determine junction barrier.

5.2 Experimental Details with the Incorporation of SWCNT

The effects of COOH - SWCNT on the organic device based on MG dye will be investigated and elaborated upon in this part.

5.2.1 Materials and Sample Preparation

A cationic dye with the chemical composition of $[C_6H_5C(C_6H_4N(CH_3)_2)_2]$ Cl is Malachite Green (MG) dye. It is atriarylmethane group member and molecular mass of it is 364.911 g/mol (chloride). On a broader scale, it is made by condensing 2 moles of dimethylaniline with 1 mole of benzaldehyde at 1000°C in presence of concentrated sulfuric acid or zinc chloride **[6]**. This dye's cationic version has an extended pi-delocalization that enables visible light absorption. This dye has a large quantum yield **[7]**. The dye and COOH - SWCNT are procured from Finar Chemicals, Ahmedabad and Sisco Research Laboratory respectively. The architectures of MG dye and COOH - SWCNT are depicted in

Fig. 5.1(a) and **Fig. 5.1(b)**, respectively. Sigma Aldrich and Merck Specialities Pvt. Ltd., both in Mumbai, are where one can procure poly methyl methacrylate (PMMA) and dichloromethane (DCM) respectively. Due to its great capacity to dissolve organic compounds, DCM was chosen as the solvent in our research **[8]**. The dichloromethane (DCM) molecule is depicted in **Fig. 5.1 (c)**.

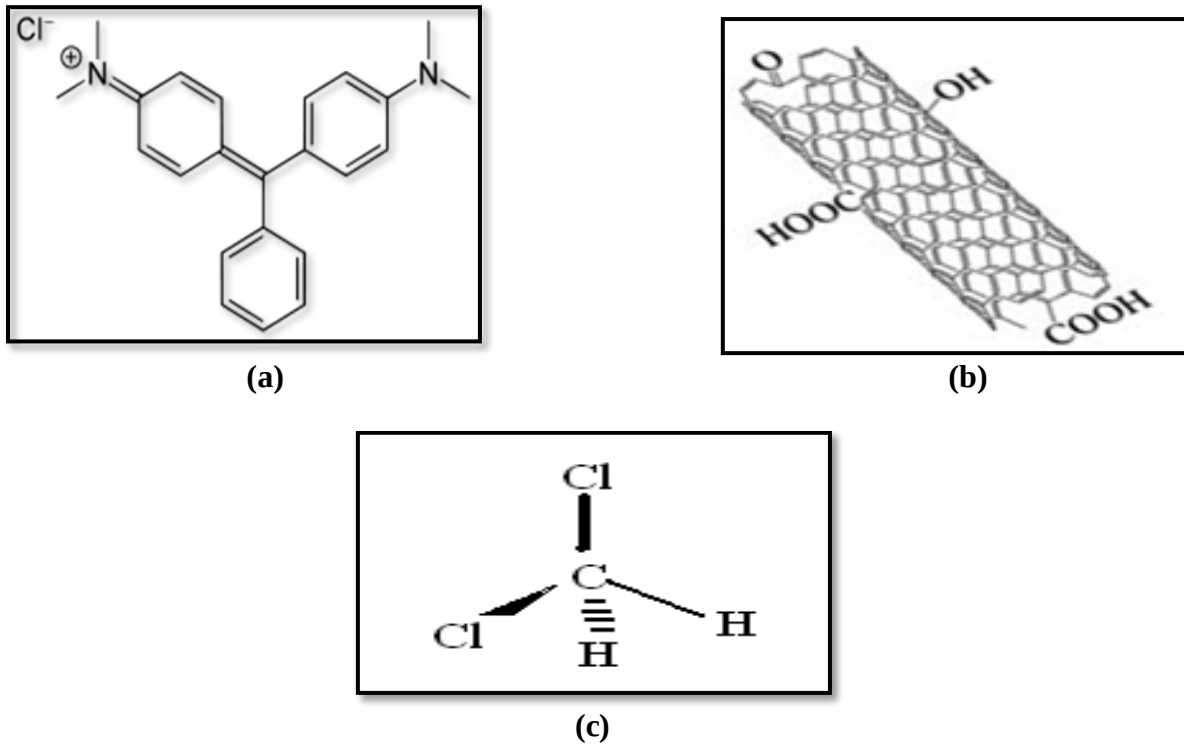

(a) **(b)**

(c)

Fig. 5.1 Structural Visualization of **(a)** MG dye, **(b)** COOH – SWCNT and **(c)** DCM

To study the impact of COOH - SWCNT on MG dye based organic device, two types of cells are prepared. While one type of cell is created using only MG dye, the other kind of cell is prepared by adding COOH - SWCNT with MG dye. Al and ITO coated glass substrates are the two electrodes that we have used in the experiment. Additionally, PMMA is used in this work to work as inert binder. 1 mg of PMMA is dissolved by adding 20 ml of DCM to prepare PMMA solution. MG dye solution is formed by adding 1 mg of MG dye with the prepared PMMA solution. In order to prepare MG dye based device with COOH - SWCNT, 1 mg of COOH - SWCNT is added to MG dye solution and then it is deposited on an ITO coated glass substrate, followed by a 1500 rpm spin coating and a 3500 rpm drying process. On an Al electrode, the same solution is spin coated in a comparable manner. Then, these electrodes are joined together in a semi-dry condition. In the similar manner, MG dye based device without any nanotube is prepared. Before electrical analysis, both these cells are dried for 12 hours in a vacuum desiccator.

5.2.2 Measurements

The measurement method is comparable to the method used in the preceding chapter. The voltage ranges from 0 to 5 V in steps of 0.5 V with a 500 ms delay.

5.2.3 Results and Discussions

Current flow has already been elucidated in **chapter 3** from **equation (3.1)** to **equation (3.3)**, in accordance with R-S thermionic emission theory. The following **equation (5.1)** can be used to estimate the barrier **[9-10]**.

$$\phi_b = \frac{kT}{q} \ln\left(\frac{AA^*T^2}{I_0}\right) \qquad \textbf{(5.1)}$$

I -V plots of organic device under the influence of COOH - SWCNT and without any nanoparticle are shown in **Fig. 5.2**. The device's current has been greatly increased, attributable to COOH - SWCNT, as seen in the **Fig. 5.2**.

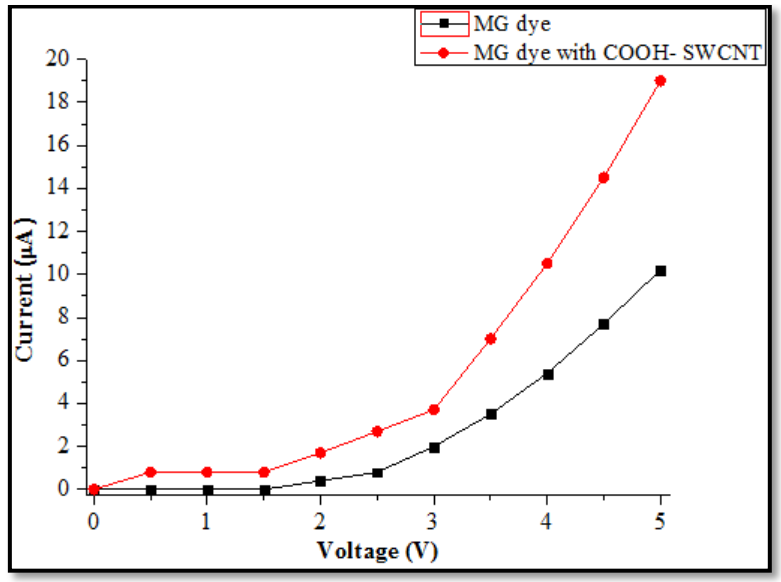

Fig. 5.2 I -V plots of device with and without COOH - SWCNT

In **Fig. 5.3**, ln I -V plots of device with and without COOH - SWCNT is analyzed to determine junction barrier.

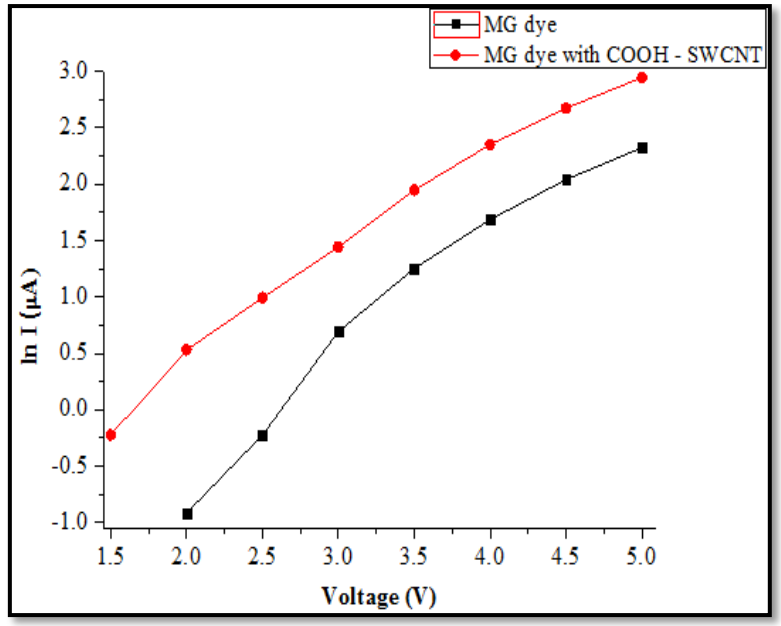

Fig. 5.3 ln I -V plots of device with and without COOH - SWCNT

Analysis of junction barrier is additionally performed using Norde function, which is described from **equation (3.5)** to **equation (3.8)** in **Chapter 3**. **Fig. 5.4** displays the Norde function plots of device with and without COOH - SWCNT.

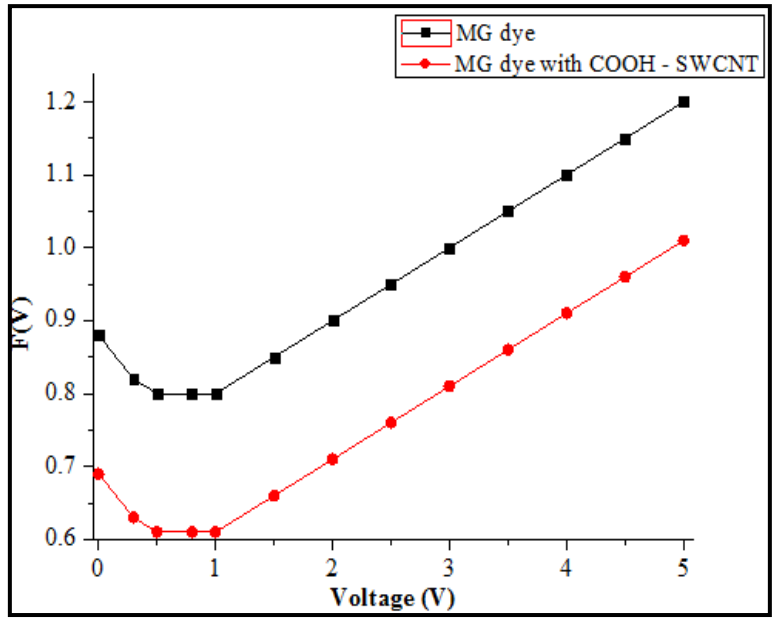

Fig. 5.4 Norde Function plots of device with and without COOH - SWCNT

Fig. 5.5 is used to estimate trap energy of the prepared device without and with COOH - SWCNT.

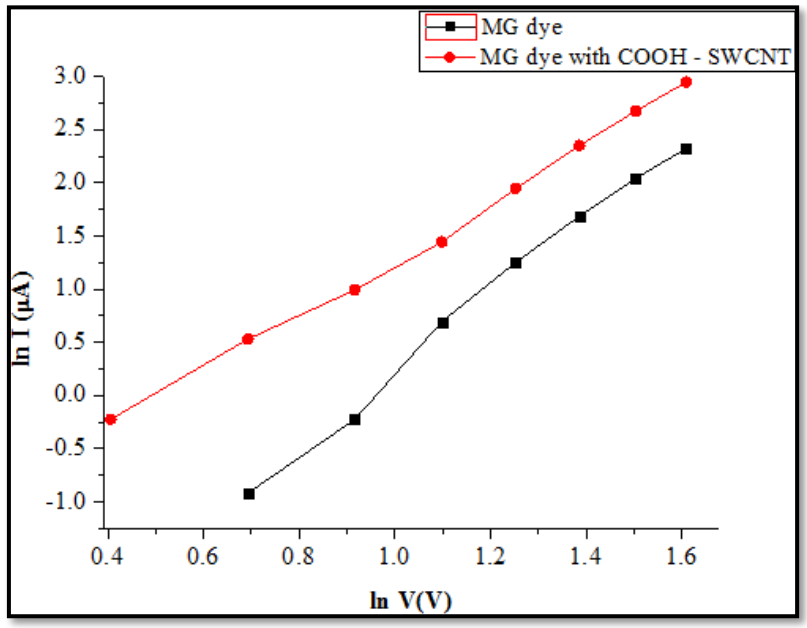

Fig. 5.5 ln I - ln V plots of device with and without COOH - SWCNT

Equation (5.2) expresses the value of trap energy.

$$E_t = mkT \qquad \textbf{(5.2)}$$

Where, all symbols carry their usual meaning.

When all parameters are held constant, it may be concluded from comparing **equation (5.1)** and **equation (5.2)**, that barrier and trap energy are comparable to one another.

5.3 Experimental Details with the Incorporation of MWCNT

This part will discuss and elucidate the effects of MWCNTs with 8 nm diameter and 30 nm diameter on the organic device.

5.3.1 Materials and Sample Preparation

Many single-walled carbon nanotubes are nested inside of one another to create MWCNTs, a unique type of carbon nanotube. MWCNTs have good electrochemical properties and a good thermal

conductivity **[11]**. One of the MWCNTs has a diameter of 8 nm, while the other has a diameter of 30 nm. Both MWCNTs have a carbon concentration of more than 99%. We have procured MWCNTs from Sigma-Aldrich. The MWCNT's schematic arrangement is depicted in **Fig. 5.6**.

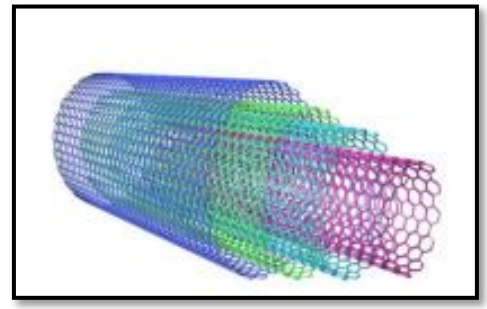

Fig. 5.6 Schematic Structure of Multi Walled Carbon Nanotubes (MWCNT)

Section 5.2.1 has already elaborated PMMA solution method. 1 mg of MG dye is introduced to PMMA solution and blended for 30 minutes. The solution is then divided into three portions and placed in beakers before being cleaned. MWCNT of 8 nm diameter and 30 nm diameter are added to the other two beakers, respectively, and stirred for three hours to produce three uniform solutions. One beaker contains only MG dye solution and other two beakers contain MG dye with 8 nm diameter MWCNT and 30 nm diameter MWCNT respectively. Before electrical measurement, all three of these cells are placed in vacuum desiccated for 12 hours at room temperature **[12]**.

5.3.2 Measurements

Section 5.2.2 has already mentioned the measurement technique. With a delay of 1000 ms, the voltage ranges from 0 to 5 V in increments of 0.5 V. A 25^0C ambient temperature is maintained throughout the experiment.

5.3.3 Results and Discussions

I -V graphs of organic devices influenced by MWCNTs with 8 nm and 30 nm in diameter are shown in **Fig. 5.7 (a)** and **Fig. 5.7 (b)**, respectively. Current rises more when 8 nm diameter MWCNT is present, compared to that of 30 nm diameter MWCNT.

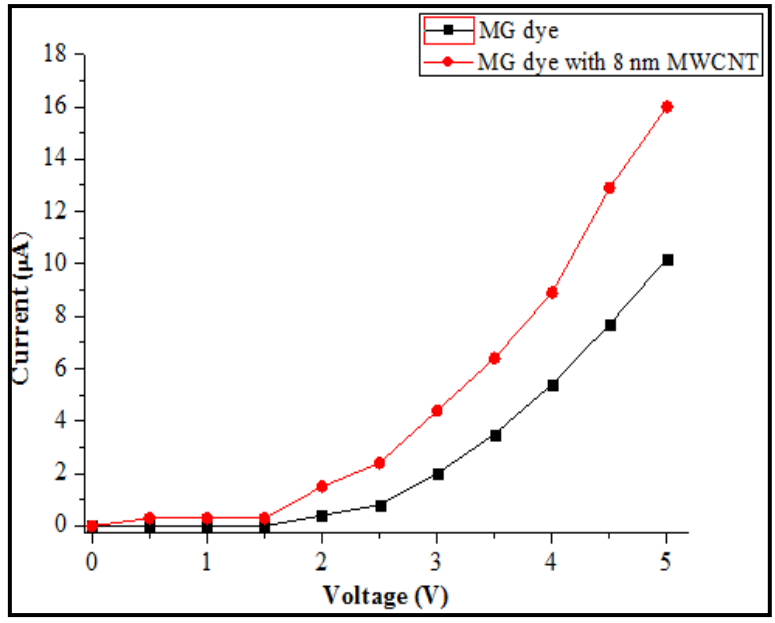

(a)

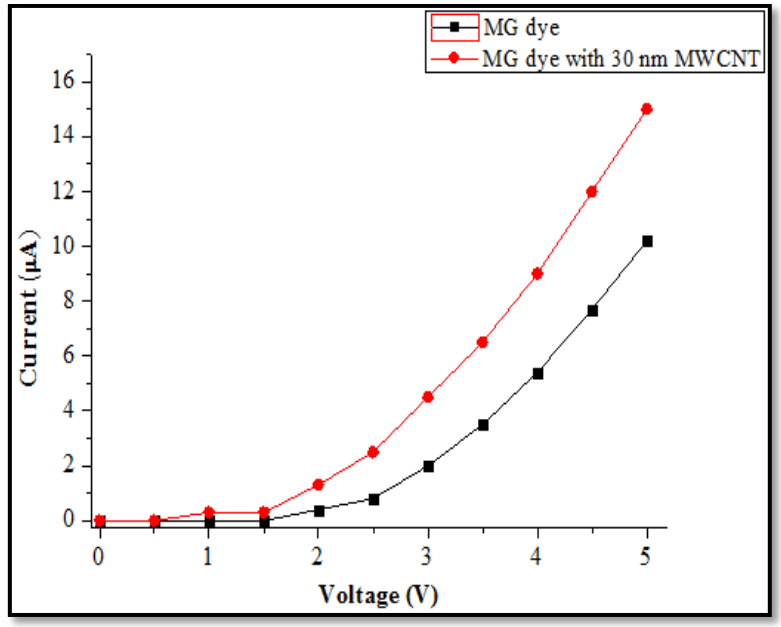

(b)

Fig. 5.7 I -V plots of device with and without **(a)** 8 nm diameter and **(b)** 30 nm diameter MWCNT

From ln I -V plots of the organic devices with and without 8 nm diameter MWCNT and 30 nm diameter MWCNT, that are depicted in **Fig. 5.8 (a)** and **Fig. 5.8 (b)**, respectively, junction barrier has been determined.

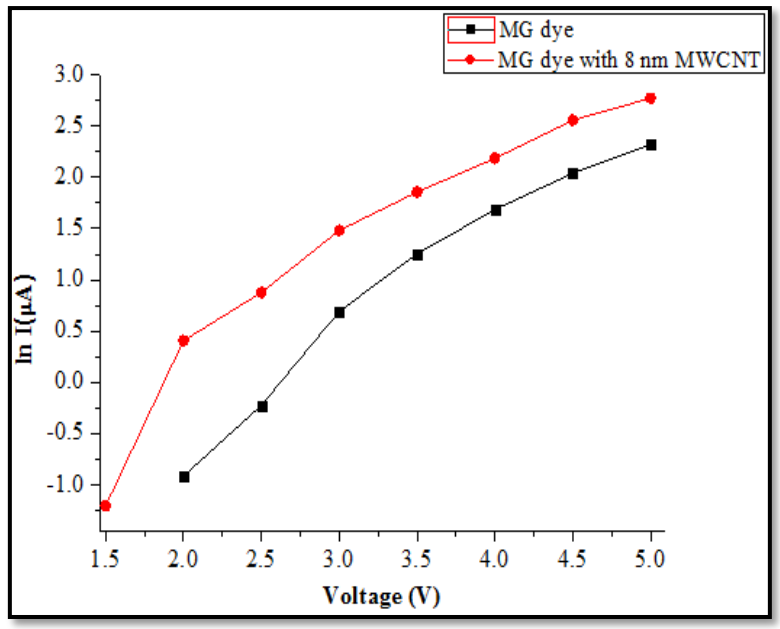

(a)

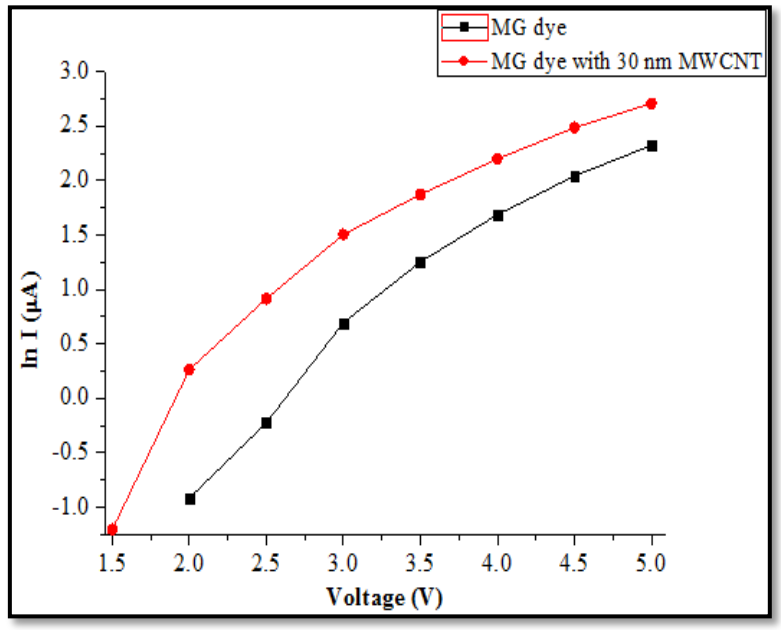

(b)

Fig. 5.8 ln I -V plots of device with and without **(a)** 8 nm diameter and **(b)** 30 nm diameter MWCNT

Identical to **Fig. 5.4**, **Fig. 5.9 (a)** and **Fig. 5.9 (b)** show the Norde function curves of MG dye both with and without 8 nm diameter and 30 nm diameter MWCNT, respectively.

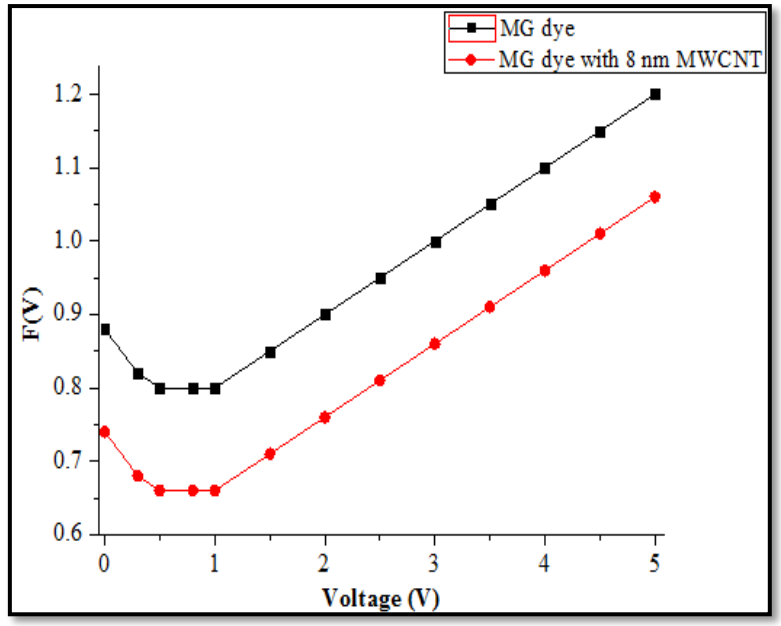

(a)

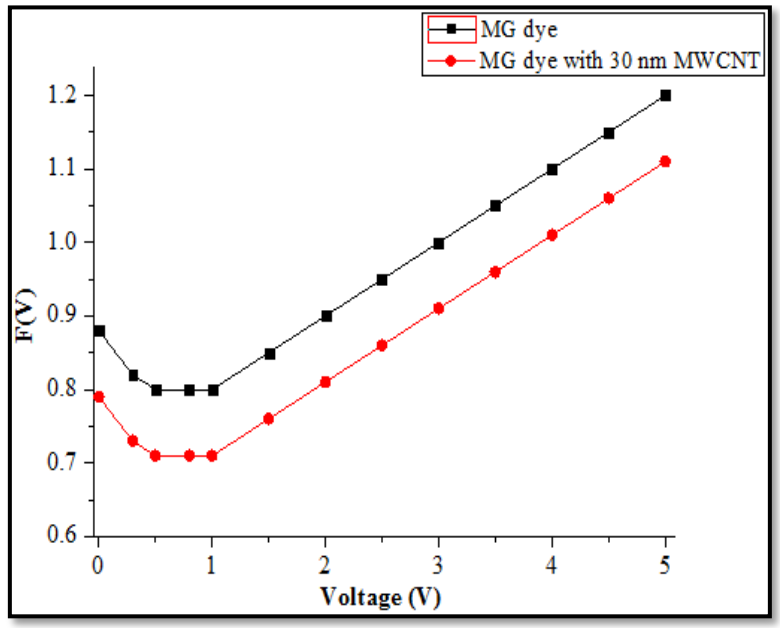

(b)

Fig. 5.9 Norde Function plots of device with and without **(a)** 8 nm diameter and **(b)** 30 nm diameter MWCNT

In **Fig. 5.10 (a)** and **Fig. 5.10 (b)**, the trap energy has been calculated without any nanotube and with 8 nm diameter and 30 nm diameter MWCNT.

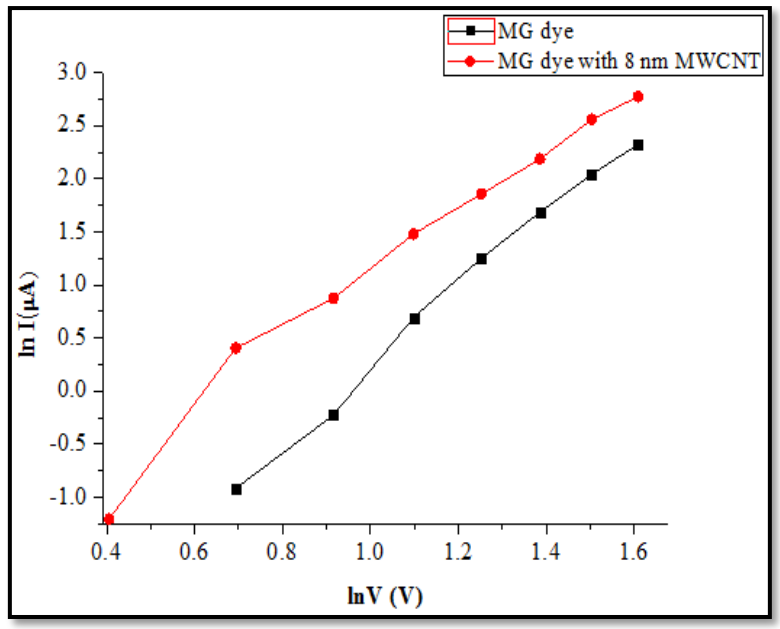

(a)

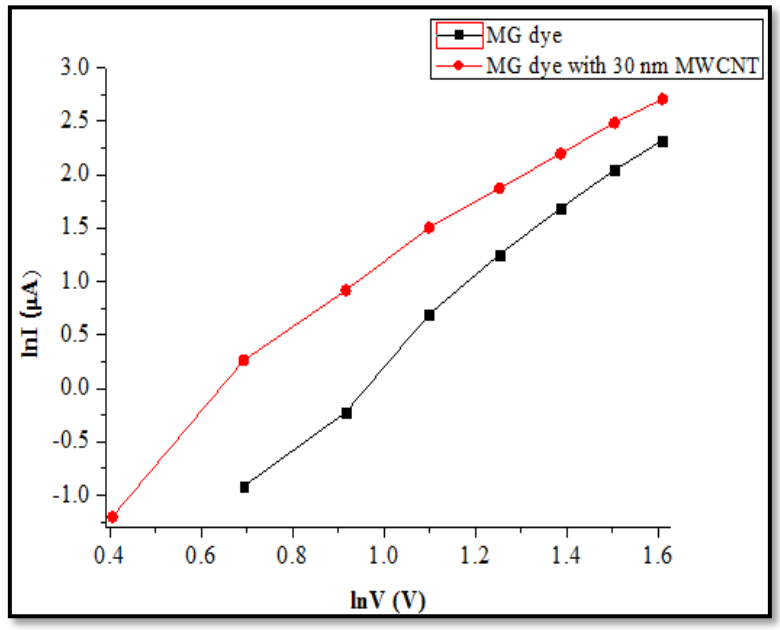

(b)

Fig. 5.10 ln I - ln V plots of device with and without **(a)** 8 nm diameter and **(b)** 30 nm diameter MWCNT

In **Table 5.1**, the values of the transition voltage, trap energy, and junction barrier of devices with and without COOH - SWCNT and MWCNTs are expressed.

Table 5.1 Calculation of transition voltage, trap energy and junction barrier of devices without any nanotube and with presence of COOH - SWCNT and MWCNTs

MG dye based devices	Transition Voltage (V)	Value of m	Trap Energy (eV)	Junction Barrier from I -V plot (eV)	Junction Barrier using Norde Function (eV)
Without any nanotube	3.900	1.770	0.046	1.120	0.880
With COOH - SWCNT	2.000	1.050	0.027	0.870	0.770
With 8 nm MWCNT	2.370	1.080	0.028	0.970	0.790
With 30 nm MWCNT	2.710	1.340	0.035	1.030	0.840

Table 5.1 demonstrates that the trap energy is reduced approximately to 41%, 39%, and 24% by COOH - SWCNT, 8 nm diameter and 30 nm diameter MWCNT, respectively, and similarly, junction barrier is decreased approximately to 22%, 13%, and 8%, by these three guest materials respectively. These conclusions are inferred from device's I -V properties. Additionally, Norde technique demonstrates that COOH - SWCNT, 8 nm diameter, and 30 nm diameter MWCNT reduce barrier potential value by about 12.5%, 10%, and 5%, respectively. The device can be switched on at low voltage caused by the presence of both COOH - SWCNT and two various sized MWCNTs.

5.4 Conclusions

The effects of COOH - SWCNT and MWCNTs, have been seen to affect trap energy and junction barrier in devices. I -V graphs are used to determine both of these parameters, influenced by COOH - SWCNT and MWCNTs. The Norde method is also used to determine junction barrier. Both COOH - SWCNT and various sized MWCNT have been shown to decrease junction barrier and trap energy. We have also demonstrated the analytical proportionality of junction barrier and trap energy, which

implies that lowering of one parameter, will also lower the other. Reduced values for both parameters improve charge injection, which improves conductivity. Due to improved charge flow, COOH - SWCNT and various-sized MWCNT lower the device's transition voltage, also known as the turn-on voltage. Pertaining to lowering junction barrier and trap energy, it is seen that the device performance under the influence of COOH - SWCNT and 8 nm diameter MWCNT is much better than MWCNT cell with 30 nm diameter. Charge separation and relaxation process is improved by smaller sizes of COOH - SWCNT and 8 nm diameter MWCNT, which improves efficacy of charge infusion in the device.

5.5 References

[1] S. Kumar and S .S. K. Iyer, "Metal–organic semiconductor interfacial barrier height determination from internal photoemission signal in spectral response measurements", Journal of Applied Physics, 2017, **121**, 143104-1−143104-6

[2] S. Chakraborty and N. B. Manik, "Effect of COOH-functionalized SWCNT addition on the electrical and photovoltaic characteristics of Malachite Green dye based photovoltaic cells", Journal of Semiconductors, 2014, **35**, 124004-1-124004-6

[3] J. G. Park, Q. Cheng, J. Lu, J. Bao, S. Li, Y. Tian, Z. Liang, C. Zhang and B. Wang, "Thermal conductivity of MWCNT/epoxy composites: The effects of length, alignment and functionalization", Carbon, 2012, **50**, 2083-2090

[4] B. Kumanek and D. Janas, "Thermal conductivity of carbon nanotube networks: a review", Journal of Materials Science, 2019, **54**, 7397-7427

[5] M. Yang, X. Li, W. Wang, S. Zhang and R. Han, "Adsorption of methyl blue from solution by carboxylic multi-walled carbon nanotubes in batch mode", Desalination and Water Treatment, 2019, **159**, 365-376

[6] A. Raducan, A. Olteanu, M. Puiu and D. Oancea, "Influence of surfactants on the fading of malachite green", Central European Journal of Chemistry, 2008, **6**, 89-92

[7] B. P. Cho, T. Yang, L. R. Blankenship, J. D. Moody, M. Churchwell, F. A. Beland and S. J. Culp, "Synthesis and characterization of N-Demethylated Metabolites of Malachite Green and Leucomalachite Green", Chemical Research in Toxicology, 2003, **16**, 285-294

[8] C. R. Shugrue, H. H. Mentzen and B. R. Linton, "A colorful solubility exercise for organic chemistry", Journal of Chemical Education, 2015, **92**, 135-138

[9] T. Zhang, C. Raynaud and D. Planson, "Measure and analysis of 4H-SiC Schottky barrier height with Mo contacts", The European Physical Journal Applied Physics, 2019, **85**, 10102-1−10102-9

[10] S. Sen and N. B. Manik, "Effect of COOH-Functionalized Single Walled Carbon Nanotubes (COOH-SWCNT) on the Interfacial Barrier Height of Malachite Green (MG) Dye Based Organic Device", Physics International, 2019, **10**, 1-7

[11] D. K. Patel, H. B. Kim, S. D. Dutta, K. Ganguly and K. T. Lim, "Carbon Nanotubes-Based Nanomaterials and Their Agricultural and Biotechnological Applications", Materials, 2020, **13**, 1679-1-1679-28

[12] S. Sen and N. B. Manik, "Effect of Different Sized Multi Walled Carbon Nanotubes on the Barrier Potential and Trap Concentration of Malachite Green Dye Based Organic Device", Advances in Materials Science, 2020, **20**, 16-26

Chapter 6

Effects of SWCNT and MWCNT on the Charge Injection Mechanism of Methyl Red (MR) Dye Based Device

6.1 Introduction

Effects of COOH - SWCNT and multifarious MWCNT on barrier potential and trap concentration of an organic device based on MG dye were investigated in the preceding chapter.

We will form an organic device based on Methyl Red (MR) dye in this chapter. We will investigate organic device's junction barrier and depletion layer width, and we will also see how SWCNT affect both of these factors. The MR dye based device will be described in this chapter using the R–S model. Utilizing I -V characteristics, we will calculate the junction barrier. The Norde technique will then be used to ensure the accuracy of the results. Additionally, the device's capacitance-voltage (C -V) characteristics will be examined to calculate junction barrier and depletion layer width. I -V diagram will be used to calculate the device's threshold voltage. We will see what SWCNT does to these factors. SWCNT possesses certain characteristics that can lower all of these parameters **[1]**.

6.2 Experimental Details with the Incorporation of SWCNT

The impact of SWCNT on various junction parameters of the M/O contact of prepared organic device will be analyzed in this part.

6.2.1 Materials and Sample Preparation

The composition of Methyl Red (4-dimethylaminobenzene-2-carboxylic acid), is a common aromatic anionic azo compound with the chemical formula $(CH_3)_2NC_6H_4N{=}NC_6H_4COOH$, is illustrated in **Fig. 6.1 (a)**. MR dye is procured from Sigma Aldrich. Two molecular rings with double bonds inside of them namely benzene rings make up the composition of Methyl Red. Two nitrogen atoms, collectively referred to as an azo group, link the two aromatic rings **[2–3]**. Additionally, Methyl Red has a carboxylic acid functional group (-COOH). A nitrogen atom is joined to two methyl ($-CH_3$) groups, which is known as an amine functional group, directly across the molecule from the carboxylic acid group. This dye's molecular structure is $C_{15}H_{15}N_3O_2$ **[4]**. The N=N group, which makes up the azo group, is stabilized by being a member of an extended delocalized system because the R and R' groups of azo compounds are aromatic **[5]**. Methyl Red is a fascinating substance for creating schottky contact at the M/O interface due to its conjugated structure and richness in 16π electrons. SWCNT, with a width of 2 nm and a length of 30 µm, is shown in **Fig. 6.1 (b)**. ITO coated glass plate and Al are used as front electrode and as back electrode respectively.

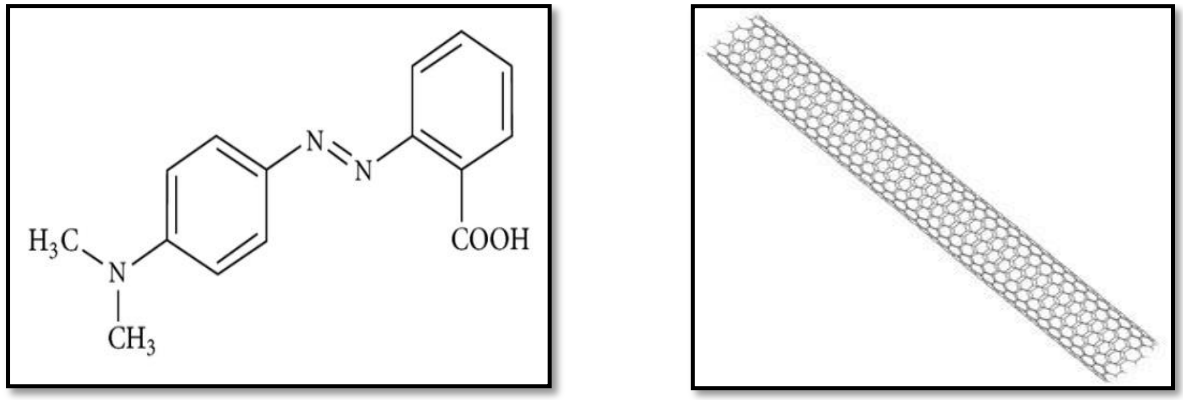

(a) **(b)**

Fig. 6.1 Structural Visualization of **(a)** MR dye and **(b)** SWCNT

PVA solution making technique has been mentioned in **chapter 3** and **chapter 4**. The PVA solution is then combined with 1 mg of MR dye, and the mixture is swirled to create MR dye solution. To retain this solution, two different test tubes are taken. One test tube contains MR dye solution. In another test tube, 1 mg of SWCNT is introduced. The MR-SWCNT mixture is thoroughly mixed for about an hour. Now, using a spin coater with a 1500 rpm spinning speed and drying at 3500 rpm, the mixture of MR and SWCNT is applied to ITO-coated glass plate. The same solution is deposited on Al anode using the same procedure as described above. Then, ITO and Al electrodes that are both in a semi-dry state are sandwiched to create the device consist of MR dye with SWCNT. Device consists of no nanotube except MR dye has also been formed using the same process. Before characterizing, these produced devices are dried in vacuum desiccator for 24 hours.

6.2.2 Measurements

Dark I -V measurement technique has already been mentioned in earlier chapters. The cells' C -V characteristics have been measured by using LCR meter. With a delay of 1000 ms, applied voltage's variation is from -5 V to 5 V with an increment of 0.25 V. Experiment is conducted at a temperature of 25°C in the laboratory's open environment.

6.2.3 Results and Discussions

Charge flow is described by using R–S model, as depicted in **equation (3.1)** to **equation (3.3)**, in the **chapter 3**. **Fig. 6.2** displays dark I -V properties of the devices. For the MR dye being used in the experiment, the dark current is quite small. But when SWCNTs are used, the current almost doubles.

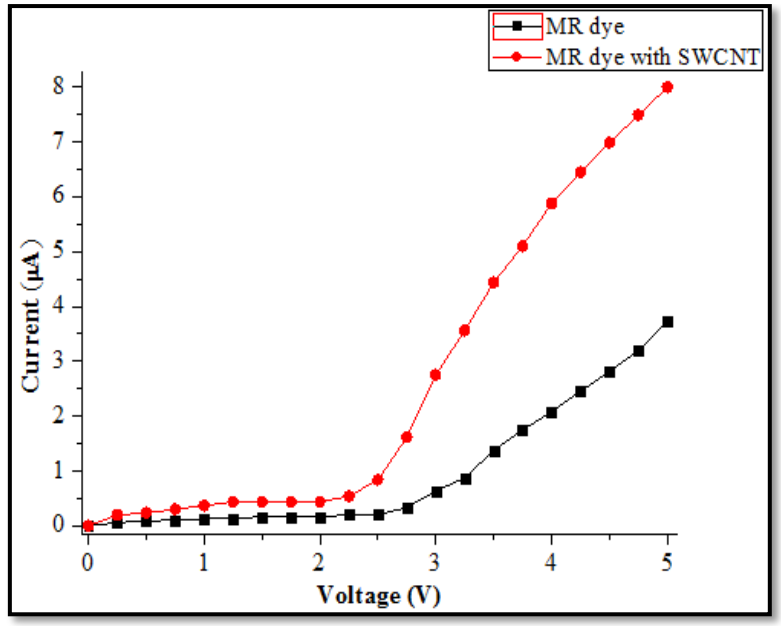

Fig. 6.2 I -V plots of device without and with SWCNT at 25°C

Fig. 6.3 displays I -V plots of an organic device based on MR dye at various temperatures and for a voltage range of -5 V to +5 V. In **Fig. 6.3**, the current flow rises with rising temperature along with increasing voltage range of -5 V to +5 V. Four different values of I_0 are estimated at four distinct temperatures i.e. 298 K, 318 K, 338 K, and 358 K respectively.

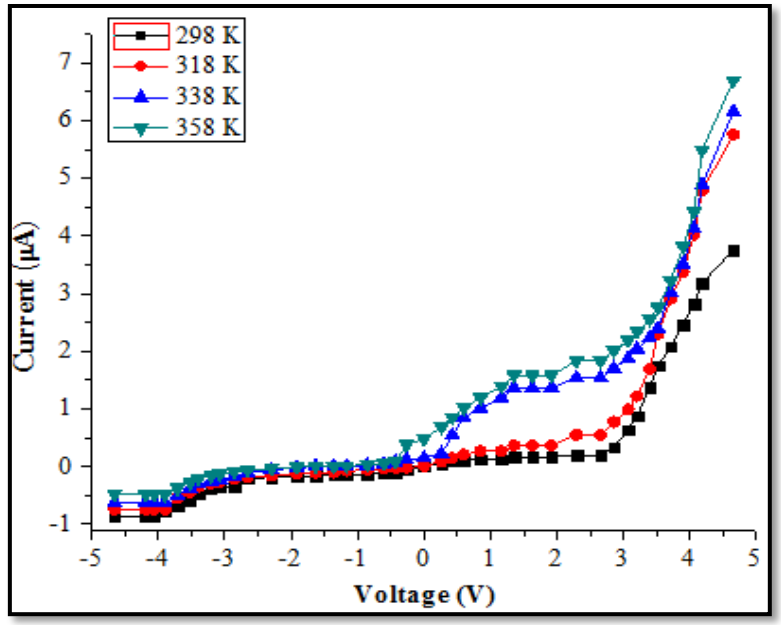

Fig. 6.3 I -V plots of device at different temperatures of 298 K, 318 K, 338 K and 358 K

From **equation (3.3)** of **chapter 3**, the derived equations are given below **[6-8]**

$$\frac{I_0}{AT^2} = A^* \exp\left(-\frac{q\phi_b}{kT}\right) \quad \textbf{(6.1)}$$

Taking logarithmic transformation of **equation (6.1)**, **equation (6.2)** can be found out.

$$\ln\left(\frac{I_0}{AT^2}\right) = \ln(A^*) - \frac{q\phi_b}{kT} \quad \textbf{(6.2)}$$

By using **equation (6.2)**, the intercept of the plot of ln $(\frac{I_0}{AT^2})$ vs. $\frac{1000}{T}$ gives the value of Richardson constant (A*). **Fig. 6.4** illustrates ln $(\frac{I_0}{AT^2})$ vs. $\frac{1000}{T}$plot of the device.

A straight line in **Fig. 6.4** has an intercept, which is specified by Richardson constant and it is estimated to be 0.012 $Acm^{-2}K^{-2}$or 120 $Acm^{-2}K^{-2}$. Because of potential variations at the M/O contact, the value of the Richardson constant is quite low.

Height of barrier can be determined from **equation (3.4)**, which is already mentioned in **chapter 3**.

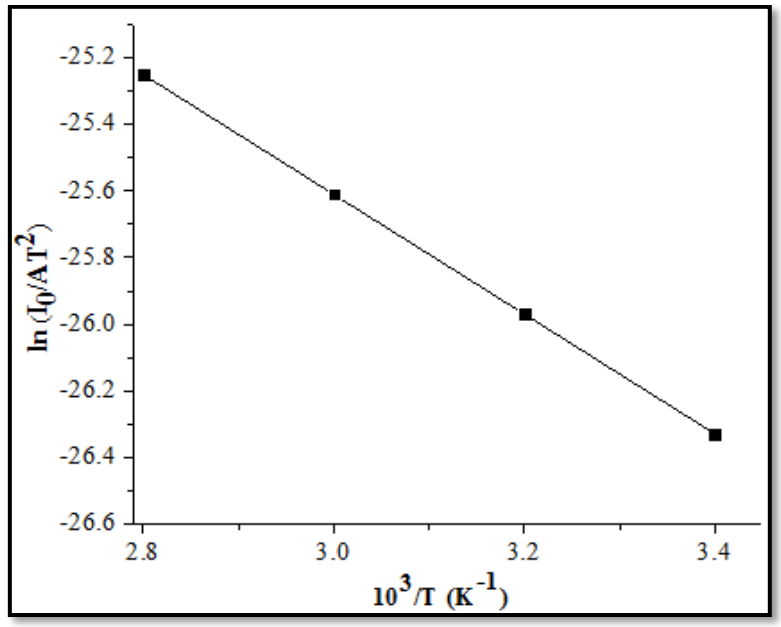

Fig. 6.4 Plot of ln $(\frac{I_0}{AT^2})$ vs. $\frac{1000}{T}$ extracted from I -V data at different temperatures of ITO/MR/Al structure

Fig. 6.5 shows ln I -V curves of device without and with SWCNT. The barrier height is calculated, which is 0.870 in absence of SWCNT and in presence of SWCNT, it reduces to 0.754 eV. I_0 is calculated from y-intercept of semilogarithmic I -V curves as shown in **Fig. 6.5**.

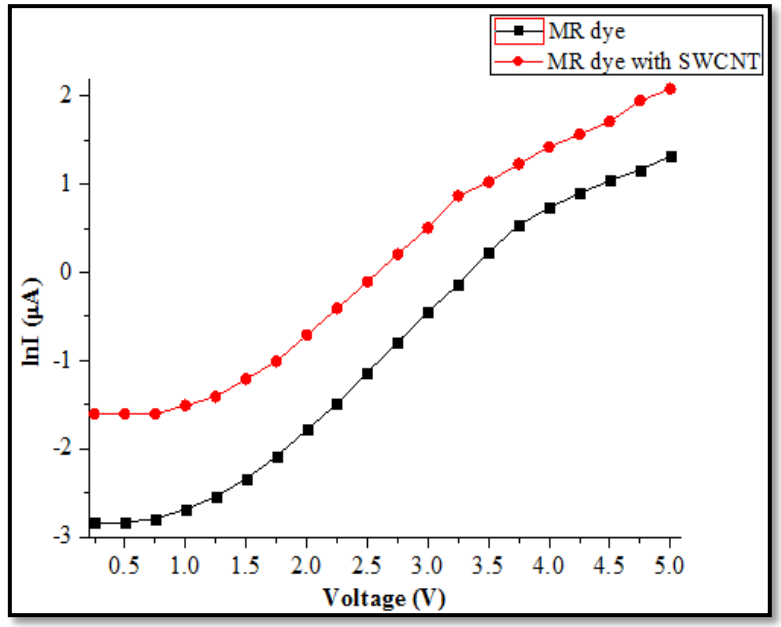

Fig. 6.5 ln I -V plots of device without and with SWCNT

Norde function, which has already been mentioned in **equation (3.5)** to **equation (3.8)** of **Chapter 3**, is used to measure barrier height. **Fig. 6.6** displays Norde function plots of devices without and with SWCNT.

This chapter also studies the influence of image charges on decreasing barriers. An external electric field and the Coulomb field work together to limit the carrier injection from metal to organic layer **[9]**. According to **equation (6.3)**, this superposition binds both carrier and the image of carrier on the electrode

$$U(x) = \phi_b - \frac{e^2}{16\pi\varepsilon_0\varepsilon x} - eFx \qquad \textbf{(6.3)}$$

Where, all symbols have their standard meaning.

To determine the effective barrier height, image charge effect has also been studied, both without and with SWCNT. The potential distribution is 3 nm from the junction and the applied field is 10^6 V/cm with a dielectric constant of 3.5.

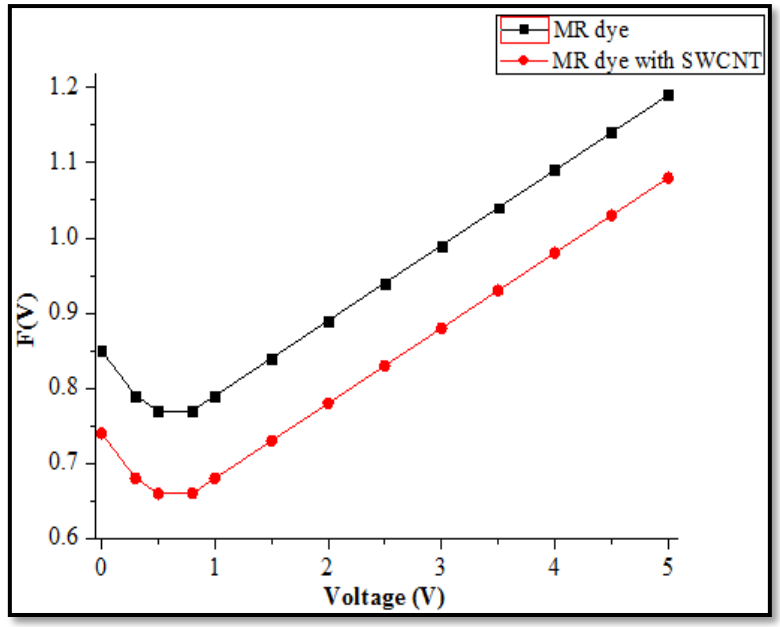

Fig. 6.6 Norde Function plots of device without and with SWCNT

The C -V characteristics have also been analyzed to determine both barrier height and the space - charge layer width of the device **[10]**.

Equation (6.4) can be used to estimate the space - charge layer width of the device.

$$W_d = \mp\sqrt{\frac{2\varepsilon_0\varepsilon_s V_d}{qN_D}} \qquad \textbf{(6.4)}$$

Where, all symbols have their standard meaning.

At a constant frequency of 10 kHz, the C -V curves of the device are shown in **Fig. 6.7** without and with SWCNT. **Fig. 6.7** shows that, the device exhibits greater capacitance with SWCNT.

The C^{-2} -V curves of device are shown in **Fig. 6.8** without and with SWCNT, respectively. The barrier height and the diffusion potential have been calculated using these characteristics.

The barrier height will differ slightly when it is measured using the C -V and I -V methods because C -V method averages the entire region to measure the height of the barrier **[11]**. The varying extraction procedures of I -V and C -V methods from various regions are the reason for the little discrepancies in barrier height **[12-13]**.

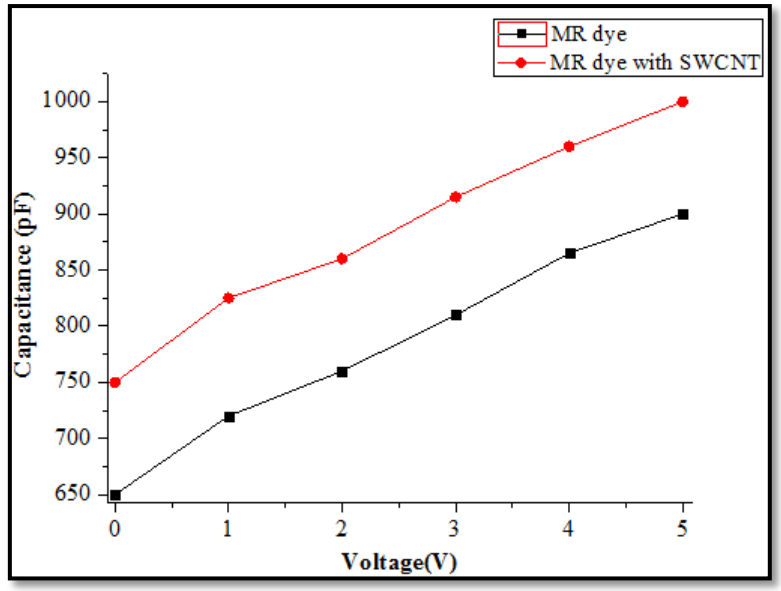

Fig. 6.7 C -V plots of device without and with SWCNT

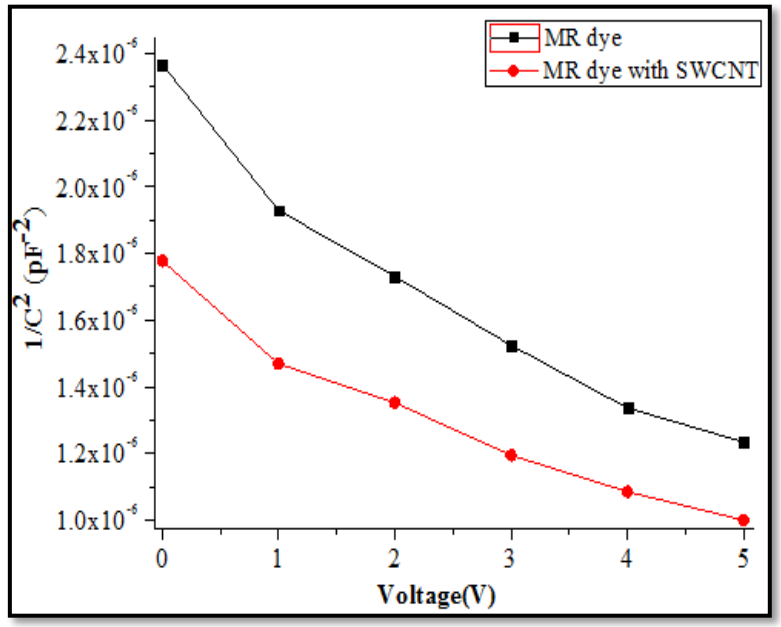

Fig.6.8 C^{-2}-V plots of device without and with SWCNT

Equation (6.5) shows the expression of the ideality factor (n) of the device.

$$n = \frac{q}{kT}\frac{dV}{d(\ln I)} \qquad \textbf{(6.5)}$$

6.3 Experimental Details with the Incorporation of MWCNT

This section will look into the effects of MWCNTs with diameters of 8 nm, 30 nm and 50 nm on the various electrical parameters of device based on MR dye.

6.3.1 Materials and Sample Preparation

Different sized MWCNT i.e. 8 nm diameter, 30 nm diameter and 50 nm diameter MWCNT are used in this work. Details of MWCNTs have already been mentioned in **chapter 5**. We have used the solvent dichloromethane (DCM), whose molecular weight is 84.93, and it is bought from Sigma Aldrich, because it readily dissolves organic compounds. The following **Fig. 6.9 (a)** and **Fig. 6.9 (b)** illustrate the structures of MWCNT and DCM respectively.

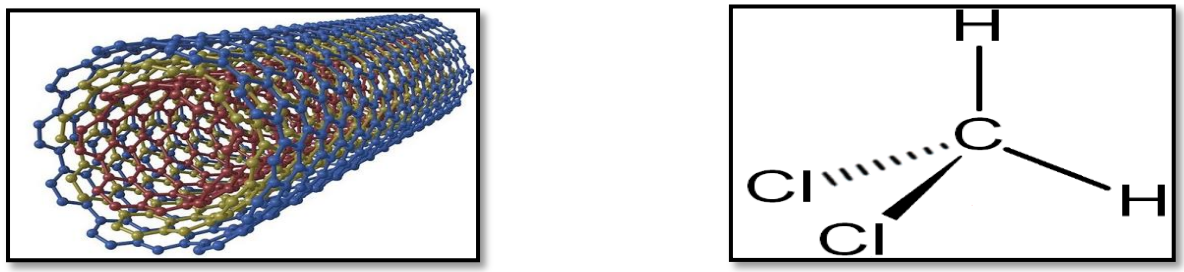

(a) **(b)**

Fig. 6.9 Structures of **(a)** MWCNT and **(b)** DCM

Details of PMMA have already been mentioned in the earlier **chapter 5**. In a clean test container, 1 mg of PMMA is dissolved by adding 15 ml of DCM. To obtain a clear solution, the combination is next stirred for 1 hour at room temperature using a magnetic stirrer. Since PMMA container solution has good weathering resistance and good transparency, it is used in our work as a binder material. PMMA solution is combined with 1 mg of MR dye and swirled for 30 minutes. Four portions of the prepared solution are divided among four test containers. The three test tubes each contains MWCNT of size 8 nm, 30 nm, and 50 nm, which are introduced and stirred separately for three hours to create well-mixed dye and MWCNT solutions. The fourth test tube only contains MR dye solution without any nanotube. The same sample preparation techniques that are described in **section 6.2.1** are used. Before analysis, all cells are vacuum-dried at room temperature for 24 hours.

6.3.2 Measurements

The same testing technique as described in **section 6.2.2** is used. At a temperature of 25^0C, measurements are made in the 0 V to 5 V regions.

6.3.3 Results and Discussions

Fig. 6.10 displays I -V plots of devices without and with various sized MWCNT.

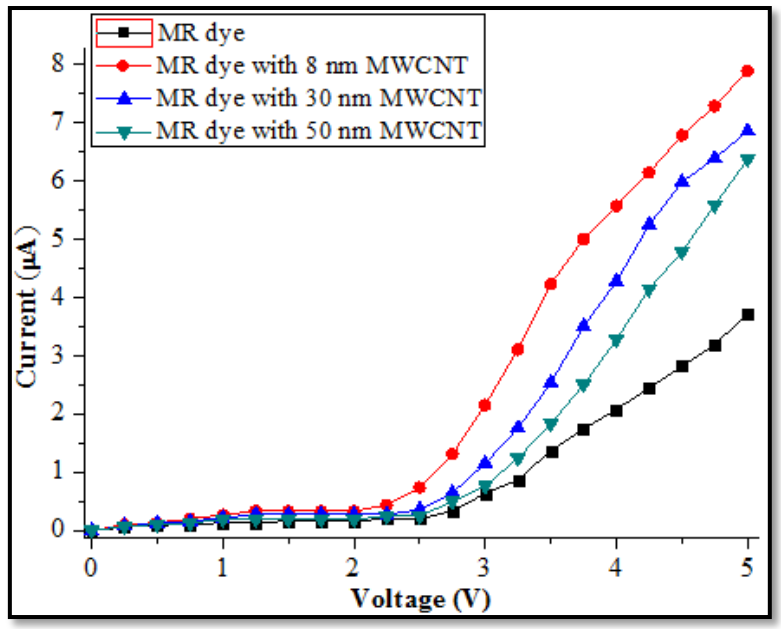

Fig. 6.10 I -V plots of device without and with different sized MWCNT

MWCNT incorporation also substantially enhances the device's current flow. Additionally, it has been noted that the current flow rises more quickly in presence of 8 nm diameter MWCNT than it does in the presence of 30 nm or 50 nm diameter MWCNT. ln I -V plots of **Fig. 6.10** have been shown in **Fig. 6.11** to calculate junction barrier and the ideality factor.

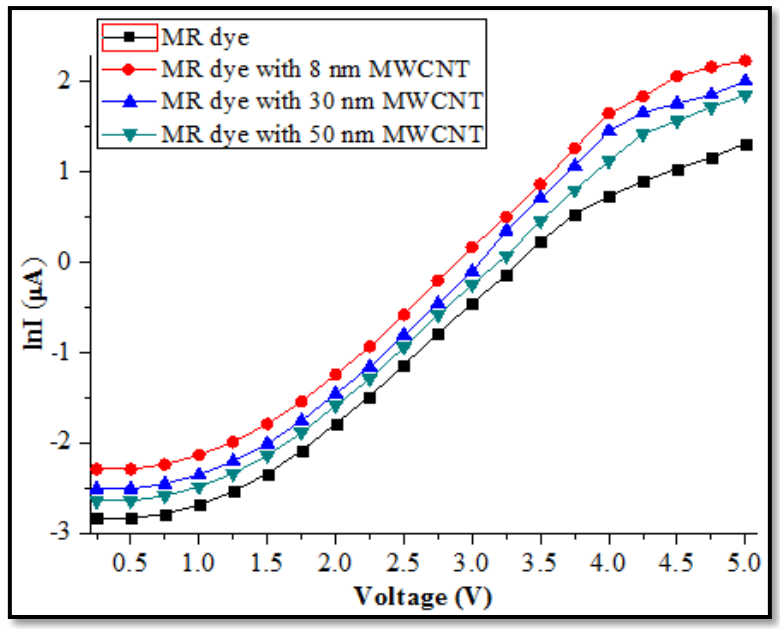

Fig. 6.11 ln I -V plots of device without and with different sized MWCNT

Norde function plots of the device in presence and in absence of various sized MWCNTs are illustrated in **Fig. 6.12**.

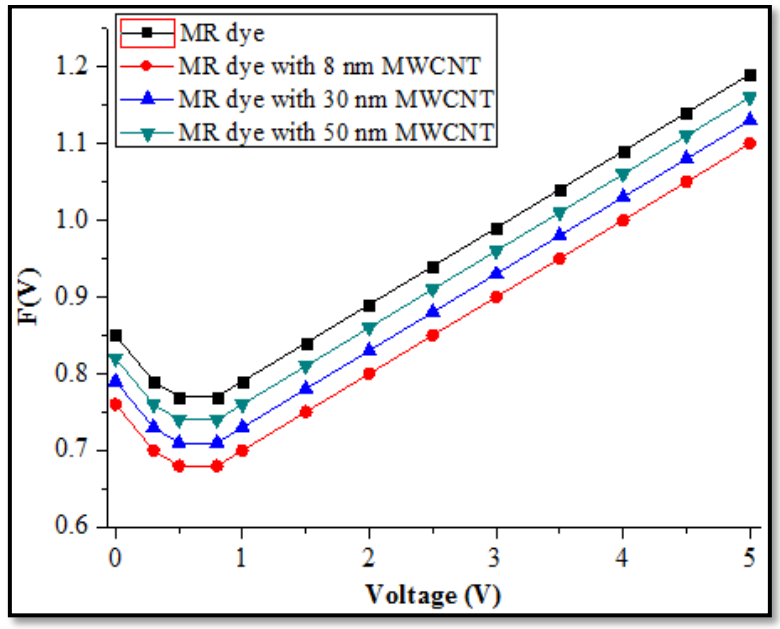

Fig. 6.12 Norde Function plots of device without and with different sized MWCNT

As it has been measured without and with SWCNT, the effective barrier is also estimated taking into account image charge effect when 8 nm, 30 nm, and 50 nm MWCNTs are present, respectively. The applied field, the dielectric constant's value, and the distribution of potential at the interface all stay the same as mentioned previously in this chapter.

C -V plots of device can also be used to estimate the barrier height and depletion layer width of device. The device's C -V properties are shown in **Fig. 6.13** both with and without MWCNTs of various sizes.

The C^{-2} -V graphs of device are shown in **Fig. 6.14** with and without MWCNTs of various sizes, respectively.

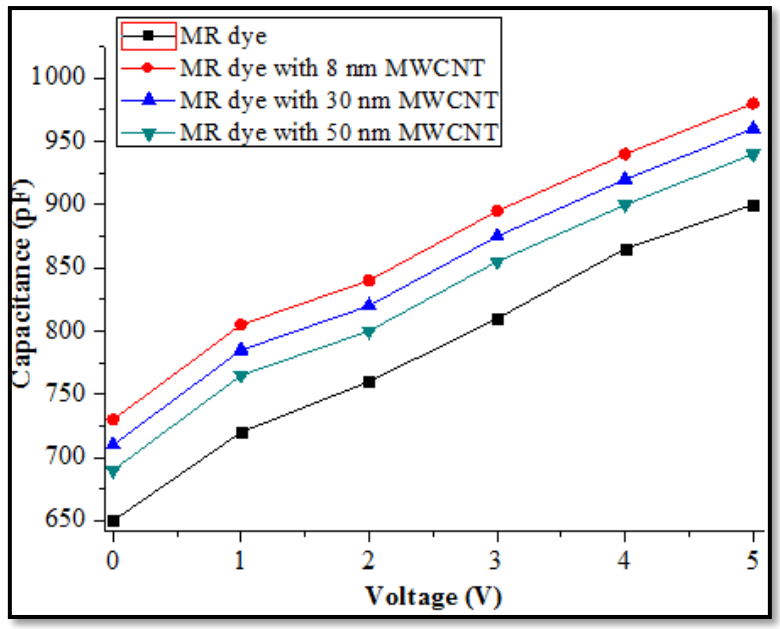

Fig. 6.13 C -V plots of device without and with different sized MWCNT

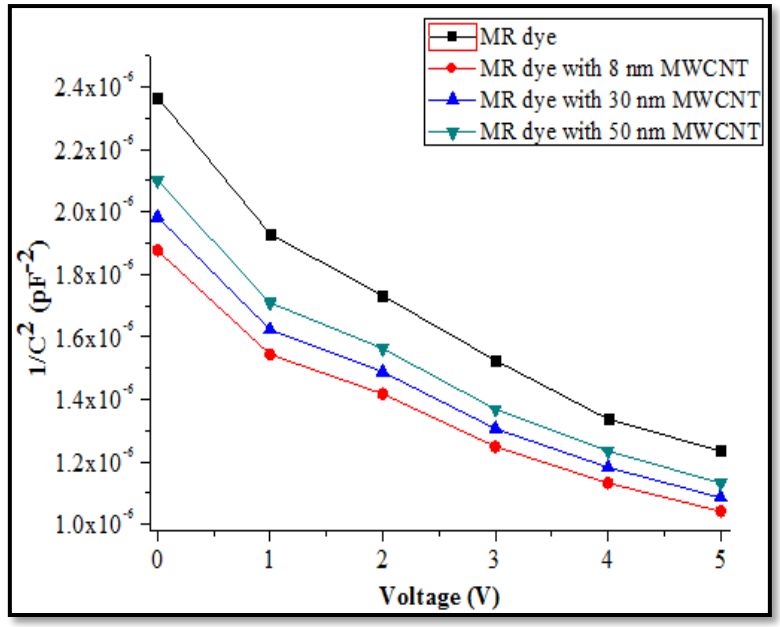

Fig. 6.14 C^{-2}-V plots of device without and with different sized MWCNT

Table 6.1 expresses the parameters of dark I -V characteristics of the device under the influence of SWCNT and different sized MWCNT.

From **Table 6.1**, it can be seen that the three methods i.e I -V, Norde and C -V methods show the reduction of barrier height as 13.79%, 12.94% and 15.47% respectively with SWCNT, 11.49%, 10.58% and 10.71% respectively with 8 nm diameter MWCNT, 5.88%, 8.23% and 8.33% respectively with 30 nm diameter MWCNT and with 50 nm diameter MWCNT, the reduction becomes 5.74%, 7.05% and 4.76% respectively. The threshold voltage and depletion layer width also exhibit reductions of 48.41% and 9.77% with SWCNT, 40.48% and 7.36% with MWCNT of 8 nm diameter, 30.55% and 5.40% with MWCNT of 30 nm diameter, and 20.63% and 4.023% with MWCNT of 50 nm diameter. When SWCNT and MWCNT of various sizes are present, the ideality factor is also significantly reduced. With SWCNT and different sized MWCNT, the effective barrier height taking image charge into account decreases considerably. Reducing barrier height and depletion layer width will aid in improving the charge infusion, which will enable device to be switched on at significantly lower voltages.

Table 6.1 Parameters of Dark I -V characteristics of MR dye based organic devices under the influence of SWCNT and different sized MWCNT

Parameters	MR Dye Based Device				
	Without any Nanotubes	**With SWCNT**	**With 8 nm MWCNT**	**With 30 nm MWCNT**	**With 50 nm MWCNT**
Threshold Voltage (V)	2.520	1.300	1.500	1.750	2.000
Ideality Factor	5.570	0.680	0.760	0.980	1.570
Barrier Height (eV) using I -V characteristics	0.870	0.750	0.770	0.800	0.820
Barrier Height (eV) using Norde Method	0.850	0.740	0.760	0.780	0.790
Barrier Height from C -V characteristics (eV)	0.840	0.710	0.750	0.770	0.800
Effective Barrier Height Considering Image Charge Lowering Effect (eV)	0.840	0.630	0.670	0.680	0.720
Depletion Layer Width (W_d) (cm) × 10^{-6}	8.700	7.850	8.060	8.230	8.350

Table 6.1 also demonstrates that, SWCNT and 8 nm MWCNT work better than MWCNTs of 30 nm and 50 nm in terms of performance. In comparison to MWCNT with middle and high (30 and 50 nm) diameters, SWCNT and MWCNT with the smallest 8 nm diameter will have the higher aspect ratio. When MWCNT is used in an organic device, its aspect ratio will have a significant impact on both its mechanical and electrical characteristics **[14]**. Smaller-diameter MWCNT exhibit superior performance. Along with the rise in aspect ratio, the electrical conductivity percolation threshold also drops **[15–16]**. Compared to 30 nm diameter and 50 nm diameter MWCNT, these characteristics make both SWCNT and 8 nm diameter MWCNT outstanding additives in electrically conductive

polymer applications, which will improve the charge infusion. The efficacy of organic optoelectronic devices will also be improved by improved charge injection processes.

6.4 Conclusions

We have looked at how SWCNT and MWCNT of various sizes – each with a width of 8 nm, 30 nm, and 50 nm – affected the various factors influencing charge infusion of devices. One of the major causes of lower infusion of carriers from M/O layer is contact barrier. I -V and C -V characteristics, as well as Norde technique, are used to analyze contact barrier values for devices. These three techniques' extractions of barrier height are fairly consistent with one another. The injection barrier and depletion layer width at M/O contact are decreased with SWCNT and various sized MWCNT. Higher conductivity is obtained by improving charge injection procedure and lowering barrier height and depletion layer width. Due to a decrease in interfacial barrier and depletion layer width, the device's threshold voltage has also been reduced. SWCNT and MWCNT of various sizes have been found to substantially reduce device's ideality factor, which can be ascribed to trap concentration lessening at interface. In this chapter, the impact of the image charge on the device's effective barrier has also been taken into account. In comparison to 30 nm diameter and 50 nm diameter MWCNT, SWCNT and 8 nm diameter MWCNT have higher aspect ratios and percolation thresholds, which leads to substantially improved charge infusion.

6.5 References

[1] G. Mittal, V. Dhand, K. Y. Rhee, S. J. Park and W. R. Lee, "A Review on Carbon Nanotubes and Graphene as Fillers in Reinforced Polymer Nanocomposites", Journal of Industrial and Engineering Chemistry, 2015, **21**, 11-25

[2] E. W. Wysiecka, N. Łukasik, J. F. Biernat and E. Luboch, "Azo group(s) in selected macrocyclic compounds", Journal of Inclusion Phenomena and Macrocyclic Chemistry, 2018, **90**, 189-257

[3] A. Banerjee, C. Ghosh and P. Chakraborty, "Methyl red/ indium-tin-oxide organic diode: an electrical and optoelectronic study", Microelectronic Engineering, 2019, **216**, 111053-1-111053-6

[4] A. Salem, "Conduction Mechanism under DC and AC Fields of Methyl Red Dye as a New Organic Semiconductor", Acta Physica Polonica A, 2019, **136**, 952-956

[5] T. Kılıçoğlu, M. E.Aydın and Y. S. Ocak, "The determination of the interface state density distribution of the Al/ methyl red/p-Si Schottky barrier diode by using a capacitance method", Physica B, 2007, **388**, 244-248

[6] C. Ghica, L. Ion, G. Epurescu, L. Nistor, S. Antohe and M Dinescu, "Organic Photovoltaic Cells Based on ZnO Thin Film Electrodes", Journal of Nanoscience and Nanotechnology, 2010, **10**, 1322-1326

[7] K. Sarpatwari, O. O. Awadelkarim, M. W. Allen, S. M. Durbin, and S. E. Mohney, "Extracting the Richardson constant: IrO_x/n-ZnO Schottky diodes", Applied Physics Letters, 2009, **94**, 242110-1-242110-3

[8] S. Sen and N. B. Manik, "Modification of Barrier Height and Depletion Layer Width of Methyl Red (MR) Dye - Based Organic Device in Presence of Single - Walled Carbon Nanotubes (SWCNT)", Indian Journal of Physics, 2022, **96**, 385-390

[9] V. I. Arkhipov, U. Wolf and H. Bässler, "Current injection from a metal to a disordered hopping system. II. Comparison between analytic theory and simulation", Physical Review B, 1998, **59**, 7514 - 7520

[10] N. Li, X. D. Gao, B. F. Ding, X. Y. Sun, X. M. Ding and X. Y. Hou, "Determination of capacitance-voltage characteristics of organic semiconductor devices by combined current-voltage and voltage decay measurements", Science China Technological Sciences, 2011, **54**, 826-829

[11] Ö. Güllü, "Barrier Modification by Methyl Violet Organic Dye Molecules of Ag/P-Inp Structures", European Journal of Interdisciplinary Studies, 2016, **2**, 7-17

[12] Ö. Güllü and A. Türüt, "Electronic parameters of MIS Schottky diodes with DNA biopolymer interlayer", Materials Science-Poland, 2015, **33**, 593-600

[13] Y. Y. Kudryk, V. V. Shynkarenko, V. S. Slipokurov, R. I. Bigun and R. Y. Kudryk, "Determination of the Schottky barrier height in diodes based on Au–TiB_2–n-SiC 6H from the current-voltage and capacitance-voltage characteristics", Semiconductor Physics, Quantum Electronics & Optoelectronics, 2014, **17**, 398-402

[14] M. R. Ayatollahi, S. Shadlou, M. M. Shokrieh and M. Chitsazzadeh, "Effect of multi –walled carbon nanotube aspect ratio on mechanical and electrical properties of epoxy – based nanocomposites", Polymer Testing, 2011, **30**, 548-556

[15] Y. Zare and K. Y. Rhee, "Calculation of the Electrical Conductivity of Polymer Nanocomposites Assuming the Interphase Layer Surrounding Carbon Nanotubes", Polymers, 2020, **12**, 404-1-404-1

[16] S. Sen and N. B. Manik, "Effect of Different Sized Multi Walled Carbon Nanotubes on the Parameters Affecting the Charge Injection Process of Methyl Red Dye Based Organic Device", Journal of Material Sciences and Engineering, 2021, **10**, 1-5

Chapter 7

Effect of Back Electrode on Trap Energy and Injection Barrier Height of Crystal Violet (CV) Dye Based Device

7.1 Introduction

In the preceding chapter, we elucidated the effects of incorporating SWCNT and various-sized MWCNT in the device and studied junction barrier of a MR dye based device without or after analyzing image charge effect and space - charge layer width. The organic device's I -V and C-V characteristics had both been analyzed in order to determine the aforementioned device parameters. Additionally, we calculated the organic device's ideality factor and threshold voltage in the presence and lack of SWCNT and various-sized MWCNT.

The effects of ZnO, TiO_2, SWCNT and MWCNT on various parameters affecting the charge infusion and charge entrapment process at M/O contact of various organic dye based devices had been studied from **chapter 3** to **chapter 6**.

Now, in this chapter, we will observe the impact of counter electrodes on the parameters that affect charge infusion in the organic dye based devices. Typically, transparent glass plates with high work functions are used as the front electrode and materials with low work functions are used as counter electrode. The impact of the back electrode on barrier height and trap energy of these devices has not received much attention.

The impact of two distinct auxiliary electrodes, namely Al coated back electrode and Al-M sheet-based back electrode, on barrier height and trap energy of devices will be examined in this chapter. As front electrode, glass is covered with ITO. Crystal Violet (CV) dye will be used as an organic material to form the device.

In essence, difference between metal's fermi energy and organic substance's energy band is what determines barrier height **[1]**. The area below threshold voltage is where injection-limited current at the M/O interface typically flows. Both thermionic injection current and tunneling current caused by a field are typically components of injection current. Field-induced tunneling current is so negligible at low voltage that it can be disregarded. Because of this, the prepared device will be described using R-S model of thermionic emission **[2–3]**.

7.2 Materials and Sample Preparation

Structure of CV dye is displayed in **Fig. 7.1** and it is purchased from Loba Chemie Private Ltd. in India. The cationic dye CV, with the molecular formula [$C_{25}N_3H_{30}Cl$], dissociates in water to produce

a positively charged coloured ion **[4-5]**. As an optically active substance, CV dye is used **[6]**. Al – M sheet has a higher reflectivity than regular Al.

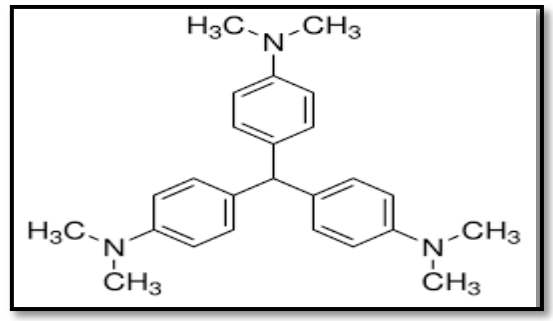

Fig. 7.1 Structural diagram of CV dye

The CV dye is recrystallized twice from an ethanol-water combination and combined with PVA to create PVA solution. PVA is partly hydrolyzed. It functions to create a gel-like solution. Its compatible structure and hydrophilic qualities are used to improve the mechanical qualities of organic dye sheets. 10 cc of double-distilled water and 5 mg of PVA were combined in a clean test container and stirred to create the transparent viscous PVA solution. The CV pigment is dissolved in 2 mg of this mixture. After being cleaned in a chloroform solution, the electrodes are dried in a vacuum desiccator. The thin film is sandwiched between ITO-coated glass and another sheet of Al-coated mylar that serves as the reflecting back surface with the aid of a viscous gel-like solid solution. The spin coating process is used to create the thin films having uniform distribution. Using aforementioned process, another thin layer is also created using an ITO-coated glass and Al plates as the counter electrode. For about 12 hours, these cells are dried in a vacuum desiccator.

7.3 Measurements

The same measurement technique is followed as mentioned in the **Measurements** section of preceding chapters. The voltage range is from 0 to 6 V with increment of 0.25 V and delay of 500 ms. Temperature is kept at 26^0C throughout the measurement process.

7.4 Results and Discussions

Equation (3.1) to **equation (3.3)** of **chapter 3** is used to explain current flow. The **equation (3.4)** in **chapter 3** is used to calculate the height of barrier.

In **Fig. 7.2**, the dark I -V properties of CV dye in presence of Al-M auxiliary electrode and an Al auxiliary electrode, are depicted. Al-M back electrode greatly improves the current flow in the device when compared to Al counter electrode.

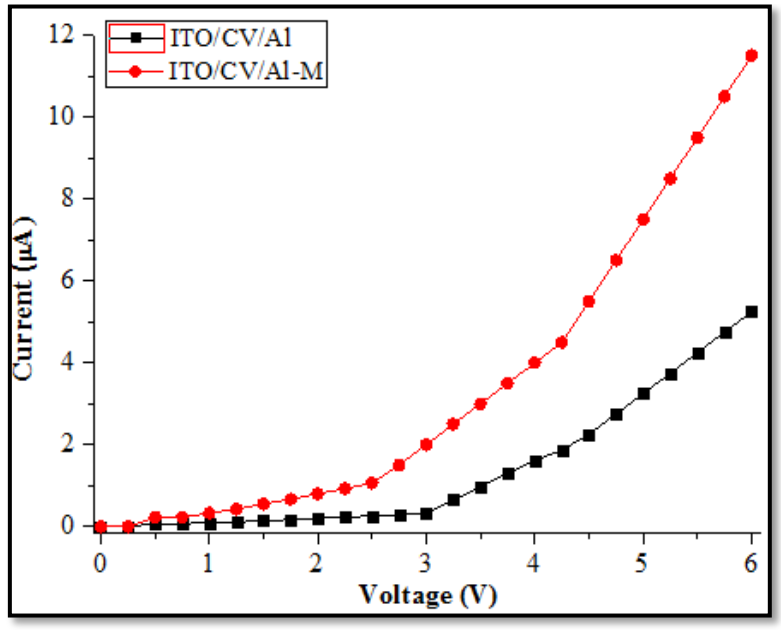

Fig. 7.2 I -V plots of ITO/CV/Al based organic device and ITO/CV/Al-M based device

We have drawn ln I -V plots of I -V graphs of both devices comprising of Al and Al-M counter electrode respectively in **Fig. 7.3**. These plots are used to determine the interfacial barrier. **Fig. 7.3** reveals that the ITO/CV/Al-M based organic device's barrier height is lower than that of the ITO/CV/Al based organic device.

While calculating barrier height, Norde function is employed. The Norde function plots of both the structures are displayed in **Fig. 7.4**.

We have drawn ln I - ln V curves of both the structures, which are shown in **Fig. 7.5**, to determine trap energy.

The expression for the trap energy concentration (N_t) is given in **equation (7.1)**

$$N_t(\epsilon) = N_0 \exp\left(-\frac{\epsilon}{kT_c}\right) \quad \textbf{(7.1)}$$

Where, ϵ denotes the depth of traps below conduction band mobility boundary and other symbols carry their standard meaning.

Equation (7.2) can be used to express trap energy **[7-10]**.

$E_t = mkT$ **(7.2)**

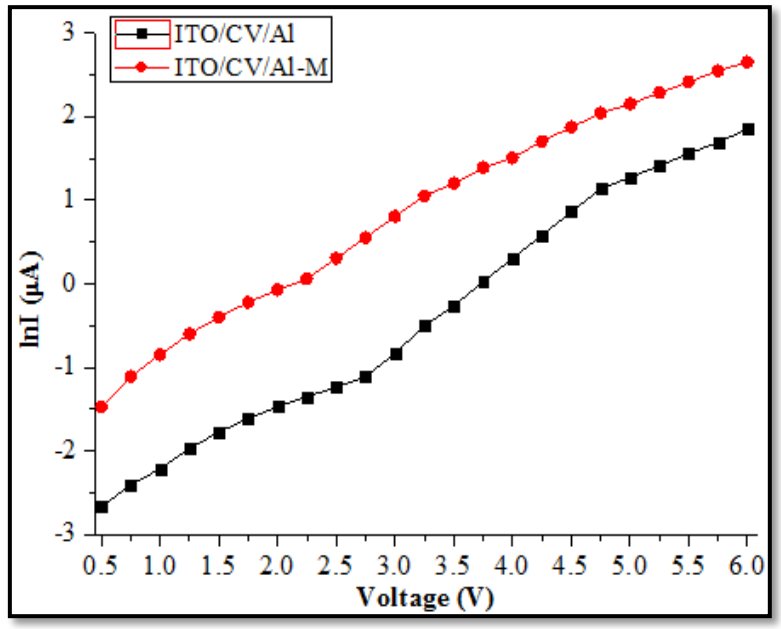

Fig. 7.3 ln I -V plots of ITO/CV/Al based organic device and ITO/CV/Al-M based device

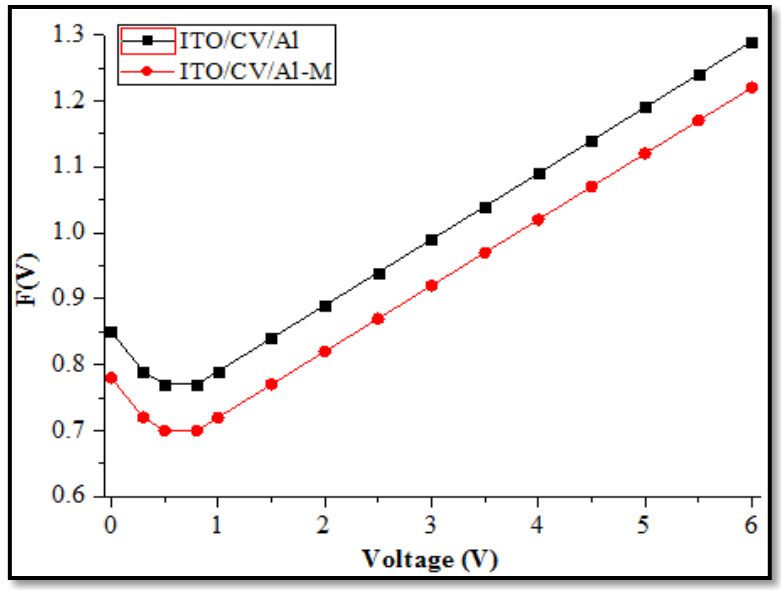

Fig. 7.4 Norde Function plots of ITO/CV/Al structure and ITO/CV/Al-M structure

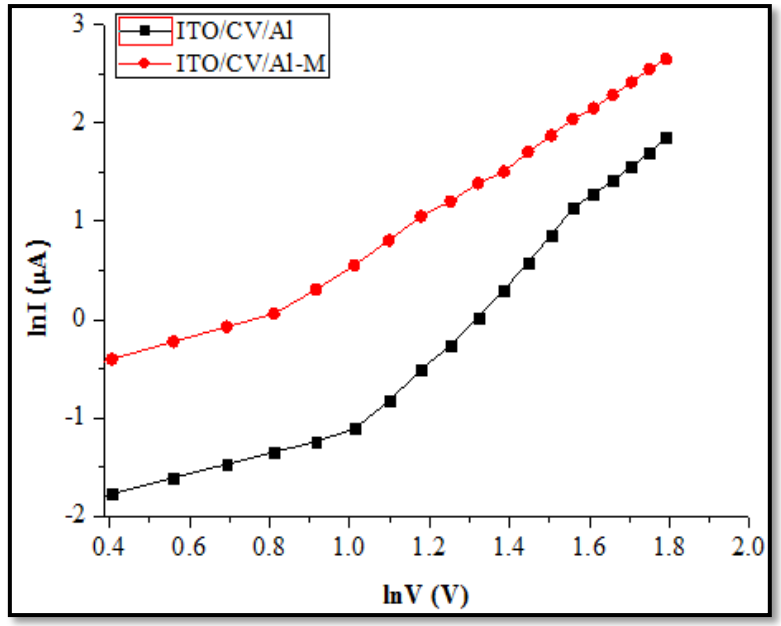

Fig. 7.5 ln I - ln V plots of ITO/CV/Al structure and ITO/CV/Al-M structure

Table 7.1 displays the estimation of barrier height and trap energy for both the structures.

Table 7.1 Calculation of barrier height and trap energy of devices with two different back electrodes

CV Dye Based Device	Value of m	Trap Energy (eV)	Barrier Height from I -V characteristics (eV)	Barrier Height using Norde Function (eV)
With Al electrode	1.710	0.044	0.800	0.830
With Al-M electrode	1.300	0.034	0.770	0.790

7.5 Conclusions

Throughout this chapter, we have looked at how the back electrode affects the organic devices' junction barrier and trap energy. When two different counter electrodes are present, the values of

junction barrier for devices are estimated by looking at the plot of I -V characteristics and also by using Norde technique. Both approaches exhibit strong agreement with one another. In comparison to Al back electrode, it can be said that barrier height and trap energy at interface have been significantly reduced with Al-M back electrode. In this device, the barrier lowering and reduction in trap energy enhance charge infusion, leading to improved conductivity.

7.6 References

[1] P. L. Bullejos, J.A. J. Tejada, M. J. Deen, O. Marinov and W. R. Datars, "Unified model for the injection and transport of charge in organic diodes", Journal of Applied Physics, 2008, **103**, 064504-1-064504-12

[2] D. K. De and O. C. Olawole, "A three-dimensional model for thermionic emission from graphene and carbon nanotube", Journal of Physics Communications, 2019, **3**, 015004-1-015004-17

[3] S. M. Sze and K. K. Ng, "Physics of Semiconductor Devices", 2007, [3rd ed.], John Wiley & Sóns, New York, 159-181

[4] D. Jayganesh, R. Tamilarasan, M. Kumar, M. Murugavelu, and V. Sivakumar, "Equilibrium and Modelling Studies for the Removal of Crystal Violet Dye from aqueous solution using eco-friendly activated carbon prepared from Sargassmwightii seaweeds", Journal of Materials and Environmental Sciences, 2017, **8**, 1508–1517

[5] R. Ragu, P. S. Latha Mageshwari, M. Akilan and S. Jerome Das, "Enhanced optical, mechanical, photoacoustic and third-order nonlinear property of pure and crystal violet (CV) dye incorporated anthracene crystal: an efficacious material for nonlinear optical applications", Applied Physics B, 2020, **126**, 95-1-95-10

[6] S. Goel, N. Sinha, H. Yadav, A. Hussain and B. Kumar, "Effect of crystal violet dye on the structural, optical, mechanical and piezoelectric properties of ADP single crystal", Materials Research Bulletin, 2016, **83**, 77-87

[7] P. Mark and W. Helfrich, "Space-Charge-Limited Currents in Organic Crystals", Journal of Applied Physics, 1962, **33**, 205-215

[8] S. M. H. Rizvi and B. Mazhari, "Investigation of Traps in Thin-Film Organic Semiconductors Using Differential Analysis of Steady-State Current–Voltage Characteristics", IEEE Transactions on Electron Devices, 2018, **65**, 3430-3437

[9] A. Haldar, S. Maity and N. B. Manik, "Effect of back electrode on photovoltaic properties of crystal-violet-dye-doped solid-state thin film", Ionics, 2008, **14**, 427-432

[10] S. Sen and N. B. Manik, "Effect of Back Electrode on Trap Energy and Interfacial Barrier Height of Crystal Violet (CV) Dye based Organic Device", Bulletin of Materials Science, 2020, **43**, 1- 4

Chapter 8

Findings and Conclusions

8.1 Summary

8.2 Findings of the Work

8.3 Overall Conclusion

8.4 Future Scopes of the Work

8.1 Summary

We have discussed charge injection and charge trapping process of organic semiconductor devices in the current thesis. These devices' charge injection is primarily controlled by the M/O interface, which is related to existence of traps because these devices are susceptible to traps. Barrier height and depletion layer width of M/O interface are typically reach a higher value due to interfacial trap density. However, there aren't many studies for organic semiconductors to determine these above mentioned parameters at M/O interface when traps are present.

In this context, interfacial barrier, trap concentration, depletion layer width, band bending, image force barrier lowering and barrier inhomogeneities at M/O interface considering charge trapping effect have been discussed. The different charge trapping models and its effect on charge injection process and different charge injection models have also been studied. The interfacial barrier height has also strong correlation with the interfacial band bending and image force barrier lowering effect of these organic devices.

We have calculated these parameters from I -V plots of these devices and correlate it with the trap energy at M/O interface. We have also observed the effect of ZnO, TiO_2, SWCNT and MWCNT on these parameters of the series of organic dyes such as PSF, Safranin - T, MG and MR dyes. We have studied the back electrode effect on the junction parameters of CV dye based devices.

We have designed our present work into the following chapters.

In **Chapter 1**, we have mentioned the objectives and background of this present work. The parameters that will affect the charge injection process, such as interfacial barrier height, concentration of traps, depletion layer width, band bending, and image force barrier lowering and barrier inhomogeneities at the metallic electrode - organic dye interface have also been mentioned.

In **Chapter 2**, we have discussed the different charge trapping and charge injection models in detail. The parameters such as interfacial barrier height, concentration of traps, depletion layer width, band bending, image force barrier lowering and barrier inhomogeneities that affect the charge trapping and charge injection process have also been mentioned. Different nanotubes and nanoparticles which have been incorporated in different organic dye based devices have also been elucidated in this chapter.

In **Chapter 3**, **Chapter 4**, **Chapter 5** and **Chapter 6**, we have investigated various junction characteristics, including trap energy, barrier potential, band bending, barrier inhomogeneity, and space - charge region width of various organic dye based devices. I -V measurements are used to

analyze the devices. We have also used Norde's approach to verify congruency of interfacial barrier calculated from I -V characteristics, and both approaches are still in strong agreement with one another. The interfacial barrier and trap energy have been analytically linked. Connection between barrier height and the depletion layer width has also been elucidated. Analysis has also been done on the relationship between applied field and depletion layer width and barrier height. The effects of ZnO and TiO_2 on PSF dye, SWCNT on Safranin - T dye, SWCNT and MWCNT on MG dye, and SWCNT and MWCNT on MR dye based organic devices have also been calculated. The above-mentioned factors are decreased by the presence of nanotubes and nanoparticles, improving charge infusion and lowering device's threshold voltage. These four chapters also provide an explanation of the potential causes of such alterations.

In **Chapter 7**, we have seen how back electrode affects trap energy and contact barrier of CV dye based device. We have found out that alteration of back electrode has decreased trap energy and junction barrier, improving charge injection at M/O contact.

8.2 Findings of the Work

Findings on PSF dye based devices without and with ZnO and TiO_2 nanoparticles

Table 8.1 shows that with ZnO and TiO_2 nanoparticles, values of threshold voltage, barrier potential, and band bending of devices have been lowered. Additionally, TiO_2 nanoparticles enhance device efficiency more than ZnO nanoparticles. It can be explained by TiO_2 nanoparticles' higher permeability when compared to ZnO nanoparticles. As a result of their large porosity, TiO_2 nanoparticles receive more injected electrons than ZnO nanoparticles and offer a more conductive path from the injection site to the collecting electrode.

From **Table 8.2**, it has been estimated how various TiO_2 nanoparticle concentrations affect threshold voltage, barrier potential, and band bending of devices. As it can be seen, both techniques reliably demonstrate that junction barrier is lessened to its lowest point at a PSF: TiO_2 nanoparticle composition of 1:4. This composition also exhibits substantial decrease in threshold voltage. The same composition ratio also significantly decreases band bending.

Table 8.1 Parameters of Dark I -V characteristics of PSF dye based devices without and with ZnO nanoparticles and TiO_2 nanoparticles

PSF dye based devices	Threshold Voltage (V)	Barrier Potential from I -V characteristics (eV)	Barrier Potential using Norde's Function (eV)	Band Bending (eV)
Without nanoparticle	4.000	0.810	0.830	0.218
With ZnO nanoparticles	3.500	0.670	0.690	0.183
With TiO_2 nanoparticles	2.500	0.440	0.470	0.153

Table 8.2 Parameters of Dark I -V characteristics of PSF dye based devices without any nanoparticle and with varying TiO_2 nanoparticles concentrations

Devices (PSF:TiO_2)	Threshold Voltage (V)	Barrier Potential from I -V plot (eV)	Barrier Potential from Norde Function (eV)	Band Bending (eV)
Without any nanoparticle	4.000	0.810	0.830	0.218
1:1	2.500	0.440	0.470	0.153
1:2	2.250	0.430	0.440	0.147
1:3	2.000	0.400	0.420	0.136
1:4	1.750	0.380	0.370	0.127

Findings on Safranin - T Dye Based Devices without and with SWCNT

From **Table 8.3**, it can be discerned that, with SWCNT, charge infusion of Safranin - T dye based device shows improved performance as the values of threshold voltage, trap energy, barrier potential without and with considering image charge effect and barrier inhomogeneity are significantly reduced in presence of SWCNT.

Table 8.3 Parameters of Dark I -V characteristics of Safranin - T dye based devices without and with SWCNT

Safranin - T dye based devices	Threshold Voltage (V)	Value of m	Trap Energy (eV)	Barrier Potential (eV)	Effective Barrier Potential considering Image Charge (eV)	Barrier Inhomogeneity (eV)
Without SWCNT	4.000	2.270	0.059	0.810	0.790	0.170
With SWCNT	3.250	1.580	0.041	0.770	0.740	0.130

Findings on MG Dye Based Devices without and with SWCNT and MWCNT

Table 8.4 compares and displays the transition voltage, trap energy, and barrier potential values of organic devices with and without COOH - SWCNT, as well as devices with and without 8 nm and 30 nm MWCNTs. In terms of barrier potential and trap energy, it can be seen that device performance of COOH - SWCNT and the 8 nm diameter MWCNT cell display better performance compared to 30 nm diameter MWCNT cell. The charge separation and relaxation process is accelerated by smaller sizes of COOH - SWCNT and 8 nm diameter MWCNT, which improves efficacy of device.

Table 8.4 Parameters of Dark I -V characteristics of MG dye based devices without any nanotube and with presence of COOH - SWCNT and MWCNTs

MG dye based devices	Transition Voltage (V)	Value of m	Trap Energy (eV)	Junction Barrier from I -V plot (eV)	Junction Barrier using Norde Function (eV)
Without any nanotube	3.900	1.770	0.046	1.120	0.880
With COOH – SWCNT	2.000	1.050	0.027	0.870	0.770
With 8 nm MWCNT	2.370	1.080	0.028	0.970	0.790
With 30 nm MWCNT	2.710	1.340	0.035	1.030	0.840

Findings on MR Dye Based Devices without and with SWCNT and MWCNT

In **Table 8.5**, the threshold voltage, ideality factor, barrier height, and depletion layer width of MR dye based devices under the impact of SWCNT and various-sized MWCNT are expressed. The threshold voltage, ideality factor, barrier height, and depletion layer width of the devices have all enhanced significantly in presence of SWCNT and MWCNT of various sizes. All of the experimental data also demonstrate that 8 nm MWCNT outperforms 30 nm and 50 nm MWCNT in terms of efficacy. When compared to MWCNT with middle and high (30 and 50 nm) diameters, MWCNT with the smallest diameter of 8 nm will have the highest aspect ratio. With a rise in aspect ratio, the electrical conductivity percolation threshold also drops. Compared to 30 nm and 50 nm MWCNT, 8 nm MWCNT exhibits the characteristics that make it a superior additive in electrically conductive polymer applications, resulting in an enhanced charge infusion mechanism.

Table 8.5 Parameters of Dark I -V characteristics of MR dye based devices under the influence of SWCNT and MWCNT

Parameters	MR dye based devices				
	Without any nanotube	**With SWCNT**	**With 8 nm MWCNT**	**With 30 nm MWCNT**	**With 50 nm MWCNT**
Threshold Voltage (V)	2.520	1.300	1.500	1.750	2.000
Ideality Factor	5.570	0.680	0.760	0.980	1.570
Barrier Height (eV) using I -V characteristics	0.870	0.750	0.770	0.800	0.820
Barrier Height (eV) using Norde Method	0.850	0.740	0.760	0.780	0.790
Barrier Height from C -V characteristics (eV)	0.840	0.710	0.750	0.770	0.800
Effective Barrier Height Considering Image Charge Lowering Effect(eV)	0.840	0.630	0.670	0.680	0.720
Depletion Layer Width (W_d) (cm) × 10^{-6}	8.700	7.850	8.060	8.230	8.350

Findings on CV Dye Based Devices in Presence of Different Back Electrodes

Table 8.6 displays the barrier height and trap energy for both ITO/CV/Al and ITO/CV/Al-M structures. It can be said that when Al-M back electrode is present, the barrier height and the trap energy are considerably lower compared to Al back electrode. In this organic device, lowering of both injection barrier and trap energy enhances charge infusion, leading to improved conductivity.

Table 8.6 Parameters of Dark I -V characteristics of CV dye based devices in presence of two different back electrodes

CV dye based devices	Value of m	Trap Energy (eV)	Barrier Height from I -V characteristics (eV)	Barrier Height using Norde Function (eV)
With Al electrode	1.710	0.044	0.800	0.830
With Al-M electrode	1.300	0.034	0.770	0.790

8.3 Overall Conclusion

In the current study, we have looked at various charge trapping models and their impact on charge injection process. Discussions of various charge injection methods have also taken place. In this context, we have investigated and calculated the height of the interfacial barrier, the concentration of traps, the width of depletion layer, band bending, image force barrier lowering and barrier inhomogeneities at M/O interface. Interfacial band bending and image force barrier lowering of these organic devices are strongly correlated with interfacial barrier. We have also demonstrated analytical proportionality of barrier potential and trap energy, which implies that lowering of one parameter will also lower the other. Reduced values for both factors improve charge injection, which also improves conductivity.

We have calculated the above stated parameters from I -V characteristics of various organic dye based devices such as PSF, Safranin - T, MG, MR dyes and correlate it with the trap energy at M/O interface. The effects of ZnO, TiO_2, SWCNT and MWCNT on M/O junction parameters of these dyes have also been noted. A reduction in interfacial barrier height, trap concentration, depletion layer width, band bending, image force barrier lowering, and barrier inhomogeneities at M/O interface has been observed to improve device performance when ZnO, TiO_2, SWCNT and different sized MWCNT are present, taking charge trapping effect into account.

Additionally back electrode effect is investigated in CV dye based devices. We have looked at how contact barrier and trap energy of the devices are affected by two distinct counter electrodes such as

Al-M sheet-based back electrode and an Al coated back electrode. In comparison to Al back electrode, it has been found out that presence of Al-M counter electrode lowers contact barrier and trap energy more considerably. Improvement of charge infusion process at M/O interface and the enhanced conductivity is made possible by reduction in both barrier height and trap concentration. Additionally, it enables device to operate at much lesser voltages.

8.4 Future Scopes of the Work

In the current work, we have investigated the interrelationship between interfacial barrier and concentration of traps as well as the relationship between junction barrier and the width of space - charge layer. Analysis has also been done on how the applied electric field affects the depletion layer width and barrier height. Impact of ZnO, TiO_2, SWCNT and MWCNT on the M/O junction parameters of series of organic dyes, including PSF, Safranin - T, MG and MR dyes, has been the subject of an extensive study. Above mentioned factors are decreased by presence of nanoparticles and nanotubes, which improves charge infusion and lowers device's threshold voltage. The device's power consumption will decrease as a result of lowering of the threshold voltage, and much lower loadings can still accomplish the desired level of conductivity. Additionally, we have looked into how the charge injection procedure for organic devices is affected by the back electrode of the device.

However, there are still some issues in this respect that require attention. In this research, the effects of different distributions of barrier potential and barrier inhomogeneities at the M/O interface are not taken into account. To gain a thorough understanding of the charge infusion of devices, it is necessary to thoroughly study these parameters. Future research on the reproducibility and durability of these organic dye based devices is required in order to gain a detail understanding of their potential applications in various newly developing areas of electronics, such as transient electronics etc. Since fully flexible devices are now of the utmost importance, devices should also be modified to achieve these features.

----------O----------

List of Publications

Journal Papers

1. **Sudipta Sen**, N. B. Manik, "Effect of COOH-Functionalized Single Walled Carbon Nanotubes (COOH-SWCNT) on the Interfacial Barrier Height of Malachite Green (MG) Dye Based Organic Device", **Physics International**, 10 (1), 1-7, (2019)

2. **Sudipta Sen**, N. B. Manik, "Effect of Back Electrode on Trap Energy and Interfacial Barrier Height of Crystal Violet (CV) Dye based Organic Device", **Bulletin of Materials Science**, 43 (60), 1 – 4, (2020)

3. **Sudipta Sen**, N. B. Manik, "Effect of Zinc Oxide (ZnO) Nanoparticles on Interfacial Barrier Height and Band Bending of Phenosafranin (PSF) Dye Based Organic Device", **Journal of Electronic Materials**, 49 (8), 4647-4652, (2020)

4. **Sudipta Sen**, N. B. Manik, "Effects of Fullerene Nanoparticles and Fullerite Nanoparticles on the Charge Injection Mechanism of Methyl Red Dye Based Organic Device", **AIP Advances**, 10 (09), 095216-1 – 095216-5, (2020)

5. Sudipta Sen, N. B. Manik, "Correlation between Barrier Potential and Charge Trapping under the Influence of Titanium Dioxide Nanomaterials in Organic Devices", **Results in Materials**, 8 (100145), 1- 6, (2020)

6. Sudipta Sen, N. B. Manik, "Effect of Different Sized Multi Walled Carbon Nanotubes on the Barrier Potential and Trap Concentration of Malachite Green Dye Based Organic Device", **Advances in Materials Science**, 20 (4), 16-26, (2020)

7. Sudipta Sen, Pallab Kumar Das, N. B. Manik, "Study on Effect of Single Walled Carbon Nanotubes on Junction Properties of Safranin –T Dye Based Organic Device", **Journal of Physics Communications**, 5 (045004), 1-9, (2021)

8. Sudipta Sen, N. B. Manik, "Effect of Different Concentrations of Titanium Di Oxide Nanoparticles on the Potential Barrier of Organic Device", **European Journal of Formal Sciences and Engineering**, 4 (1), 1-10, (2021)

9. Pallab Kumar Das, **Sudipta Sen**, N. B. Manik, "Effect of Single Walled Carbon Nanotubes on the Series Resistance and Trap Energy of Malachite Green Dye Based Organic Device", **Journal of Nano Research**, 69 (5), 43-52, (2021)

10. **Sudipta Sen**, N. B. Manik, "Effect of Different Sized Multi Walled Carbon Nanotubes on the Parameters Affecting the Charge Injection Process of Methyl Red Dye Based Organic Device", **Journal of Material Sciences and Engineering**, 10 (5), 01-05, (2021)

11. Sudipta Sen, N. B. Manik, "Effect of Fullerene Nanoparticles on the Barrier height of Copper Phthalocyanine Dye Based Organic Device", **Advanced Materials Research**, 1167, 35-42, (2021)

12. Sudipta Sen, N. B. Manik, "Effects of Two Different Solvents on Schottky Barrier of Organic Device", **Journal of Physics Communications**, 5 (095010), 1-10, (2021)

13. Sudipta Sen, N. B. Manik, "Modification of Barrier Height and Depletion Layer Width of Methyl Red (MR) Dye - Based Organic Device in Presence of Single - Walled Carbon Nanotubes (SWCNT)", **Indian Journal of Physics**, 96 (2), 385-390, (2022)

14. Pallab Kumar Das, **Sudipta Sen**, N. B. Manik, "Study on the Series Resistance of Crystal Violet Dye - Based Organic Photovoltaic Device in Presence of Single Walled Carbon Nanotubes", **Indian Journal of Physics**, 96 (5), 1423-1431, (2022)

15. Sudipta Sen, Pallab Kumar Das, N. B. Manik, "Modification of Interfacial Properties of Organic Device in Presence of Single Walled Carbon Nanotubes", **Journal of Materials Science and Surface Engineering**, 9 (1), 1067-1070, (2022)

List of International or National Conferences/ Seminars

1. Sudipta Sen, Sujata Chakraborty, Swapan Bhunia, Nabin Baran Manik, "Effect of Single Walled Carbon Nanotubes (SWCNT) on the Band Bending of Rose Bengal (RB) Dye Based Photovoltaic Devices", **National Conference on Condensed Matter Physics (CMDAYS 2017)**, Department of Physics, Tezpur University, 29th –31st August, (2017)

2. Sudipta Sen, Sujata Chakraborty, Nabin Baran Manik, "Effect of Single Walled Carbon Nanotubes (SWCNT) on the Barrier Potential of Crystal Violet (CV) Dye Based Organic Diode", **National**

Conference on Condensed Matter Physics (CMDAYS 2018), Bose - 125 Event, Department of Physics, The University of Burdwan, 29th –31st August, (2018)

3. Sudipta Sen, Sujata Chakraborty, Nabin Baran Manik, "Study on the Effect of Single Walled Carbon Nanotubes (SWCNT) on Trap Energy and Barrier Potential in Rose Bengal (RB) Dye Based Organic Device", **National Seminar on Emerging Frontiers in Materials Science (EFMS 2019)**, Department of Physics in collaboration with Department of Electronics, Behala College, Kolkata, 15th –16th February, (2019)

4. Sudipta Sen, Nabin Baran Manik, "Modification of Trap Energy and Barrier Height in Crystal Violet (CV) Dye based Organic Device in Presence of Single Walled Carbon Nanotubes (SWCNT)", **14th International Conference on Recent Trends in Engineering, Applied Science and Management (ICRTESM 2019)**, Proceedings on International Journal of Scientific Research and Review (2019), Vedant College of Engineering and Technology, Bundi, Rajasthan, 16th –17th February, (2019)

5. **Sudipta Sen**, Nabin Baran Manik, "Study on the Effect of 8 nm Size Multi Walled Carbon Nanotubes (MWCNT) on the Barrier Height of Malachite Green (MG) Dye Based Organic Device", **2nd International Conference on Current Trends in Materials Science and Engineering (CTMSE 2019)**, Proceedings on International Journal of Advanced Science and Engineering (2020), S. N. Bose National Centre for Basic Sciences, Kolkata, 18th –20th July, (2019)

6. Sudipta Sen, Nabin Baran Manik, "Effect of Fullerene Nanoparticles on Barrier Height of Crystal Violet Dye Based Organic Device", **3rd International Conference on Electronics, Materials Engineering & Nano –Technology (IEMENTECH 2019)**, **IEEE Conference # 48150**, Proceedings on IEEE Xplore (2020), Department of Electronics, Institute of Engineering and Management, Kolkata, 29th – 31st August, (2019)

7. Sudipta Sen, Nabin Baran Manik, "Influence of Single Walled Carbon Nanotubes on the Ideality Factor of Rose Bengal Dye Based Organic Device", **National Conference on Flatlands and Beyond (2019) – A meet on 2D materials**, S. N. Bose National Centre for Basic Sciences, Kolkata, 5th – 6th September, (2019)

8. Sudipta Sen, Nabin Baran Manik, "Effect of Zinc Oxide (ZnO) Nanoparticles on the Barrier Potential of Phenosafranin (PSF) Dye Based Organic Device", **National Seminar on Physics at**

Surfaces and Interfaces of Soft Materials (PSISM 2019), Condensed Matter Physics Research Centre, Department of Physics, Jadavpur University, Kolkata, 26th – 27th September, (2019)

9. Sudipta Sen, Nabin Baran Manik, "Study on the Effect of Zinc Oxide Nanoparticles on Injection Barrier Height of Crystal Violet Dye Based Organic Device", **1st International Conference on Condensed Matter Physics (IEMPHYS 19)**, Proceedings on International Journal of Innovative Research in Physics, Department of Basic Science & Humanities, Institute of Engineering and Management, Kolkata, in association with IEM Society of Physics Students (SPS) Chapter and American Institute of Physics, 14th –16th November, (2019)

10. Sudipta Sen, Pallab Kumar Das, Swapan Bhunia, Nabin Baran Manik, "Effect of Single Walled Carbon Nanotubes (SWCNT) on the Barrier Potential of Methyl Red (MR) Dye Based Organic Device", **One Day National Seminar on New Directions in Physical Sciences 2020: Special Emphasis on Material Science & Biophysics (NDPS 2020)**, Condensed Matter Physics Research Centre, Department of Physics, Jadavpur University, Kolkata, 25th February, (2020)

11. **Sudipta Sen**, Nabin Baran Manik, "Effect of Two Different Sized Multi Walled Carbon Nanotubes (MWCNT)on the Ideality Factor and Threshold Voltage of Methyl Red (MR) DyeBased Organic Device", **3rd International Conference on Current Trends in Materials Science and Engineering (CTMSE 2021)**, Department of Basic Science & Humanities, Institute of Engineering and Management, Kolkata, 11th –13th March, (2021)

12. Sudipta Sen, Nabin Baran Manik, "Modification of Barrier Height of Azure – B Dye Based Organic Device in Presence of Single Walled Carbon Nanotubes (SWCNT)", **2nd International Conference on Advanced Physics (IEMPHYS 21)**, Department of Basic Science & Humanities, Institute of Engineering and Management, Kolkata, in association with IEM Society of Physics Students (SPS) Chapter, American Institute of Physics and Smart Society, USA, 1st – 3rd April, (2021)

13. Arnab Kanti Karan, Dipankar Sahoo, **Sudipta Sen**, Swapan Bhunia, Subhra Rakshit, Nabin Baran Manik, "Estimation of Activation Energy of Tartrazine Dye based Natural Organic Device", **4th International Conference on Current Trends in Materials Science and Engineering (CTMSE 2022)**, Department of Basic Science & Humanities, Institute of Engineering and Management, Kolkata, 28th – 30th July, (2022)

14. Arnab Kanti Karan, Dipankar Sahoo, **Sudipta Sen**, Nabin Baran Manik, "Evaluation of Richardson Constant of Fruit dyes using Carmoisine and Tartrazine", **3rd International Conference**

on Advanced Physics (IEMPHYS 22), Proceedings on International Journal of Innovative Research in Physics, Department of Basic Science & Humanities, Institute of Engineering and Management, Kolkata, in association with IEM Society of Physics Students (SPS) Chapter, American Institute of Physics and Smart Society, USA, 22nd – 24th September, (2022)

15. **Sudipta Sen**, Nabin Baran Manik, "Influence of Multi Walled Carbon Nanotubes (MWCNTs) on Parameters Affecting Charge Injection Process at M/O Contact", **6th International Conference on Electronics, Materials Engineering & Nano–Technology (IEMENTECH 2022)**, IEEE Conference, Department of Electronics, Institute of Engineering and Management, Kolkata, 2nd – 4th December, (2022)

16. Sudipta Sen, Arnab Kanti Karan, Dipankar Sahoo, Nabin Baran Manik, "Impact of Single Walled Carbon Nanotubes (SWCNTs) on Injection Barrier of Thionine Dye Based Organic Device", **International Conference on Nanotechnology (ICNT 2022)**, Sponsored by Science and Engineering Research Board (SERB), Govt. of India, Institute of Fire and Safety Engineering, Haldia, 23rd – 24th December, (2022)

17. **Sudipta Sen**, Arnab Kanti Karan, Dipankar Sahoo, Nabin Baran Manik, "Single Walled Carbon Nanotubes: Its effect on Parameters Related to Charge Injection Process of Organic Device", **7th International Conference on Nanoscience and Nanotechnology (ICONN 2023)**, SRM Institute of Science and Technology, Tamil Nadu, India, 27th – 29th March, (2023)

Book Chapter

1. Sudipta Sen, Nabin Baran Manik, "Estimation and Modification of Electrical Parameters of Organic Device in the Presence of Single Walled Carbon Nanotubes", IntechOpen, (2022)

Awards

1. Best award in poster presentation for paper entitled "Effect of Two Different Sized Multi Walled Carbon Nanotubes (MWCNT) on the Ideality Factor and Threshold Voltage of Methyl Red (MR) Dye Based Organic Device" by **Sudipta Sen**, Nabin Baran Manik at **3rd International Conference on Current Trends in Materials Science and Engineering (CTMSE 2021)**, Kolkata, 11th-13th March, (2021)

2. Best award in poster presentation for paper entitled "Modification of Barrier Height of Azure – B Dye Based Organic Device in Presence of Single Walled Carbon Nanotubes (SWCNT)" by **Sudipta Sen**, Nabin Baran Manik at **2nd International Conference on Advanced Physics (IEMPHYS 21)**, Kolkata, 1st-3rd April, (2021)

3. Best award in paper presentation for paper entitled "Impact of Single Walled Carbon Nanotubes (SWCNTs) on Injection Barrier of Thionine Dye Based Organic Device", by **Sudipta Sen**, Arnab Kanti Karan, Dipankar Sahoo, Nabin Baran Manik at **International Conference on Nanotechnology (ICNT 2022)**, **Sponsored by Science and Engineering Research Board (SERB)**, **Govt. of India**, Haldia, 23rd – 24th December, (2022)

Workshops/ Seminars/ Webinars/ Conferences Attended

1. One day Seminar on "Recent Trend in Frontier Research in Physics (RTFRP 2018)*"*,Department of Physics, Jadavpur", Department of Physics, Jadavpur University, 6th March, (2018)

2. One day UGC-SAP Sponsored National Seminar on "Advances in Nanoscience and Nanotechnology Applications", Department of Chemical Engineering, Jadavpur University, 10th January, (2020)

3. Five days Short Term Training Program (STTP) on "Evolution of RF Electromagnetics from Microwave to mm Wave Technologies", Centre of Excellence in Complex and Nonlinear Dynamical Systems, VJTI, Mumbai, 19th December – 23rd December, (2020)

4. One day MDPI Webinar on "Materials: Advanced Porous Materials", 12th May, (2021)

5. Three days International Conference on "Recent Trends in Green Chemistry (ICRTGC-2021)", Department of Chemistry, Akal University and Indian Chemical Society, Kolkata, 28th September – 30th September, (2021)

6. One day National Virtual Conference on "Smart Nanomaterials- 2021", Faculty of Allied Health Sciences, Chettinad Academy of Research and Education, Kelambakkam, Tamil Nadu, 16th October, (2021)

7. One day National Virtual Conference on "Biomedical Applications of Nanotechnology", Faculty of Allied Health Sciences, Chettinad Academy of Research and Education, Kelambakkam, Tamil Nadu, 07th May, (2022)

8. Five Days Workshop on "Interpretation of Instrumental Methods (WIIM-2023)", Sathyabama Institute of Science and Technology and CSIR - NML Madras Centre, Chennai, Tamil Nadu, 2nd January – 6th January, (2023)

Sudipta Sen
24/04/2023